MICROCOPY RESOLUTION TEST CHART

NATIONAL BUREAU OF STANDARDS 1963 A

AFWAL-TR-81-3075
PART I

AD A112626

ASSESSMENT OF LIGHTNING SIMULATION
TEST TECHNIQUES

W. G. Butters
D. W. Clifford
K. P. Murphy
K. S. Zeisel

McDonnell Aircraft Company
P. O. Box 516
St. Louis, Missouri 63166

October 1981

FINAL REPORT – PART I FOR PERIOD JULY 1980 – OCTOBER 1981

DTIC FILE COPY

DTIC
ELECTE
MAR 30 1982
S   D
B

Prepared for

FLIGHT DYNAMICS LABORATORY
AIR FORCE WRIGHT AERONAUTICAL LABORATORIES
AIR FORCE SYSTEMS COMMAND
WRIGHT-PATTERSON AIR FORCE BASE, OHIO 45433

82 03 29 020

This technical report has been reviewed and is approved for publication.

BRIAN P. KUHLMAN, 1Lt, USAF
Project Engineer

GARY A. DUBRO, Chief
Atmospheric Electricity Hazards Group
Flight Vehicle Protection Branch
Vehicle Equipment Division

FOR THE COMMANDER

SOLOMON R. METRES
Director
Vehicle Equipment Division

REPORT DOCUMENTATION PAGE	READ INSTRUCTIONS BEFORE COMPLETING FORM

1. REPORT NUMBER	2. GOVT ACCESSION NO.	3. RECIPIENT'S CATALOG NUMBER
AFWAL-TR-81-3075	AD-A112 626	

4. TITLE *(and Subtitle)*	5. TYPE OF REPORT & PERIOD COVERED
ASSESSMENT OF LIGHTNING SIMULATION TEST TECHNIQUES	Final, Part I – July 1980 to October 1981
	6. PERFORMING ORG. REPORT NUMBER

7. AUTHOR(s)	8. CONTRACT OR GRANT NUMBER(s)
W. G. Butters, D. W. Clifford K. P. Murphy, K. S. Zeisel	F33615-80-3406 C

9. PERFORMING ORGANIZATION NAME AND ADDRESS	10. PROGRAM ELEMENT, PROJECT, TASK AREA & WORK UNIT NUMBERS
McDonnell Aircraft Company P.O. Box 516 St. Louis, Missouri 63166	24020234

11. CONTROLLING OFFICE NAME AND ADDRESS	12. REPORT DATE
Flight Dynamics Laboratory Air Force Systems Command Wright-Patterson Air Force Base, Ohio 45433	October 1981
	13. NUMBER OF PAGES
	116

14. MONITORING AGENCY NAME & ADDRESS(if different from Controlling Office)	15. SECURITY CLASS. (of this report)
Air Force Flight Dynamics Laboratory Flight Vehicle Protection Branch Vehicle Equipment Division	Unclassified
	15a. DECLASSIFICATION/DOWNGRADING SCHEDULE

16. DISTRIBUTION STATEMENT *(of this Report)*

Approved for public release; distribution unlimited.

17. DISTRIBUTION STATEMENT *(of the abstract entered in Block 20, if different from Report)*

18. SUPPLEMENTARY NOTES

19. KEY WORDS *(Continue on reverse side if necessary and identify by block number)*

Lightning Simulation Testing	Transmission Line Model
Induced Voltage	Capacitive Coupling
Indirect Lightning Effects	Inductive Coupling

20. ABSTRACT *(Continue on reverse side if necessary and identify by block number)*

The program objective was to assess the current pulse and shock-excitation lightning simulation test techniques. The current pulse test technique applies a pulsed current stimulus to the test article, while the shock-excitation technique first charges the test article to a high voltage which then produces a rapid voltage/current pulse on the test article as the spark gap (between the test article and the return conductors) breaks down. Direct comparisons of the induced voltage response on interior circuits were made for the two test techniques. The interior circuits were high-impedance differential wire pairs -

DD FORM 1 JAN 73 **1473** EDITION OF 1 NOV 65 IS OBSOLETE

typical of many flight-critical circuits in advanced aircraft.

The program was divided into three tasks: 1) an analytical task to model both test techniques to provide a theoretical base, 2) comparative tests using an aluminum cylinder and simple interior circuits that were readily modeled, and 3) comparative tests on the flight control circuits of a full-scale YF-16 fighter aircraft.

The cylinder test configuration was modeled as two coupled transmission line circuits. The generator, cylinder, return lines, and the output configuration between the cylinder and the return line comprise the primary transmission line that interacts with an interior circuit transmission line via aperture coupling. The current pulse test technique (shorted output) and both the charging (open output) and discharging (arc output) phases of the shock-excitation test technique were studied. The analysis showed that capacitive coupling should dominate for high-impedance circuits while inductive coupling should dominate for low-impedance circuits. Sensitivity studies showed that aperture location, cylinder dissipation, cylinder characteristic impedance, and cylinder length were important parameters.

The system and induced voltage responses of the cylinder test configuration agreed very well with the analytically-predicted waveforms. Simple RLC circuit modeling was sufficient to predict the induced voltage behavior during the charging phase of the shock-excitation test. The discharge phase of the shock-excitation test contained both the fast discharge of the previously charged cylinder and the slower current response produced by the generator as in the current pulse technique. For the same test conditions, the fast discharge of the shock-excitation test produced induced voltage transients an order of magnitude larger than those for the current pulse test. For the high-impedance circuits tested, the shock-excited induced voltage scaled like the time rate of change of the cylinder voltage, in agreement with the analytical predictions.

The tests on the YF-16 flight control circuits produced time domain waveforms that were similar to those of the cylinder tests. The complexity of the aircraft system was most evident in the frequency domain where system resonances could not readily be explained and in the test technique complications caused by the aircraft's physical size and weight. The fast discharge of the shock-excitation test technique produced near threat level rates of voltage and current change; however, the induced voltage on the flight control circuits was only two to five times as large as the respective current pulse test. More detailed tests are required to fully interpret the YF-16 test results.

PREFACE

This report describes the work performed by McDonnell Aircraft Company (MCAIR) on Contract F33615-80-C-3406 sponsored by the Flight Vehicle Protection Branch of the Air Force Flight Dynamics Laboratory, Wright-Patterson Air Force Base, Ohio and funded by the Naval Air Development Center in Warminster, Pennsylvania.

The MCAIR lightning laboratory performed the work reported herein between July 1980 and January 1981. Besides the authors, Dr. C. J. Skouby and Dr. R. A. Pearlman of the MCAIR Avionics Division made significant contributions to the program.

The authors wish to thank Mr. G. A. DuBro and Lt. B. P. Kuhlman of the Electromagnetic Hazards Group Laboratory of the Flight Dynamics Laboratory for their assistance throughout the program.

This report (Part I) includes an analytical and experimental comparison of the current pulse and shock-excitation lightning simulation test techniques on both a simplified cylindrical geometry and a YF-16 fighter aircraft. Part II of the final report will describe the results of lightning simulation tests on the NOAA C-130 aircraft used in the FDL/NOAA Airborne Lightning Characterization Program. Testing is to be performed in November 1981.

Accession For

NTIS GRA&I ☑
DTIC TAB ☐
Unannounced ☐
Justification

By
Distribution/
Availability Codes

Dist | Avail and/or Special

A

iii/iv

TABLE OF CONTENTS

LIST OF ILLUSTRATIONS

(cont'd)

(cont'd)

LIST OF TABLES

SECTION I
INTRODUCTION

The potential threat of atmospheric hazards to new generation aircraft has
been increased by the widespread use of sensitive microelectronics in flight-
critical avionics and by the reduced shielding effectiveness afforded by
advanced composite structural materials. Induced electromagnetic transients
coupled to internal wiring during a lightning strike can readily damage or
upset avionics if protective measures are not implemented. Ground-based
lightning simulation testing is necessary to optimize the design measures
and to assure the survivability of aircraft avionics after an actual strike.
Ground tests should simulate all the important electromagnetic coupling
mechanisms of the aircraft/lightning interaction as realistically as possible.

Induced transient tests have generally been conducted by passing a low-level
current pulse waveform through an aircraft structure. The induced signals on
selected interior circuits are measured and then linearly scaled to peak
lightning threat levels. This current pulse technique, which has been
applied to several aircraft, has been referred to as the lightning transient
analysis (TA) technique. The test results have been consistent as long as
current induced coupling mechanisms are dominant and nonlinear effects are
not present.

Because of concerns about possible nonlinearities and apparent inconsis-
tencies in the early-time response of the measured transients, the McDonnell
Aircraft Company (MCAIR) launched a program in 1977 to further develop the
test technique. The resulting MCAIR technique differs in several respects
from the current pulse technique. The MCAIR approach, referred to as the
shock-excitation technique, isolates the aircraft from both the generator and
ground by spark gaps. A very high voltage generator is used to spark over the
gaps and to provide both voltage and current stimuli. This technique allows
the simulation of three phases of a lightning strike: 1) the fast electric
field changes produced by nearby flashes, 2) the stepped-leader attachment to
the aircraft, and 3) the direct attachment return stroke.

The primary objective of this program was to compare the induced transient responses of the hard-wired current pulse technique and the shock-excitation test. Three tasks were defined for the program. Task 1 was an analytical task designed to theoretically determine the correct coupling mechanisms and to provide an analytical base for Task 2. In Task 2, comparative current pulse and shock-excitation tests were conducted on an aluminum cylinder under conditions amenable to predictive analysis. Task 3 extended the test evaluation to full-scale tests on the YF-16 fighter aircraft tested at the Flight Dynamics Laboratory, Air Force Wright Aeronautical Laboratories, at Wright-Patterson Air Force Base, Ohio.

SECTION II
BACKGROUND

1. The Current Pulse Test

The transient current pulse technique was first developed by General Electric Company's high-voltage laboratory and applied to an F-89 aircraft in 1971. Since that time, the current pulse test has been further refined and applied to a number of additional aircraft by the USAF Flight Dynamics Laboratory and Lightning Technologies, Inc. The test technique and results are well documented and will not be repeated here.[1,2,3,4] The typical current pulse test setup uses a lightning pulse generator and waveshaping network connected to an aircraft attach point as the system stimulus. The current path is completed by a hard-wire connection from a second aircraft location to the other side of the generator. The general assumptions are that at low-current levels induced transients on interior wiring can be scaled linearly as long as the driving current waveform is identical in shape (and, therefore, in frequency content) to the full-threat waveform. Diffusion or resistively-coupled transients scale linearly with the peak current, and inductively-coupled transients scale as the time rate of change of the current (dI/dt). At higher current levels, the possibility of nonlinear effects such as arcing at joints or surface tracking along dielectrics is recognized. Such effects can cause a distortion of the current paths and, therefore, a deviation from linear scaling. However, it is argued that any such deviations should be in a direction to make the scaled values more conservative.

2. The Shock-Excitation Test

a. Development History - The shock-excitation test technique was developed under a MCAIR Independent Research and Development (IRAD) program to provide a full-scale aircraft lightning test that would better simulate the

natural lightning environment. The results of the continuing IRAD program are briefly summarized here to establish background for their application to this test program.

Figure 1 is a simplified schematic of the flexible experimental layout used in test development. A long aluminum cylinder with a wire pair strung on axis represents the aircraft fuselage and interior wiring. The cylinder is 15 inches in diameter, and its length can be varied in 8-foot sections from 8 to 48 feet. The cylinder is isolated well above the floor on insulating supports. A high-voltage Marx generator is the system stimulus and data are transmitted from internal and external sensors by fiber-optic data links to a computer-controlled data acquisition system in a screen room. A typical set of data is shown in Appendix A, together with the data processing routines that have been developed for transient analysis.

Because of the extremely large number of system variables, most of the MCAIR testing has concentrated on the differential circuit response of interior wiring due to aperture coupling. Aperture coupling is the dominant coupling mechanism to the internal wiring of metal-skinned aircraft, and the majority of flight-critical circuits are the differential type using two wires, as opposed to a single wire and structural return. The differential (line-to-line) response has been shown to be more sensitive to the high-voltage, high-frequency shock stimulus.[5]

The initial test development is documented in References 5 and 6; the key findings include:
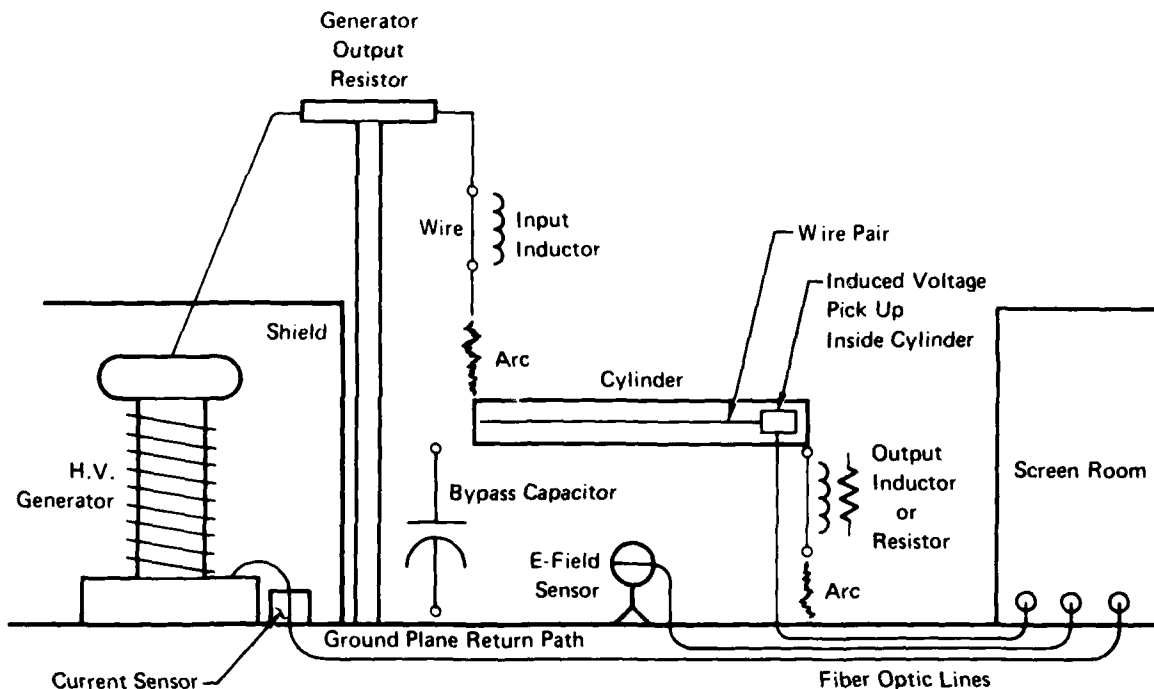
FIGURE 1. EXPERIMENTAL LAYOUT

GP11-0312-1

(1) Long arcs to and from an isolated test article produce rapid electric
field changes, rapid vehicle charging, and a return stroke type dis-
charge condition in which the article is fully charged to a high
potential before the arrival of the return stroke ground wave
(Figure 2).

(2) High-frequency induced voltage transients are excited in all three
phases. The magnitudes and frequencies of the various responses are
dependent upon test configuration.
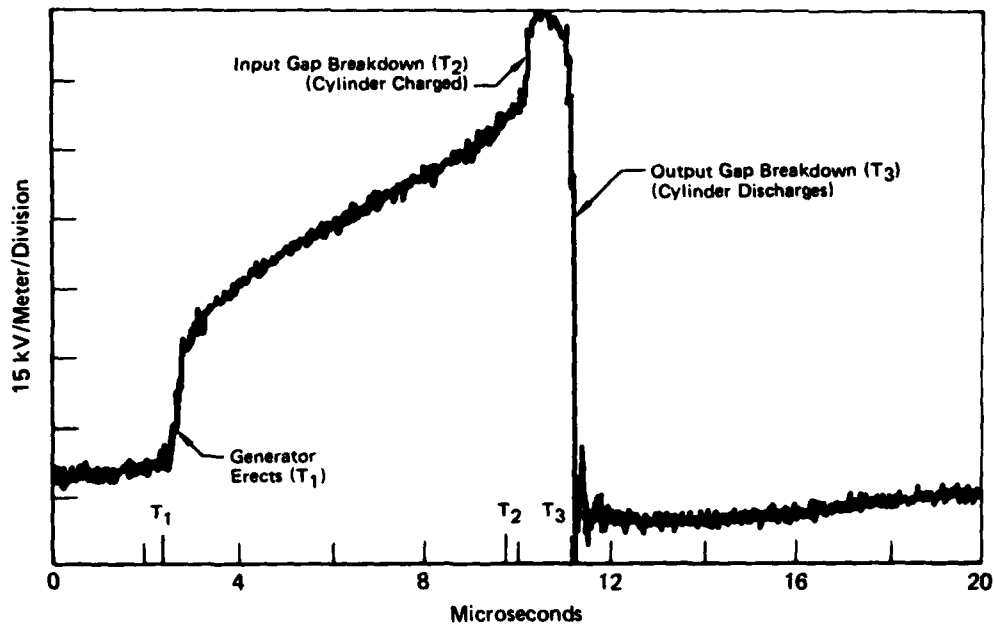
FIGURE 2. ELECTRIC FIELD NEAR THE CYLINDER
Input and Output Spark Gaps

(3) The magnitude of the interior wire transient induced during the charging of an isolated test article (i.e., stepped-leader attachment) is proportional to dV/dt for high impedance circuits ($\dot{V}$ transient).

(4) For a hard-wired test article (as in the current pulse test), the *magnitude of the induced transient is proportional to dI/dt(0+) and not related to the peak current unless the waveform is held invariant.*

(5) The discharge of a lightning simulation generator into an isolated test article causes the test article to be first charged and then discharged as it is allowed to arc to ground potential. This type of test produces a much larger induced voltage on interior high impedance circuits than is produced by discharging the same generator output through a grounded test article. The increased induced voltage is due to the rapid discharge of the article to ground potential ($dV/dt \approx 10^{12}$ v/sec, $dI/dt \approx 10^{11}$ amps/sec) before the slower discharge of the generator can take place. This finding is important because it relates to the simulation requirement produced by recent

6

measurements of natural lightning which show that return stroke
current transitions often occur in less than 200 nsec. Allowing the
aircraft to discharge from a very high potential through a spark
channel is possibly the most realistic and yet the simplest way to
accomplish this simulation.

Many experimental test sequences have been conducted to determine the effects
of system parameter variations on the shock-excitation transient response.
The parameter variations studied include:

o Interior circuit type: differential, common mode

o Cylinder stimulus (input/output configuration): radiated, hard-wired,
   arcs, various output resistances.

o Input waveform: voltage levels, current levels, different Marx
   generators, various waveshaping components

o Cylinder configurations: length; number, size, and location of
   apertures; current paths; internal wire type (twin-lead, coax, etc.)

o Return path configurations: wire, ground plane, coaxial.

It is instructive to separate the results of the many parameter variation
sequences into the two categories of time and frequency domain responses. The
time domain responses are more predictable and are important for scaling to
threat level. The frequency domain responses are important in circuit design,
but resonances and transmission line effects make them less predictable.

b. _Time Domain Response_ - The magnitude and form or envelope of the
induced voltage response are the important features that are scaled to threat
level to determine if component damage or digital upset can be anticipated.
Understanding of the variation of these characteristics with changes in the
system parameters is critical to the development of the simulation test
technique. Several generalizations can be made from the past test results.

(1) For a given set of cylinder test conditions, the form of transient
    responses can be consistently predicted for the system current, the
    induced voltage, and the electric field in the vicinity of the
    cylinder.

(2) The magnitude and frequency of the system current can be predicted in
    most cases using simple, lumped-parameter RLC circuit analysis. In
    cases employing an output spark gap, a more sophisticated many-loop,
    time-dependent solution is required to match the current waveform.
    Such a solution has been obtained.

(3) The form of the induced voltage response is primarily determined by
    the circuit type and the cylinder stimulus. Differential circuits
    exhibit a high-frequency damped sinusoidal response with very little
    magnetic ($d\phi/dt$) response. Common mode circuits have significant
    $d\phi/dt$ response, with a high-frequency transient modulating the early
    response.

(4) Either magnetic or capacitive coupling can dominate, depending upon
    the circuit configuration and impedance. For the high impedance,
    differential circuits typically used in the critical circuits of
    fighter aircraft, capacitive coupling should dominate. Where capaci-
    tive coupling dominates, a hard-wired low-level current pulse test is
    not appropriate because the high E-fields are not simulated.

(5) The cylinder output condition (whether hard-wired or an output arc)
    has a significant effect on the magnitude of the induced voltage.

(6) Variation of the input waveform, cylinder configuration, and return
    wire configuration parameters have an effect on the magnitude of the
    induced voltage, but little effect on the form of the response.

(7) For a given set of conditions, scaling relationships based on the
    input waveform can be observed and have predictive capability.

8

These generalizations qualitatively identify the key parameters that are important in any lightning test formation. The principal difference in the shock-excitation and current pulse test is whether or not the aircraft is hard-wired to the low voltage side of the pulse generator. It is significant that this factor has the largest effect on induced voltage magnitudes, particularly where capacitive coupling to important circuits is involved.

c. <u>Frequency Domain Response</u> - The frequency content of the transient response is obtained by the computer calculation of the Fourier transform of the digitally recorded time domain response. The causes of the frequency peaks (resonances) have been investigated by varying the circuit configuration and termination, by time domain reflectometry, by sweep frequency techniques, and by standing wave measurements. In the idealized geometry of the laboratory test setup, most of the dominant frequency peaks can be explained by lumped-parameter resonance or line length effects; however, some peaks remain unexplained. In an actual aircraft, the complexity of the circuit interactions makes the understanding of the frequency spectra far more difficult.

The variation of the frequency content of the skin current and the induced voltage is not as predictable as the time domain response. The characteristic frequencies calculated from simple RLC theory are present in current measurements; however, they are generally complicated by the addition of secondary resonances and transmission line effects that are dependent upon system configuration. The frequency content of the induced voltage is very dependent on the coupling mechanism (inductive or capacitive), system geometry, line lengths, and terminations. Again some generalizations can be made from the numerous test sequences performed:

(1) Radiated fields incident on an isolated cylinder produce a single dominant frequency peak on the cylinder characteristic of a half-wavelength resonance. Skin current resonances as a function of cylinder length and test configuration are discussed in Reference 7.

9

(2) Skin current resonances on the cylinder, when the cylinder is isolated from ground but connected to high impedance waveshaping elements from the Marx generator, also show the half-wavelength resonance; however, the frequency is shifted, and secondary resonances may be present.

(3) Skin current resonances on the cylinder connected to ground by a wire or an arc show a quarter-wavelength resonance. Standing waves are established at the resonant frequency and have a current maximum at the cylinder to ground connection. Termination of the cylinder to ground return transmission line in a resistance near its characteristic impedance greatly damps the quarter-wavelength resonance.

(4) The frequency content of the induced voltage response is generally more complicated and less predictable than that of the skin current.

(5) Inductive coupling in common mode circuits produces resonant frequencies consistent with those of the skin currents, but additional high-frequency resonances due to interior wiring line length effects are also present.

(6) Induced voltage spectra of differential mode circuits are generally dominated by interior wire transmission line effects, but also contain secondary frequencies that are not readily explained.

SECTION III
TASK 1 - CYLINDER ANALYSIS

The analysis of the transient responses of the aluminum cylinder test configuration provides the theoretical background necessary to understand the subsequent experimental results. The objective of Task 1 was to model the geometrically-simple test configuration in order to provide insight into the coupling dynamics and to validate the experimental results for the various lightning simulation conditions applied to the cylinder. No attempt was made to model the YF-16 test circuits due to the aircraft complexity and a lack of sufficient detail.

Figure 3 depicts the modeled test configuration. The high-voltage Marx generator is connected by waveshaping elements to the test cylinder which is generally isolated from ground by an output spark gap. Variation of the spark gap spacing produces three distinct output test configurations which were studied analytically and, later, experimentally. These variations include: 1) the open cylinder output in which the gap spacing is so large that gap breakdown does not occur, 2) the hard-wired output in which the gap electrodes are connected together to ground the cylinder, and 3) the intermediate gap spacings in which the cylinder is charged to high voltage until the spark gap breaks down to complete the generator discharge path through the cylinder.

For the computer model, a single interior wire with arbitrary terminations was used as the interior test circuit whose induced response was studied. Coupling to the wire was through an open aperture near the generator end of the cylinder. Both low and high impedance interior wire terminations were studied analytically; however, only high impedance circuits (which simulated the YF-16 flight control circuits) were investigated experimentally.

1. Analytical Approach

The experimental setup was modeled as two coupled transmission line circuits with a time-dependent arc resistance (see Appendix B). The cylinder and its ground return were modeled as the source transmission line. The internal wires were modeled as a coupled transmission line excited by the EM

GP11-0312-5
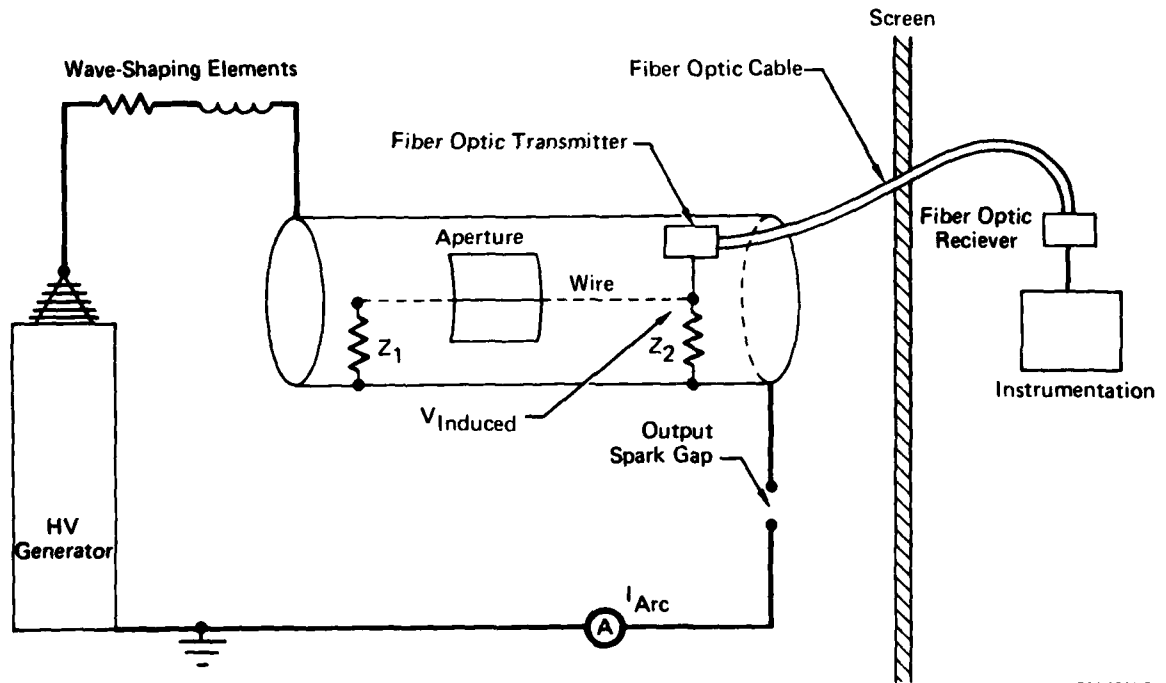
FIGURE 3. MODELED TEST CONFIGURATION

fields, generated by the source skin currents and voltages, which couple to
the wires through the aperture in the cylinder wall.

Initially, SCEPTRE and ECAP circuit codes were employed to compute time domain
waveforms. Lumped L-C sections were used to represent the transmission lines
and both mutual capacitance and inductance were used to represent the E-field
and H-field coupling between the two lines. Predicted cylinder voltage and
current waveforms roughly resembled test results, but the predicted induced
voltage waveforms did not. This problem was resolved by using a computer
program called TRANSIMM which can employ a distributed circuit model with a
variable arc resistance to more accurately represent the transmission lines.

TRANSIMM (transient simulation model) is an analytical code developed under a
concurrent industrial research and development effort. The TRANSIMM model
utilizes two coupled transmission line circuits, and is shown schematically in
Figure 4. The upper circuit models the generator and waveshaping components
as lumped parameters, and the spark gap as a time-varying arc resistance. The

12
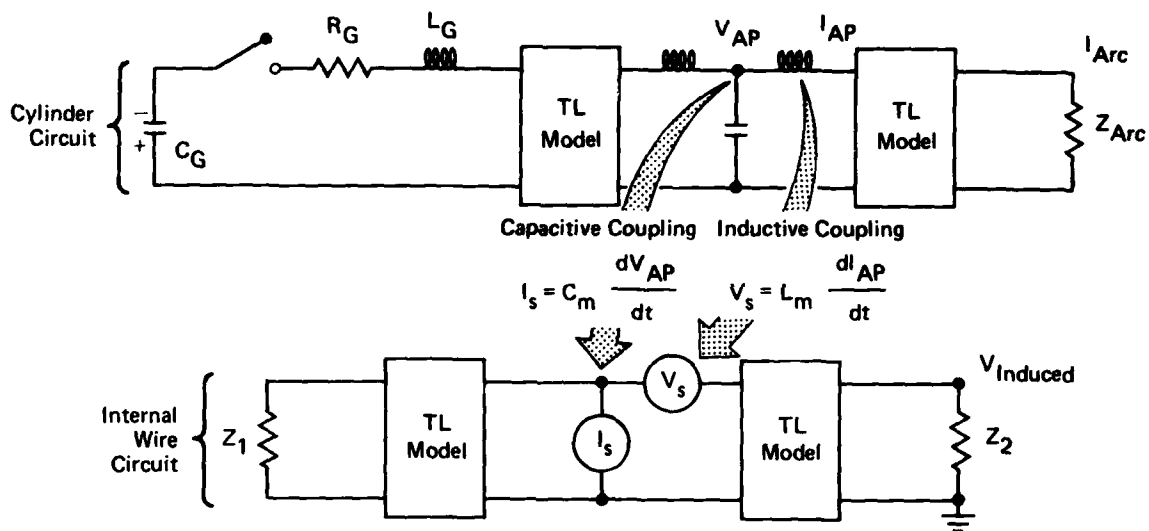
GP11-0312-8

FIGURE 4. TRANSIMM MODEL

cylinder-to-ground interaction is described with a transmission line model that is segmented in two parts, in order to give voltage and current outputs at the appropriate aperture location. These voltage and current values are then coupled to the interior wire-to-cylinder transmission line circuit as an equivalent current source ($I_s = C\frac{dV}{dt}$) in parallel with the line and a voltage source ($V_s = L\frac{dI}{dt}$) in series with the line. Solutions for the various voltage and current time waveforms are obtained using an interactive version of the SPICE circuit program with terminal graphics capability. The code employs a finite difference method using an implicit integration technique with multiple iterations to solve for the node voltages and currents, given the initial voltage on the capacitor bank.

Since TRANSIMM could incorporate either a distributed or lumped parameter transmission line model, the effects of transmission line resonances were easily determined. Reflections back and forth along the cylinder due to impedance mismatch at the ends were faithfully reproduced by the model. However, abrupt voltage transitions, such as generator triggering and output spark gap breakdown, initially resulted in a sequence of abrupt pulses repeated at multiples of the back and forth time. In some cases the very

13

high frequency components of these pulses propagated without substantial dissipation and caused numerical instabilities in the computer solution technique.

The high frequency difficulty was solved for the frequency range of interest (0 to 25 MHz) by: 1) using a realistic rise time ($\approx$10 ns) for the input voltage and a decay time of $\approx$200 ns for the arc resistance, 2) adding some dissipation to the transmission line to damp the high-frequency components, and 3) using small lumped elements to eliminate the very high-frequency components that cause numerical difficulty but do not contribute significantly to the cylinder or wire response.

Once these modifications were incorporated into the model, the TRANSIMM-predicted waveforms closely matched the test results. A sensitivity study then showed that the measured waveforms could be accurately produced by using a minimum of five lumped RLC sections to represent each transmission line. In order to reduce the computer costs, most of the analytic results were then obtained using TRANSIMM with the lumped transmission line model.

2. Analysis Results

The analysis confirmed the test results in showing that the magnitude and waveform of the induced response are very sensitive to the various cylinder terminations: floating, hard-wired, or spark gap. For the open cylinder tests where the cylinder is floating, the results are almost identical to the approximate solutions obtained using a series RLC circuit where C is the series capacitance of the cylinder and capacitor bank. Transmission line effects are not significant here and confirm the test results. For the hard-wired and spark gap tests, however, the quarter-wave resonance dominates the response in many cases. Predicted cylinder current and induced voltage waveforms exhibiting these effects closely match test results when a phase velocity of approximately .8 c is used (c = speed of light).

    a. <u>Cylinder Charging Analysis (Open Cylinder)</u> - TRANSIMM was used to simulate open cylinder tests where the charged 4000 pf capacitor bank is suddenly connected in series with a 48-foot floating cylinder through various

14

inductors to shape the waveform. The predicted cylinder current and voltage waveforms were in most cases very close to those for a simple RLC circuit.

$$I_{CYL}(t) = \frac{V_o}{\omega L} e^{-\alpha t} \sin(\omega t) \tag{1}$$

$$V_{CYL}(t) = \frac{1}{C_c} \int_o^t I_{CYL} dt \tag{2}$$

$$= V_o \frac{C_G}{C_G + C_c} \{1 - \cos(\omega t) - \frac{\alpha}{\omega} \sin(\omega t)\}^{-\alpha t}$$

where

V_o = generator voltage (480 kV)

C_c = cylinder capacitance (284 pf)

C_G = generator capacitance (4000 pf)

C = equivalent series capacitance (265 pf)

L_c = cylinder inductance (8.4 µh)

L_g = external inductance

L = total series inductance

R = series resistance

$\alpha = R/2L$

$\omega^2 = 1/LC - \alpha^2$

Figure 5 shows the TRANSIMM predicted current and voltage waveforms for a simulated open cylinder test with a total inductance of 550 µh and a resistance of 85 ohms. These waveforms are virtually identical to those of the simplified RLC circuit with a frequency of 417 kHz and a damping factor of 8×10^4 sec^{-1}. In this case, the damping is relatively small ($\frac{\alpha}{\omega} \ll 1$) and the cylinder voltage varies as the negative cosine, lagging the current by 90°. These waveforms are consistent with the test data. The predicted induced voltage waveform is illustrated in Figure 6 for the case where a single internal wire is open-circuited at the aperture end. This represents the

15
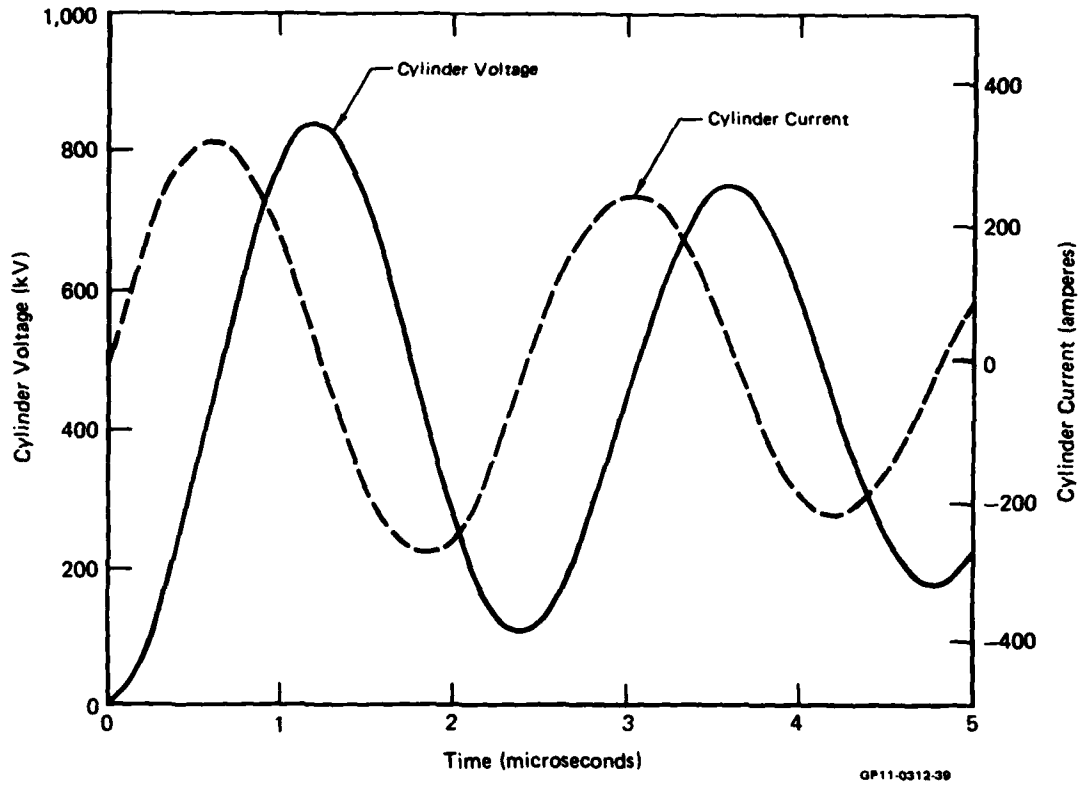
FIGURE 5. TRANSIMM — PREDICTED CYLINDER VOLTAGE AND CURRENT OPEN CYLINDER TEST
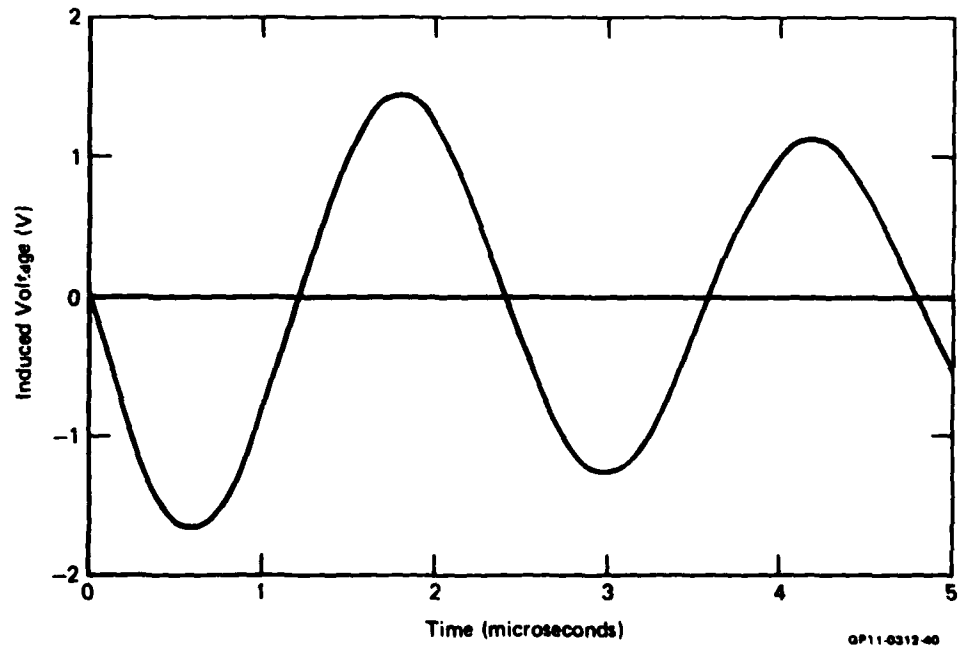
FIGURE 6. TRANSIMM - PREDICTED INDUCED VOLTAGE - OPEN CYLINDER TEST
Interior Wire Open-Circuited Near Aperture

16

effects of capacitive coupling, since inductive coupling is effectively elimi-
nated by the open circuit. The mutual capacitance C_{12}, estimated at .33 pf
(see Appendix B) using a simple electrostatics approximation, was adjusted to
.03 pf so that the magnitude of the predicted voltage, as well as the wave-
shape, matched the test result.

It is seen in Figure 6 that the induced voltage waveform has the same waveform
(except for sign) as the cylinder current. An explanation can be found in the
simple RLC approximation. Taking the derivative of equation (2), it is seen
that the cylinder current is proportional to the time derivative of the
cylinder voltage:

$$\frac{dV_{CYL}}{dt} = \frac{I_{CYL}}{C_c} \tag{3}$$

However, the capacitively-induced current in the wire is also proportional to
the time derivative of the cylinder voltage.

$$I_{INDUCED} = C_{12} \frac{dV_{CYL}}{dt} \tag{4}$$

Combining equations (3) and (4) and assuming a termination $R_2(50\Omega)$ at the other
end of the wire, the induced voltage in the RLC approximation is given by

$$V_{INDUCED} = \frac{R_2 C_{12}}{C_c} I_{CYL} \tag{5}$$

The peak value of the induced voltage is proportional to the peak value of the
cylinder current, obtained from maximizing equation (1)

$$V_{INDUCED_{PEAK}} = V_o \frac{R_2 C_{12}}{C_c} \sqrt{\frac{C}{L}} \ e^{-\{\frac{\alpha}{\omega} \tan^{-1} \frac{\omega}{\alpha}\}} \tag{6}$$

For a mutual capacitance of .03 pf, this corresponds to a peak voltage of 1.7
volts, equal to that predicted by TRANSIMM.

TRANSIMM calculations, run for other values of series inductance, predicted
that the peak induced voltage would be proportional to the peak dV/dt of the
cylinder. Figure 7 plots the peak induced voltage versus peak dV/dt predicted
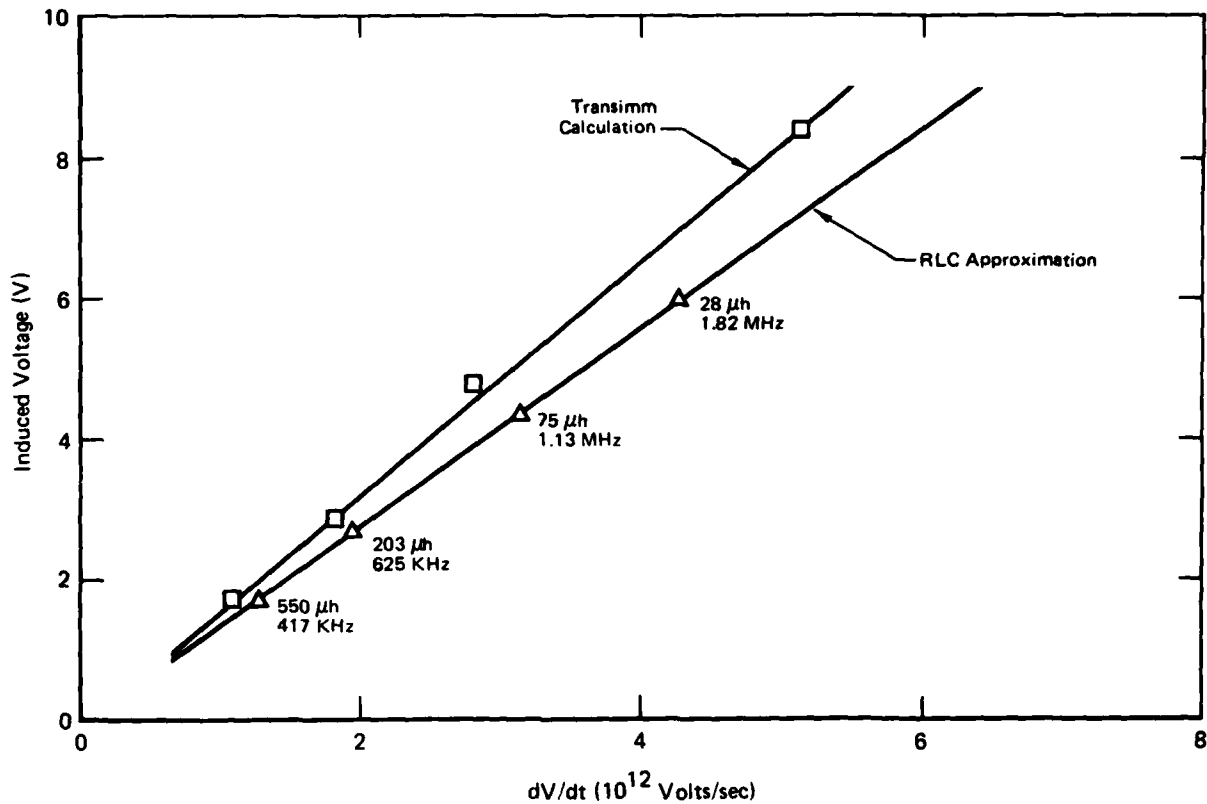
FIGURE 7. INDUCED VOLTAGE VERSUS dV/dt - OPEN CYLINDER CASE
Interior Wire Open-Circuited

by TRANSIMM, for inductances ranging from 28 μh (minimum system inductance) to 550 μh. The relationship is clearly linear. A similar plot of induced voltage versus dV/dt, based on the approximations of equations (3) and (6), is also shown. For high values of total inductance (low frequencies), the two curves are close. For low values of inductance, the curves begin to diverge. Above 1 MHz, the RLC approximation begins to break down, indicating that distributed circuit effects become significant.

If the internal wire is shorted at the aperture, capacitive coupling is effectively shunted out, leaving only magnetic coupling. Figure 8 compares the open circuit and short circuit induced voltage waveforms predicted by TRANSIMM with an external inductance of 550 μh. (The open circuit case is identical to that pictured in Figure 6). The magnetically-coupled induced waveform is a simple damped sinusoid leading the capacitively-induced waveform by approximately 50°.

18
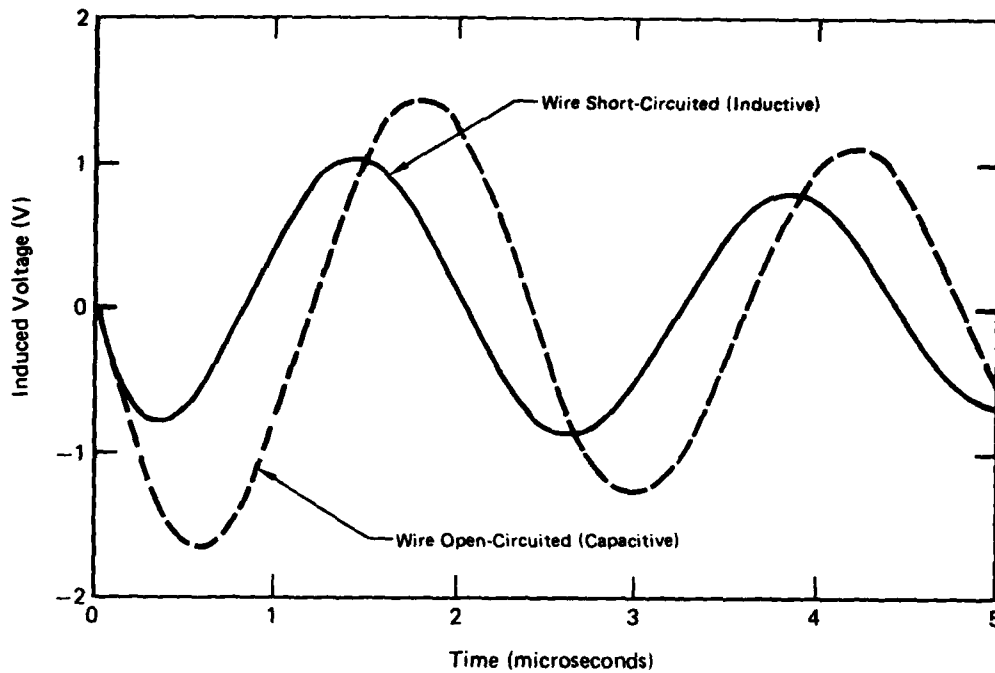
FIGURE 8. COMPARISON OF CAPACITIVE AND INDUCTIVE COUPLING
Open Cylinder Case

This phase shift can be explained as follows. The equivalent electromotive force on the internal wire due to magnetic coupling at the aperture is proportional to the time derivative of the cylinder current

$$EMF = L_{12} \frac{dI_{CYL}}{dt}$$

where L_{12} is the mutual inductance, estimated at 22 μh in Appendix B. Recalling from the simple RLC approximation that the capacitively-induced voltage is proportional to the cylinder current, the inductively-coupled electromotive force leads both the cylinder current and the capacitively-induced voltage by 90°. However, at 417 kHz, the 15.56 μh inductance of the internal wire in series with the 50-ohm termination retards the terminal voltage with respect to the electromotive force by about 40°. The net phase shift is therefore a 50° lead.

   b. <u>Hard-Wired Analysis</u> - It has been shown that distributed effects are not significant in the response of the floating cylinder for either inductive or capacitive coupling for the values modeled. This is no longer the case

19

when the cylinder is hard-wired to ground. Figures 9 and 10 show the TRANSIMM-simulated cylinder current (at the shorted termination) and cylinder voltage (at the aperture) for the hard-wired case, keeping the total inductance at 550 μh. The cylinder response is a damped sinusoid at 108 kHz which corresponds very well to the natural frequency of a series RLC circuit. (For this case the total capacitance C is the 4000 pf generator capacitance, since the cylinder capacitance is shorted out.) The cylinder voltage waveform in Figure 10, on the other hand, shows a high-frequency transient superimposed on the 108 kHz fundamental. The low-frequency component can be thought of as an inductive voltage drop corresponding to $L_c \frac{dI}{dt}$ where L_c is the inductance of the cylinder and its return path.

The magnitude of the low-frequency component is approximately L_c/L or .015 times the generator voltage waveform in the RLC representation. The high-frequency component is a 4-MHz damped waveform that corresponds to a quarter-wave cylinder resonance. The mismatch of a virtually open circuit at the generator end and short circuit at the other end results in reflections that must traverse back and forth twice to regain their original polarity.

Figure 11 depicts the TRANSIMM-simulated induced voltage when the internal wire is open at the aperture. The transmission line resonance (free response of the system) is seen to dominate, while the externally-applied 108-kHz component (forced response) is relatively negligible. The rapid variation of the cylinder voltage, during the first few microseconds after the generator is triggered, is responsible for the high-frequency capacitively-induced transient. Then, as the cylinder voltage settles down to its relatively slow variation at 108 kHz, the amplitude of the induced voltage is relatively small.

The induced voltage, when the internal wire is shorted near the aperture, is shown in Figure 12. The large external inductance at the generator end prevents rapid variations in the cylinder current, which is a slow damped sinusoid. Since the magnetically-induced voltage is proportional to the derivative of this current, it has a slow damped cosine form without significant free response components. This is consistent with hard-wired test results. The measured induced voltage exhibits a fast free response when the wire is open and slow forced response when the wire is shorted.
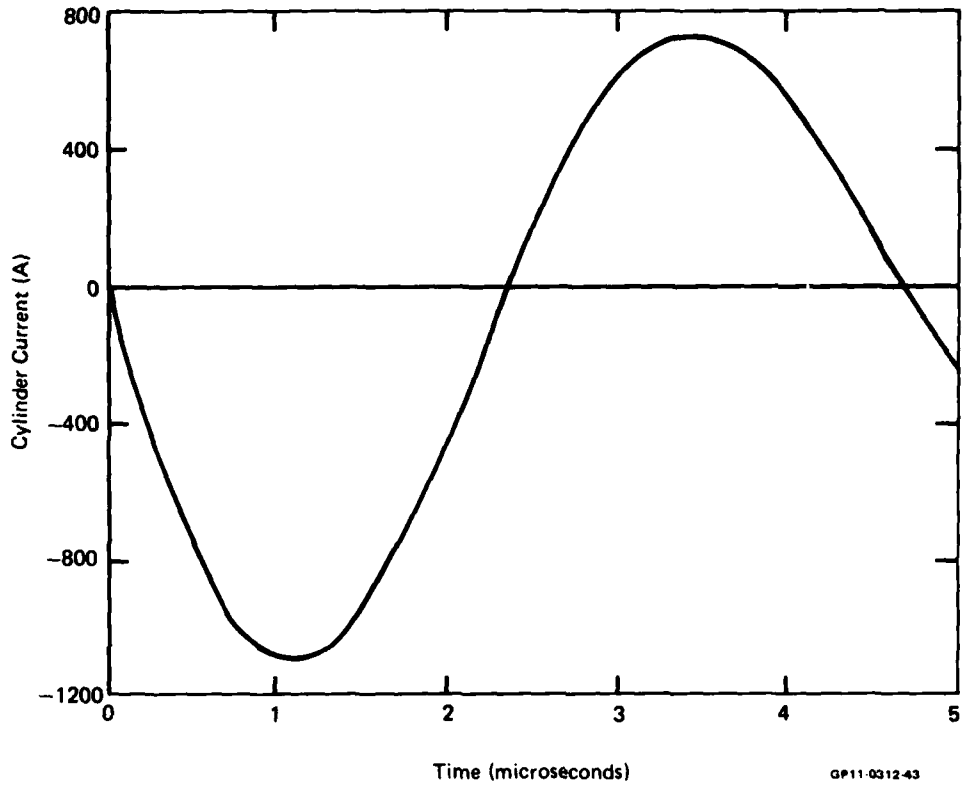
FIGURE 9. TRANSIMM - PREDICTED CYLINDER CURRENT
Hard-Wired Output
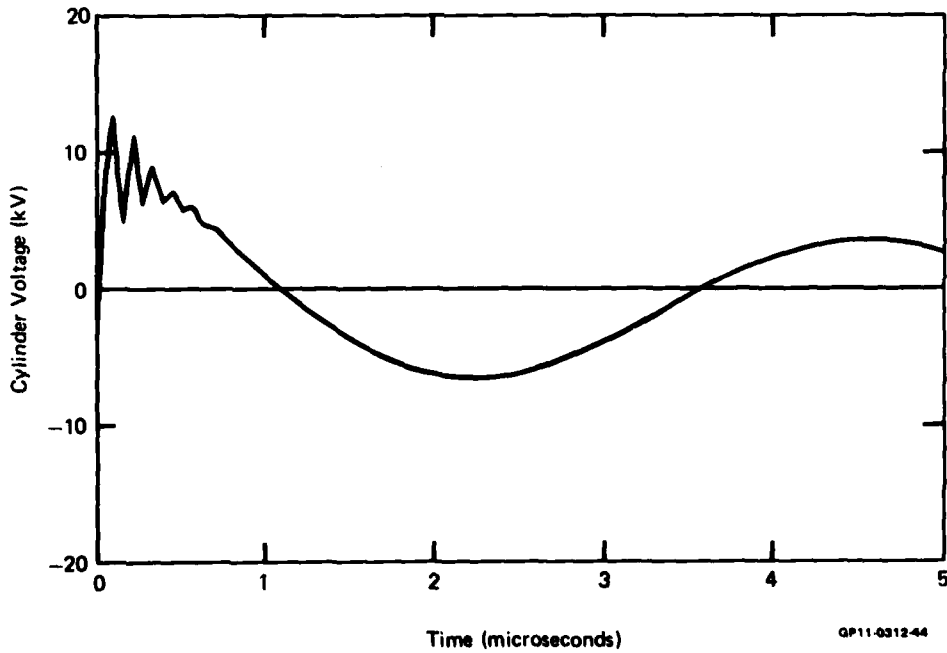
FIGURE 10. TRANSIMM - PREDICTED CYLINDER VOLTAGE AT APERTURE
Hard-Wired Output

21
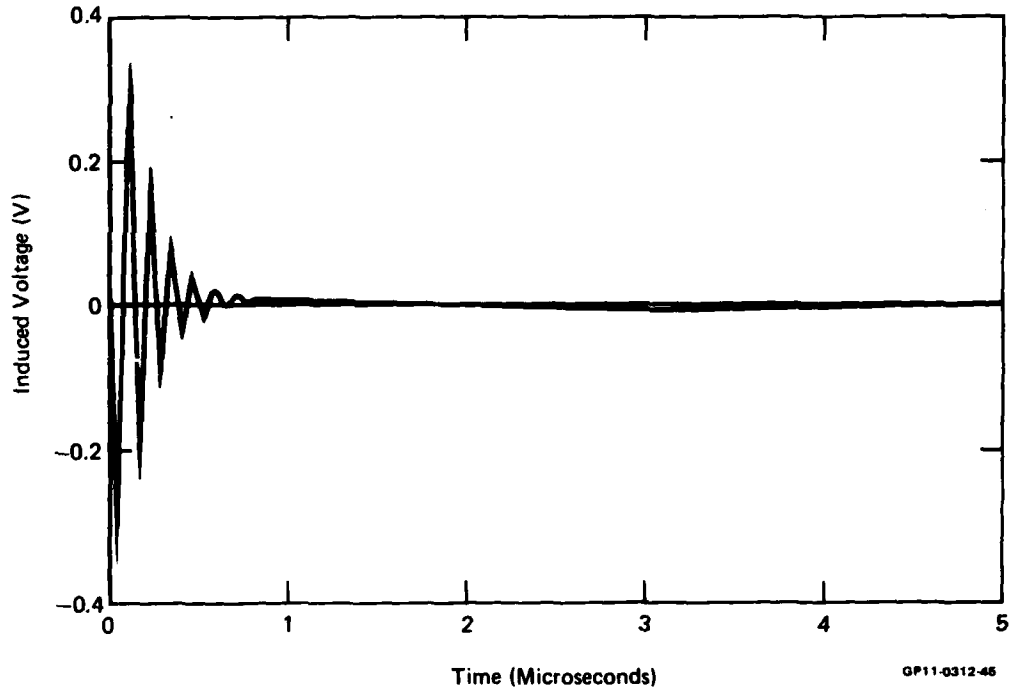
FIGURE 11. TRANSIMM - PREDICTED INDUCED VOLTAGE FOR HARD-WIRED OUTPUT
Interior Wire Open - Circuited Near Aperture
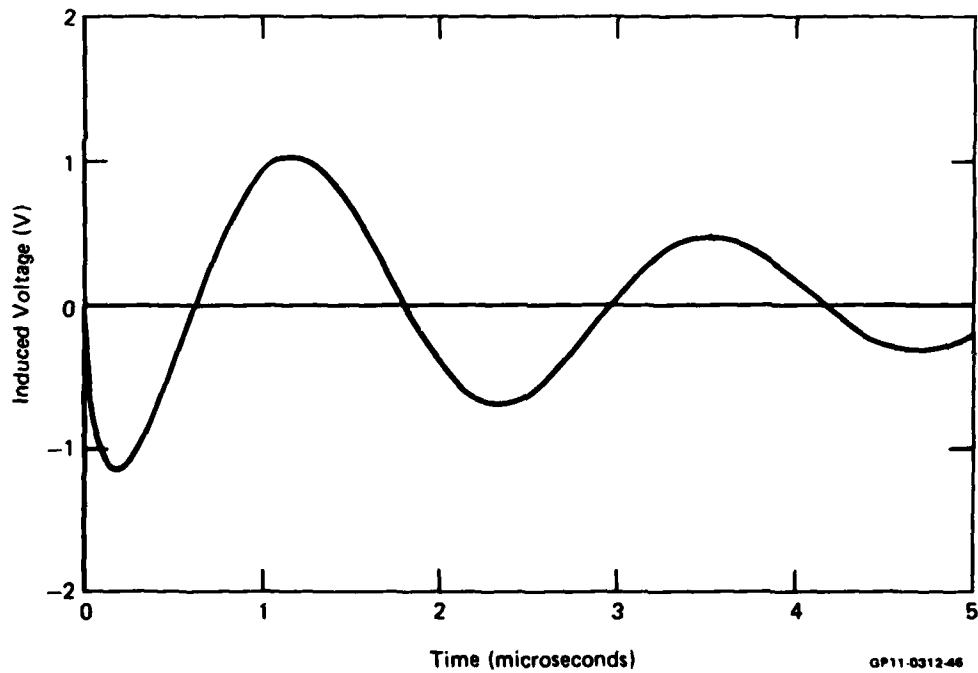
FIGURE 12. TRANSIMM - PREDICTED INDUCED VOLTAGE FOR HARD-WIRED OUTPUT
Interior Wire Shorted Near Aperture

22

Figure 13 is a summary of the TRANSIMM-predicted results for the various cylinder/internal wire configurations. When the cylinder is floating, the capacitively-coupled (open wire) peak voltage exceeds the magnetically-coupled (shorted wire) peak voltage. The reverse is true when the cylinder is hard-wired. The capacitively coupled voltage is still significant, however, despite the fact that the cylinder is hard-wired to ground.

L_{total} = 550 μh
C_{total} = 265 pf
R_{total} = 85 ohms
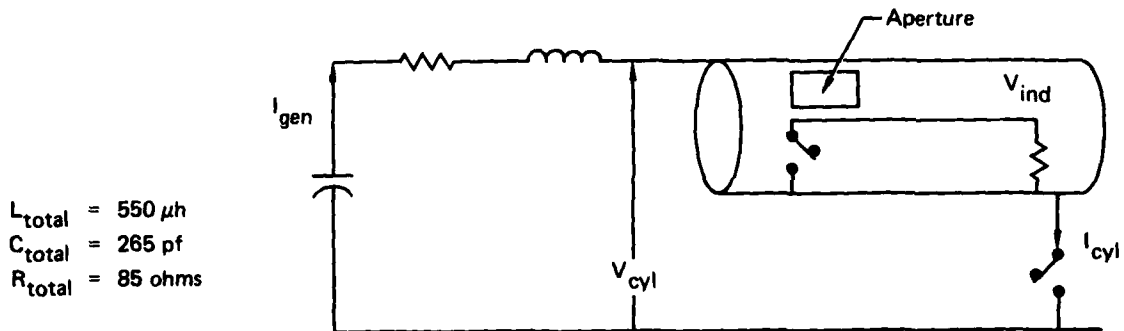
	A Cylinder Open Wire Open	B Cylinder Open Wire Shorted	C Cylinder Shorted Wire Open	D Cylinder Shorted Wire Shorted
I_{gen} (amps)	320	320	1,080	1,080
I_{cyl} (amps)	0	0	1,080	1,080
V_{cyl} (volts)	840,000	840,000	14,000	14,000
V_{ind} (volts)	1.7	1.0	0.33	1.2

QP11-0312-47

FIGURE 13. SPICE SIMULATION FOR VARIOUS CONFIGURATIONS
Peak Values

c. <u>Spark Gap Analysis</u> - The case where the cylinder is permitted to arc to ground across a spark gap was also simulated using TRANSIMM. The arc is modeled as a time-varying resistance, very large before breakdown and very small after breakdown. If the arc resistance changes abruptly, the quarter-wave oscillations in the predicted current and voltage do not damp out as fast as the test results indicate they should. If, instead, the arc resistance is allowed to decay gradually in steps over a few hundred nanoseconds (see Appendix B), the predicted waveforms correspond closely with test results. A similar result can be obtained alternatively by putting dissipation into the transmission line model (such as corona and radiation loss), but the magnitude of the dissipation required to match test results cannot be accounted for physically. It appears that most of the dissipation is in the arc.

The arc breakdown forces the voltage at the spark gap end of the cylinder to change rapidly (no more than a few tens of nanoseconds) from nearly a million volts to zero, initiating a large free response component. Even the cylinder current at that end exhibits strong high-frequency oscillations. Figure 14 shows the measured arc current for a spark gap test, with a total inductance of 280 μh and resistance of 240 ohms. The current remains negligible from the time when the generator is triggered (t = 0) until the time when the spark gap fires (t = 1 μs). It then exhibits a strong 4-MHz free response with a peak current of 1500 amps, superimposed on the slower 140 kHz forced response, with a peak amplitude of about 500 amps. The free response damps out quickly, leaving only the forced response for times greater than 2 μs. Figure 14 shows the TRANSIMM-predicted arc current, closely matching the test result. For this case, the simulated arc resistance remains at a million ohms until break-down, after which it decays to one ohm in nanoseconds. The measured and computed induced voltage waveforms are presented in Figure 15 for the case where the internal wire is open-circuited. The capacitively-induced voltage exhibits a 4-MHz free response with higher frequency ripples, corresponding to the rapid oscillations in cylinder voltage excited at breakdown. After two μs, the response is negligible. The simulated waveform corresponds very closely with the test result.

MEASURED   CALCULATED
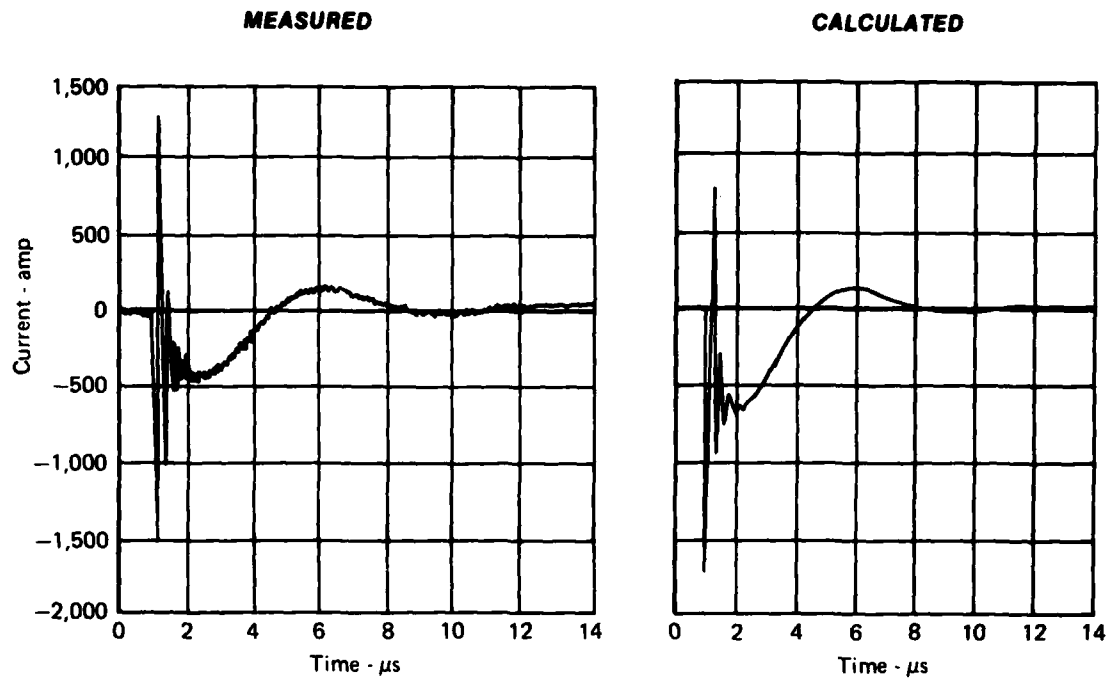
FIGURE 14. CYLINDER CURRENT

MEASURED   CALCULATED
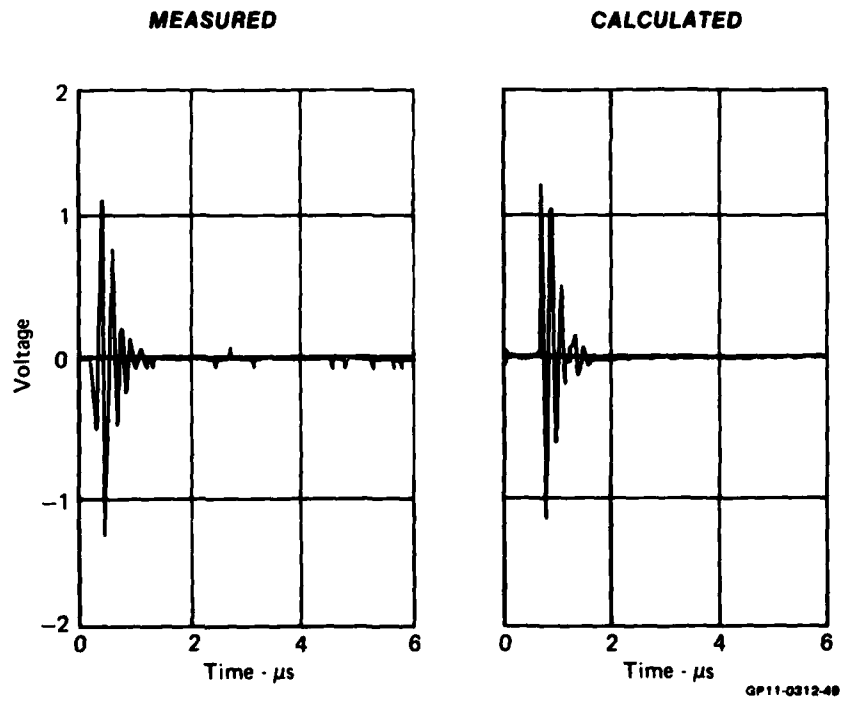
FIGURE 15. INDUCED VOLTAGE

25

When the internal wire is shorted near the aperture, test results indicate
that the induced voltage measured exhibits a predominantly low-frequency
forced response, with a very small free response riding on it. Similar
results are obtained using TRANSIMM. The large external inductance prevents
rapid oscillations in the cylinder current at the aperture, which is smoother
than the current at the arc, and prevents the magnetically-induced voltage
from varying too rapidly. It also isolates the cylinder from the generator at
high frequencies, permitting rapid variation of the cylinder voltage, the
source of capacitive coupling.

TRANSIMM was used to determine the sensitivity of the induced voltage to test
parameters. For a fixed aperture location, the most important parameters were
found to be system dissipation, cylinder characteristic impedance, and cylinder
length. The dissipation determines how fast the free response dies out. The
characteristic impedance determines the magnitude of the cylinder current free
response: lower values of impedance result in a larger free response.
Finally, the cylinder length determines the fundamental quarter-wave resonance
of the free response. Variation of the aperture location could also have a
significant effect on the amplitude and type of coupling.

3. Analysis Capabilities

The results of the analysis closely match test results and show the role that
transmission line resonances play in the overall response. The type of mis-
match at the cylinder termination largely determines the nature of the
response. The TRANSIMM model, having proved itself for the cylinder tests,
can be extended to analyze other test configurations. Coordinating analysis
with experimentation, the model can be further refined in an iterative
fashion. With suitable definition of parameters, it can also be used to
model aircraft wiring responses, predict the relationship between the labora-
tory tests and natural lightning, and model the surge impedance of the channel
and the mismatch at the aircraft attach points.

SECTION IV
EXPERIMENTAL PROGRAM DESCRIPTION

The experimental program was planned and conducted in two phases or tasks. Task 2 included an extensive series of comparative tests on a long aluminum cylinder with internal wiring that was configured to be amenable to analytical modeling. Task 3 included a similar test series on three flight control circuits of the Air Force YF-16 aircraft at Wright-Patterson Air Force Base. Nearly identical test techniques, test equipment, and instrumentation were employed on the cylinder and aircraft tests.

Three distinct lightning simulation test conditions were investigated and are discussed in the remainder of the report. This section describes the cylinder and aircraft test configurations used in all experiments. Section V describes the results of high-voltage charging tests on the electrically-isolated test articles to simulate stepped-leader attachment, and Section VI presents results and comparisons of the shock-excitation and current pulse test techniques on the two test articles.

To provide a more direct comparison of the cylinder and aircraft data, a number of test constraints were incorporated to limit the number of parameters that would be varied in the experimental program. These test limitations are listed below.

(1) Exactly the same test equipment was used in both the cylinder and YF-16 aircraft tests. This equipment includes the Marx generator system, sensors, fiber optic data links, and data acquisition system.

(2) An underdamped sinusoidal current waveform was used exclusively.

(3) Since high impedance flight-control circuits were to be monitored in the aircraft, three different open circuit wire configurations were used in the cylinder tests.

(4) The test cylinder was extended to a length of 48 feet and the interior wire pairs were made 40 feet long to simulate the YF-16 fuselage and maximum circuit lengths, respectively.

(5) A single aperture (11.25"x11.25") was used as the primary coupling source in the cylinder tests. The electromagnetic sources (apertures) on the aircraft were not as clearly defined.

(6) Similar test sequences were run on the cylinder and the aircraft. Only one configuration parameter change was made at a time.

(7) The test articles were wired directly to the generator output through waveshaping components. No input arc testing was done to simulate the electric field change before stepped-leader attachment, since the induced voltages produced by these field changes are generally less than those which occur during charging and discharging of the test article.

1. Cylinder Test Configurations

Figures 16 and 17 show a schematic of the high-voltage laboratory setup and a picture of the cylinder configured with a coaxial wire return. The test cylinder was screened from the generator by a grounded aluminum electrostatic shield. The cylinder was 14.7 inches in diameter and 48 feet long with an internal wire pair strung on axis. The interior wires were 40 feet long (starting 8 feet from the attach point end and running the length of the cylinder). Data were gathered by sensor and transmitted via analog fiber optic links to the recording instrumentation in the screen room. The principal test components used for both cylinder and YF-16 testing are described in Appendix C, while the cylinder and internal wire configurations are described in the following paragraphs.

The cylinder was constructed using typical airframe construction techniques. It was made in sections from rolled 4'x8' sheets of 0.063" 6061-T6 aluminum to give a 14.7-inch diameter. The seam was fastened using rivets on 6-inch centers. Each cylinder section has three ports (5.25"x5.25", 7.25"x7.25", and
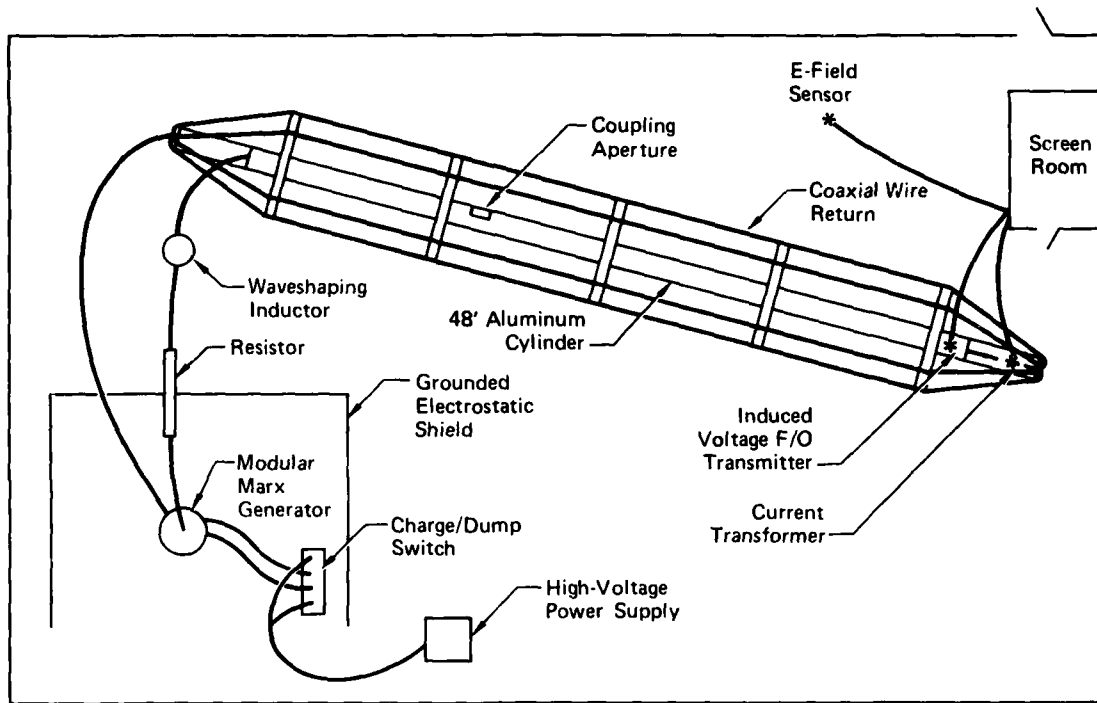
FIGURE 16. SCHEMATIC OF HIGH-VOLTAGE LABORATORY SETUP
Cylinder With Coaxial Wire Return
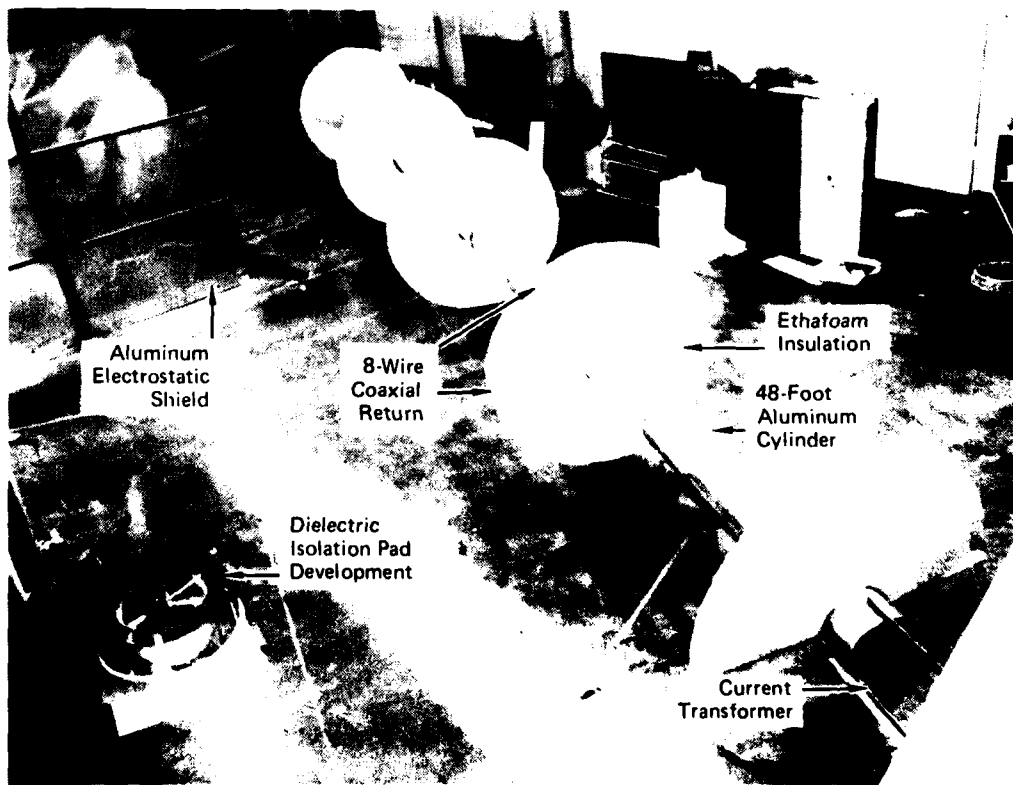
FIGURE 17. LABORATORY LAYOUT - CYLINDER WITH COAXIAL WIRE RETURN

29

11.25"x11.25") which could be covered with a flush-mounted metal plate using 8-32 screws on 2-inch centers. An insert extension was incorporated in one end of each cylinder. The extension and the mating cylinder end were matched drilled around their circumference so that the six cylinders could be connected to yield the 48-foot length. Circular aluminum disks were used as end caps. For this test program, a third disk was inserted after the first section to simulate an aircraft bulkhead. This disk segmented the cylinder into 8-foot and 40-foot interval sections. The test wires were run on axis down the length of the 40-foot section. Only one (11.25"x11.25") port 8-1/2 inches from the simulated bulkhead was left uncovered to provide aperture coupling to the interior wires.

Two test configurations were used. In one case, the cylinder was supported on dielectric tripods approximately 5 feet above an 8-foot-wide aluminum ground plane which ran the length of the cylinder. This configuration was extremely flexible because output wires can readily be incorporated to hard-wire, arc, or isolate the cylinder from the ground return. In the second configuration, an eight-wire coaxial return, as shown in Figure 17, was used. The eight 12-gauge wires were symmetrically distributed about the cylinder at a distance of 2-1/2 feet. The return wires were periodically supported on ethafoam semi-circles to maintain their spacing. This configuration provides a more "free-field" current distribution; however, it limits the potential difference which can be applied between the cylinder and return wires. During preliminary testing, substantial standing waves were excited on the cylinder to coaxial return wire transmission line when the output was shorted either by a hard-wire or an arc. Output resistors were added after the spark gap to approximately terminate the transmission line in its characteristic impedance so that reflections would be minimized.

For each test configuration, three different interior wire circuits were tested. Since the tests of the YF-16 were to be done on high-impedance differential flight control circuits, simple high impedance circuits were selected for testing on the cylinder. The three interior circuits were:

(1) Single, 22-gauge wire: isolated from the cylinder at the aperture end (end nearest the generator) and connected to the cylinder through

a 50Ω terminator at the output end. Induced voltages were measured across the 50Ω terminator. The wire-to-cylinder characteristic impedance was ≈380 ohms.

(2) Two-wire pairs: two 22-gauge wires separated by 3 inches with dielectric spacers. The wires were isolated from each other and the cylinder at the aperture end. Each wire was connected to the output end of the cylinder by a 50Ω terminator. Differential induced measurements were made across the 100Ω line-to-line resistance. The wire-to-wire characteristic impedance was 325 ohms.

(3) 300Ω twin-lead: standard television antenna wire. The same termination and measurement scheme as the two-wire pair was used.

Only one wire circuit was strung on the axis of the cylinder at a time. The wires were periodically supported by ethafoam semicircles to maintain their position on axis. Induced voltage measurements were made by a differential, high-bandwidth F/O transmitter. Attenuation was adjusted by adding standard Tektronix attenuators designed for use with the 50Ω terminators.

2. YF-16 Test Configuration

The YF-16 tests were conducted at the Atmospheric Electricity Hazards Group Laboratory in Building 13-Area C at Wright-Patterson Air Force Base, Ohio. Figure 18 is a sketch of the experimental layout, and Figures 19 through 21 are photographs of the side, nose, and tail areas, respectively.

The test aircraft was YF-16 prototype number 1 (USAF serial number 01-1567) built by General Dynamics Corporation of Fort Worth, Texas. The aircraft was brought to Dayton in December 1978 inside a C-5A and reconstructed in January 1979. The aircraft has undergone substantial lightning testing as a test bed aircraft since its arrival at the Atmospheric Electrical Hazards Group Laboratory. Laboratory personnel have subjected the aircraft to voltages up to a million volts and currents up to 30 kA. The aircraft has a fly-by-wire flight control system which utilizes computer control of all moving surfaces. The aircraft has three redundant flight control circuits with no mechanical backup.

* E-Field Sensor

RFI Enclosure

Power Supply

Current Transformer
Output Spark Gap

F/O Cable

Charge/Dump Switch

YF-16, No. 1

Sheet Coxial Return

Waveshaping Component

Electrostatic Shield

Modular Marx Generator
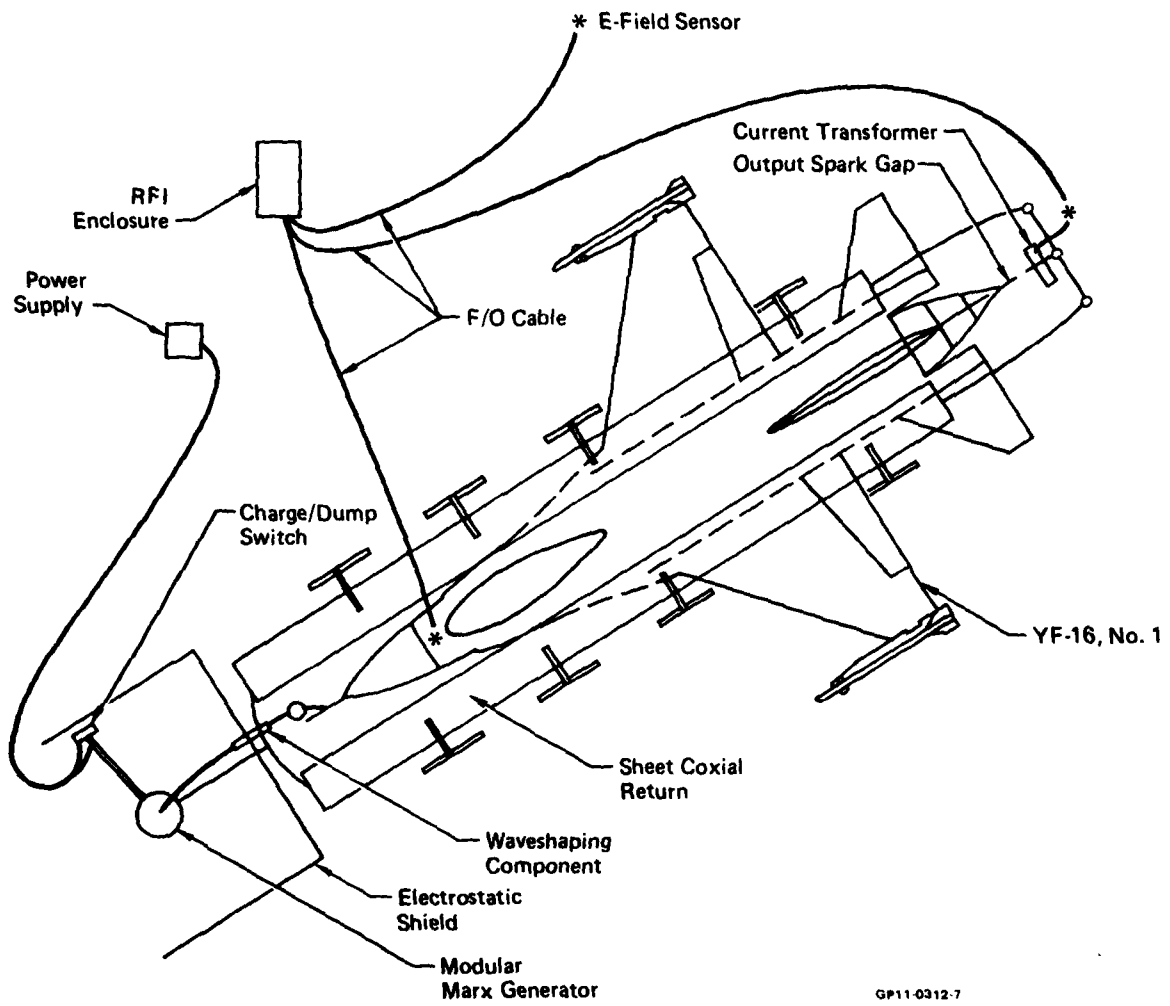
GP11-0312-7

FIGURE 18. YF-16 EXPERIMENTAL TEST CONFIGURATION

32
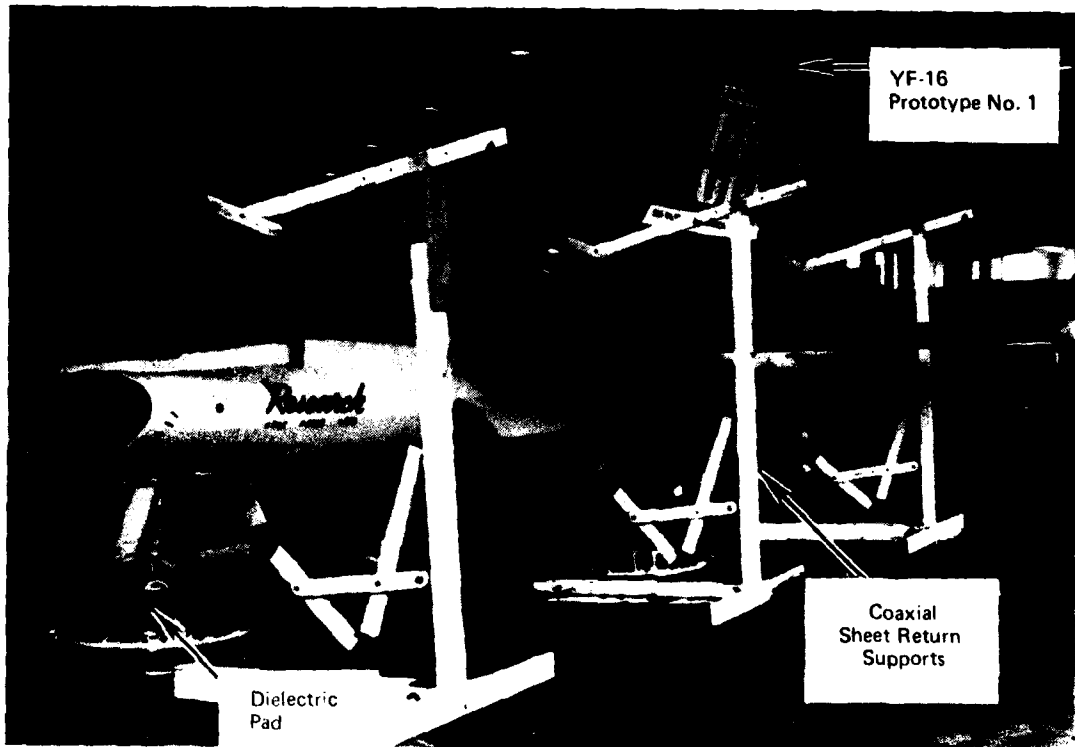
FIGURE 19. YF-16 TEST ARRANGEMENT - SIDE VIEW
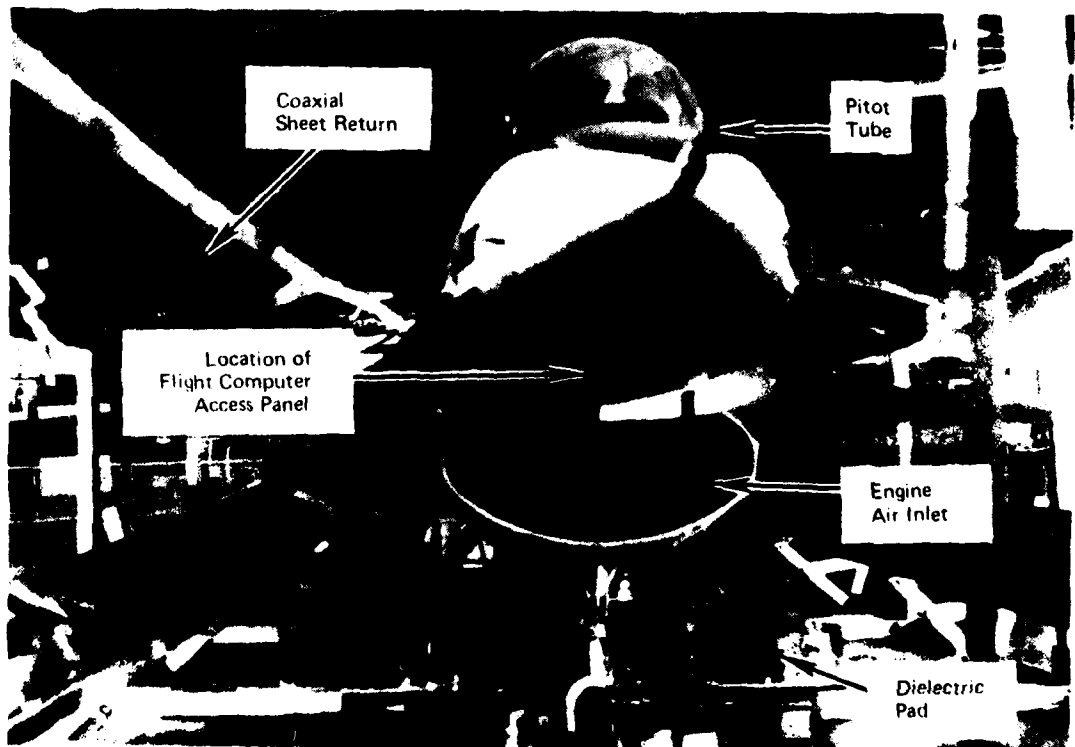
FIGURE 20. YF-16 TEST ARRANGEMENT - NOSE VIEW

Engine
Exhaust Duct

Wire to
Return Sheet

Either Arc or
Hard-Wire Connection

Current
Transformer
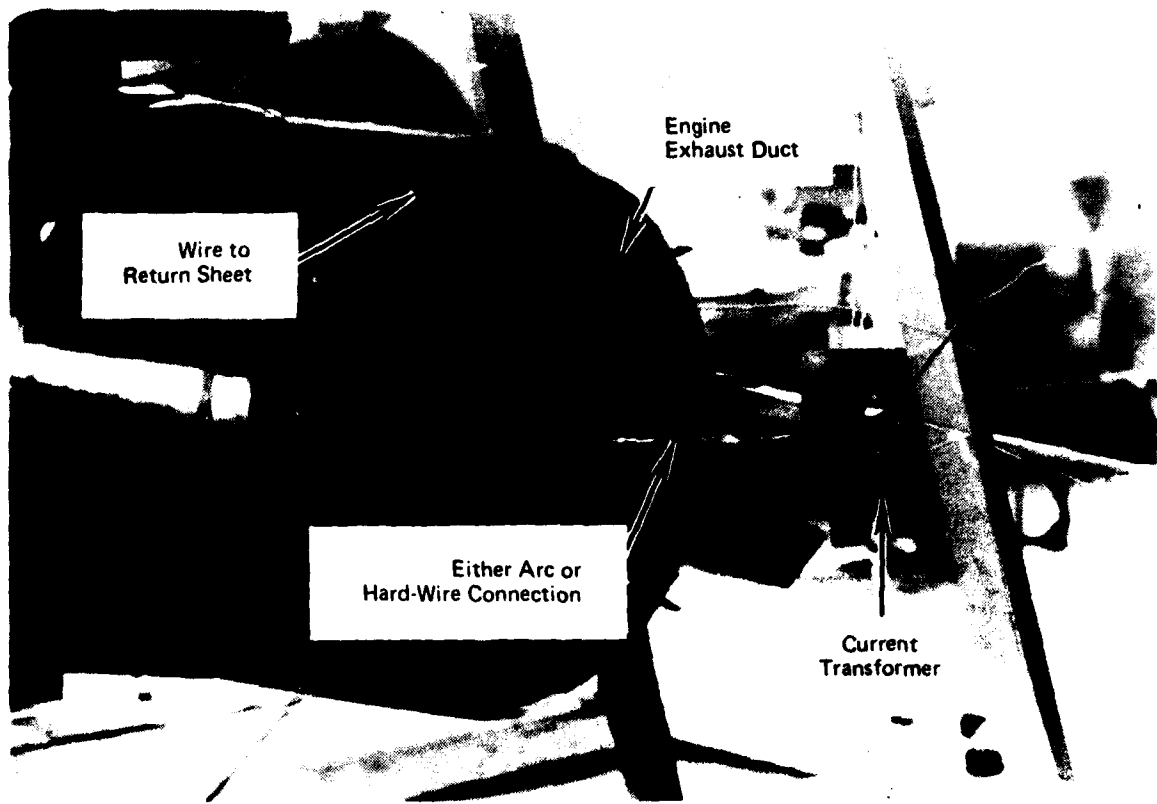
GP11-0312-10

FIGURE 21. YF-16 TEST ARRANGEMENT - TAIL VIEW

For these lightning simulation tests, the aircraft was configured with a four-sheet coaxial return, as shown in the photographs. The aircraft was positioned on specially designed dielectric pads to isolate its wheels from ground potential. The aircraft faced the high-voltage generator which was enclosed on three sides by an electrostatic shield consisting of overlapping five-mil aluminum foil supported on a wooden frame. The generator was hard-wired to aircraft's pitot tube through a 20Ω graphite resistor and inductors for wave-shaping. At the tail, the connection to the return sheets was made by four 12-gauge wires configured to be either electrically shorted or to include a series spark gap. System current was measured by a Pearson current transformer on the return sheet side of the spark gap. All measurements were converted to analog F/O signals at the sensor and routed to an RFI shielded enclosure for processing.

All induced voltage measurements were made on flight control circuits with no power applied. Access to the circuits was through a fuselage panel located on the underside of the nose approximately halfway between the radome and the engine air inlet. Data were taken near the input connector to the flight computer by cutting each wire and splicing in a breakout measurement wire in a crimped connector. All induced voltages were measured differentially across a flight control circuit using a 50Ω terminator and attenuators as appropriate. Only one circuit was monitored at a time.

Initially tests were conducted on each of three redundant yaw circuits. These circuits gave very similar results, as expected. To obtain more diversified data, tests were conducted on the yaw, left flaperon, and right flaperon circuits of Branch C. These circuits comprise one of the four redundant branches and were used for all further testing. The circuit identification and measured resistance values are shown in Table 1.

TABLE 1 - RESISTANCE OF MONITORED CIRCUITS

Circuit	Branch	Flight Computer Connection	Pins	Pin-to-Frame Resistance (Ω)	Pin-to-Pin Resistance (Ω)
Yaw Servo	C	J1003	42	100	82
			43	182	
Right Flaperon Servo	C	J1003	37	476	476
			38	0	
Left Flaperon Servo	C	J1003	52	181	81
			53	100	

GP11-0312-11

SECTION V
CHARGING TRANSIENTS

The experimental program studied three distinct lightning simulation conditions for both the cylinder and the YF-16. Section VI describes the results of the current pulse technique and the vehicle discharge portion of the shock-excitation tests which simulate the return stroke conditions. This section describes the results of shock-excitation high-voltage charging of the test article which simulates, or at least is analogous to, the traditional view of stepped-leader attachment.

When a stepped-leader attaches to an aircraft, the plane is quickly charged to a high potential by displacement currents that flow along the fuselage. A similar process occurs in the laboratory if the output of a high-voltage generator is rapidly switched to a test article that is electrically isolated from ground potential. When the generator output is switched, displacement currents flow to charge the test article-to-ground capacitance to the output voltage of the generator. The transients induced on interior wires by the displacement currents should be qualitatively representative of the induced transients produced by stepped-leader attachment. Since virtually no data exist on the effects of an actual stepped-leader attachment, the quantitative accuracy of the simulation cannot be determined; however, the isolated test article does permit the study of the vehicle response to the particular charging transients used. As data become available from flight programs, the charging transient can be modified, if necessary, to better approximate the natural conditions.

1. Cylinder Charging Tests (Open Cylinder)

The cylinder charging tests were conducted with the cylinder supported 58 inches above an 8-foot-wide aluminum ground plane. One end of the cylinder was connected through an inductor and resistor to the high-voltage generator. The other end was left open-circuited. The rate of charging the cylinder was varied by changing the input inductance. The generator charge voltage was 480 kV.

This test configuration can be simply modeled for the low-frequency charging effects as a series RLC circuit with two capacitors, as shown in Figure 22. The generator capacitance, C_G, and the cylinder capacitance, C_c, are equivalent to the single capacitor given by $C = \frac{C_G \times C_c}{C_G + C_c}$. For the underdamped condition, this circuit has the familiar damped sinusoid current response discussed in Section III 2.a and repeated below with some other useful relationships.

$$I_{CYL}(t) = \frac{V_o}{\omega L} e^{-\alpha t} \sin(\omega t) \tag{7}$$

$$\dot{I}_{CYL} = \frac{d\ I_{CYL}}{dt} = \frac{V_o}{\omega L} \{\omega\cos(\omega t) - \alpha \sin(\omega t)\}e^{-\alpha t}$$

$$= \frac{V_o}{L} \text{ at time } t = 0$$

$$V_{CYL}(t) = \frac{1}{C_c}\int_0^t I_{CYL}\ dt \tag{8}$$

$$= \frac{V_o C_G}{C_c + C_G} \{1 - \cos(\omega t) - \frac{\alpha}{\omega} \sin(\omega t)\}\ e^{-\alpha t}$$

$$\dot{V}_{CYL} = \frac{d\ V_{CYL}}{dt} = \frac{I_{CYL}}{C_c} = \frac{V_o\ \sqrt{C}}{\sqrt{C}\ C_c} e^{-\alpha t} \sin(\omega t) \tag{9}$$

These expressions show that both $\dot{V}_{CYL}$ and $\dot{I}_{CYL}$ are varied as the inductance L is changed. $\dot{V}_{CYL}$ varies as a damped sinusoid proportional to $1/L$, and $\dot{I}_{CYL}$ varies as $1/L$ for small t. The voltage on the cylinder for two different system inductances is shown in Figure 23. Note that the voltage rises sharply from zero at a rate determined by the amount of inductance, L, in the charging line. Neglecting the slow self-decay of the generator, the voltage oscillates about the steady-state generator output level. The oscillations damp out more quickly for lower inductances since $\alpha = \frac{R}{2L}$ is larger.

Each open-ended interior wire circuit was tested for three system inductances which were achieved by adding coils between the generator and the cylinder. For the three system inductances, typical data traces for the cylinder voltage (as measured with the E-field sensor) are shown in Figure 24, and their

38
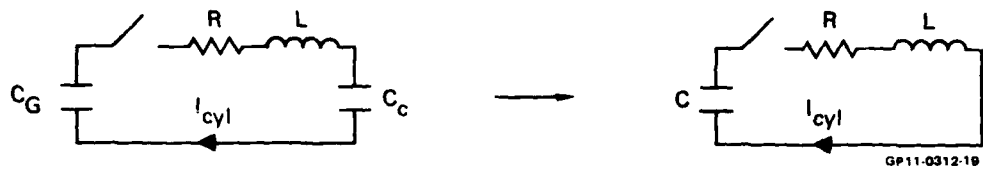
FIGURE 22. EQUIVALENT CIRCUIT FOR OPEN CYLINDER CASE
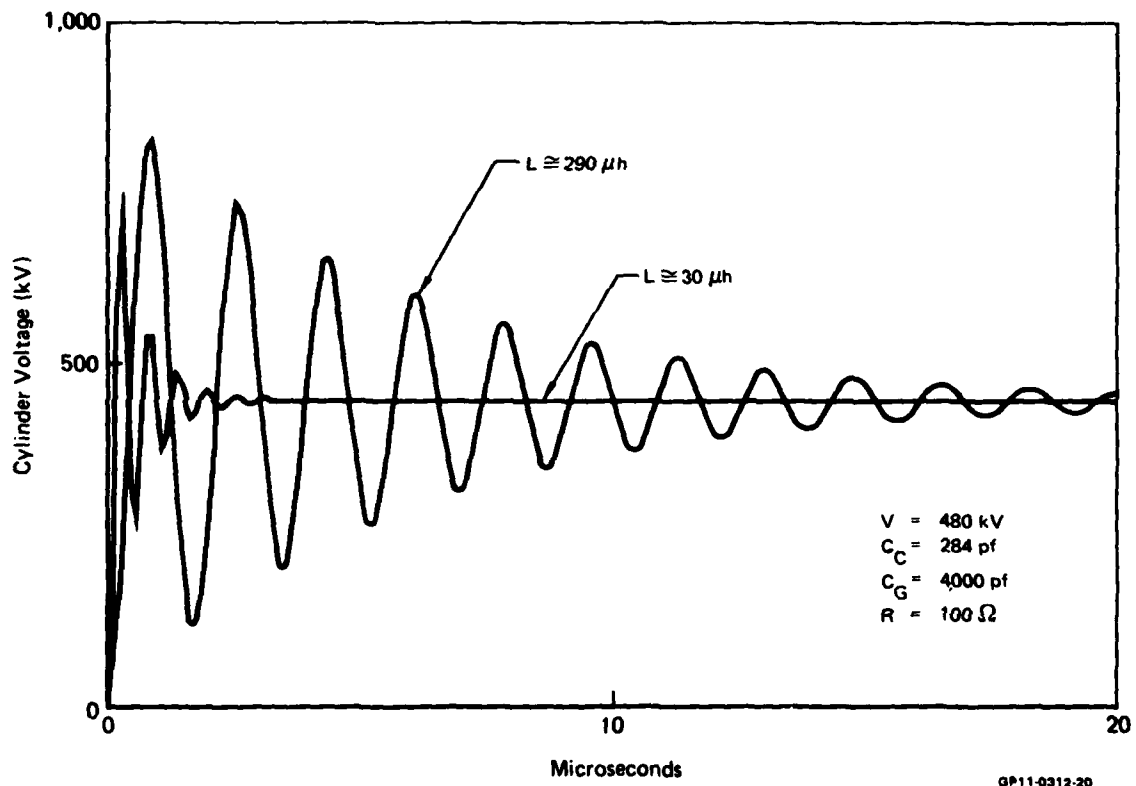
FIGURE 23. OPEN CYLINDER VOLTAGE

39
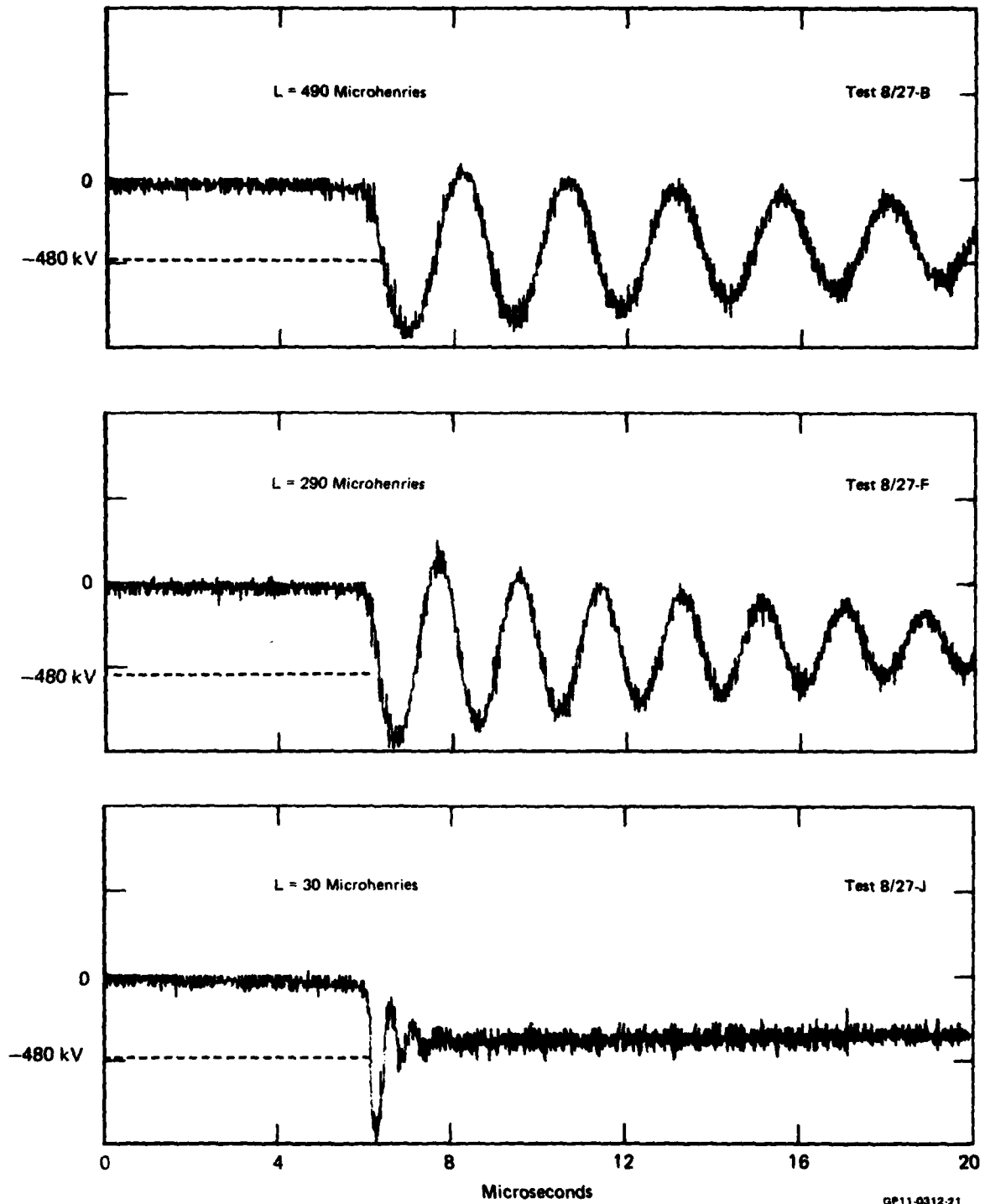
FIGURE 24. CYLINDER VOLTAGE VERSUS CHARGING INDUCTANCE
FOR THE OPEN CYLINDER CASE

40

resulting induced voltages on the high impedance single wire circuit are shown in Figure 25. The E-field sensor is a noncontacting spherical dipole antenna whose output is proportional to the E-field at the sensor. The voltage on the cylinder has the same waveshape as the field measured at the E-field sensor, and the relative magnitude is inferred by comparison to the peak calculated value.

Several important conclusions are derived from the data.

(1)   The cylinder voltage traces are similar to the RLC-modeled curves in Figure 23. The agreement of the tests with theory is shown in Table 2. The measured resonant frequency is approximately ten percent below the calculated value using the theoretical cylinder capacitance and the measured system inductance for the hard-wired output configuration. This deviation is primarily attributed to an increased cylinder-to-ground capacitance due to either (a) the close proximity of the generator's electrostatic shield and laboratory wall or (b) the presence of a corona sheath around the cylinder. Photographs taken in a darkened room during previous cylinder test programs show extensive streamering from the end of the cylinder.

TABLE 2. CIRCUIT ELECTRICAL PARAMETERS FOR CYLINDER TESTS

$L(\mu h)^*$	Theoretical** C_c (pf)	C_G (pf)	Expected f(KHz)	Measured f(KHz)
493	284	4,000	440	417
291	284	4,000	572	534
$\approx$ 30	284	4,000	1,785	1,727

*   L as calculated from hard-wire tests   GP11-0312-24

**$C_c = \dfrac{\ell \cdot 2\pi\epsilon}{\ell n\,(2h/r)}$ for a cylinder over an infinite ground plane

41
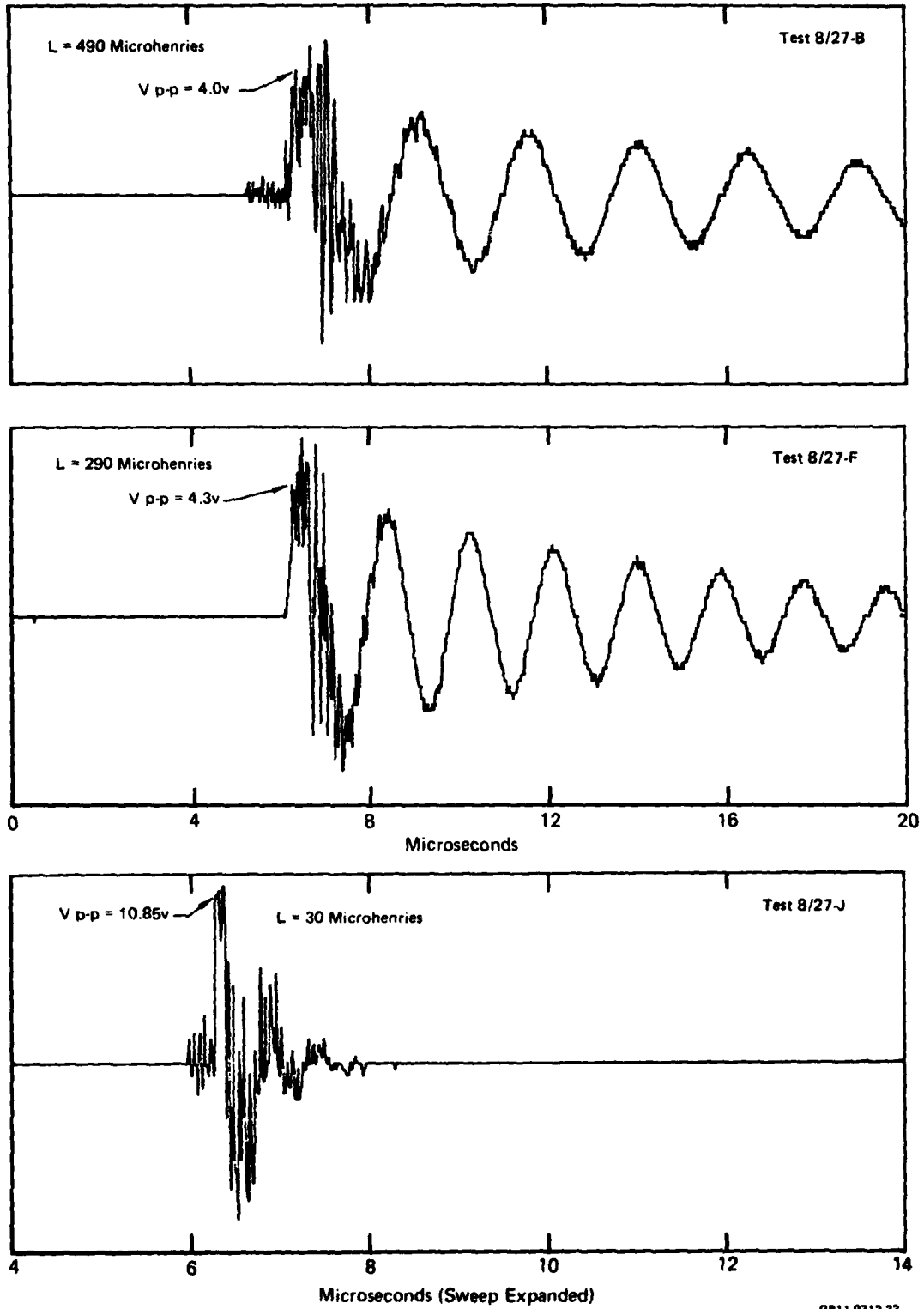
FIGURE 25. INDUCED VOLTAGE ON SINGLE WIRE (OPEN CIRCUIT) FOR VARIOUS
CHARGING RATES (LINE INDUCTANCES) FOR OPEN CYLINDER CASE

42

(2) Ignoring the early high-frequency oscillations, the induced voltage
     waveforms in Figure 25 exhibit a damped sinusoidal waveshape that is
     in phase with the displacement current. From equation (9), $\dot{V}_{CYL}$ is
     also proportional to the displacement current. Therefore, the induced
     voltage varies like d V_{CYL}/dt which is consistent with the analytical
     finding that capacitive coupling is dominant for high-impedance cir-
     cuits. There is no evidence of inductive (d I_{CYL}/dt) coupling which
     would have a cosine form near t = 0.

(3) The peak induced voltage (neglecting the high-frequency oscillations)
     is plotted in Figure 26 against the RLC-calculated $\dot{V}$ maximum for each
     of the three interior circuits. The data scatter is minimal and
     verifies the linear relationship between the induced voltage (V_I) and
     the time rate of change of the cylinder voltage (d V_{CYL}/dt) as the
     system inductance is varied. Therefore, capacitive coupling is
     apparently the dominant coupling mechanism for the high impedance
     circuits that were tested. This agrees with the analytical results
     predicted by TRANSIMM.

(4) Figure 27 shows an induced voltage trace and its fast Fourier trans-
     form (FFT) plotted on a normalized linear scale. The trace itself
     shows that the induced voltage is modulated by higher frequency com-
     ponents during the first cycle. The FFT frequencies at 5.7 MHz and
     16.8 MHz closely correlate to the quarter and three-quarter-wave-
     length resonance of the 40-foot-long interior circuit which is open
     at the aperture end and has a 50Ω impedance at the other end. The
     small 9.5 MHz resonance similarly relates to the half-wavelength
     resonance of the open 48-foot-long cylinder which is coupled to the
     interior wire. In both cases, a signal velocity of 92 percent the
     speed of light is required to match the data. These characteristic
     resonances were also observed for the other interior circuits. The
     presence of the transmission line oscillations indicates that the
     forced response of the wire due to d V_{CYL}/dt coupling can excite the
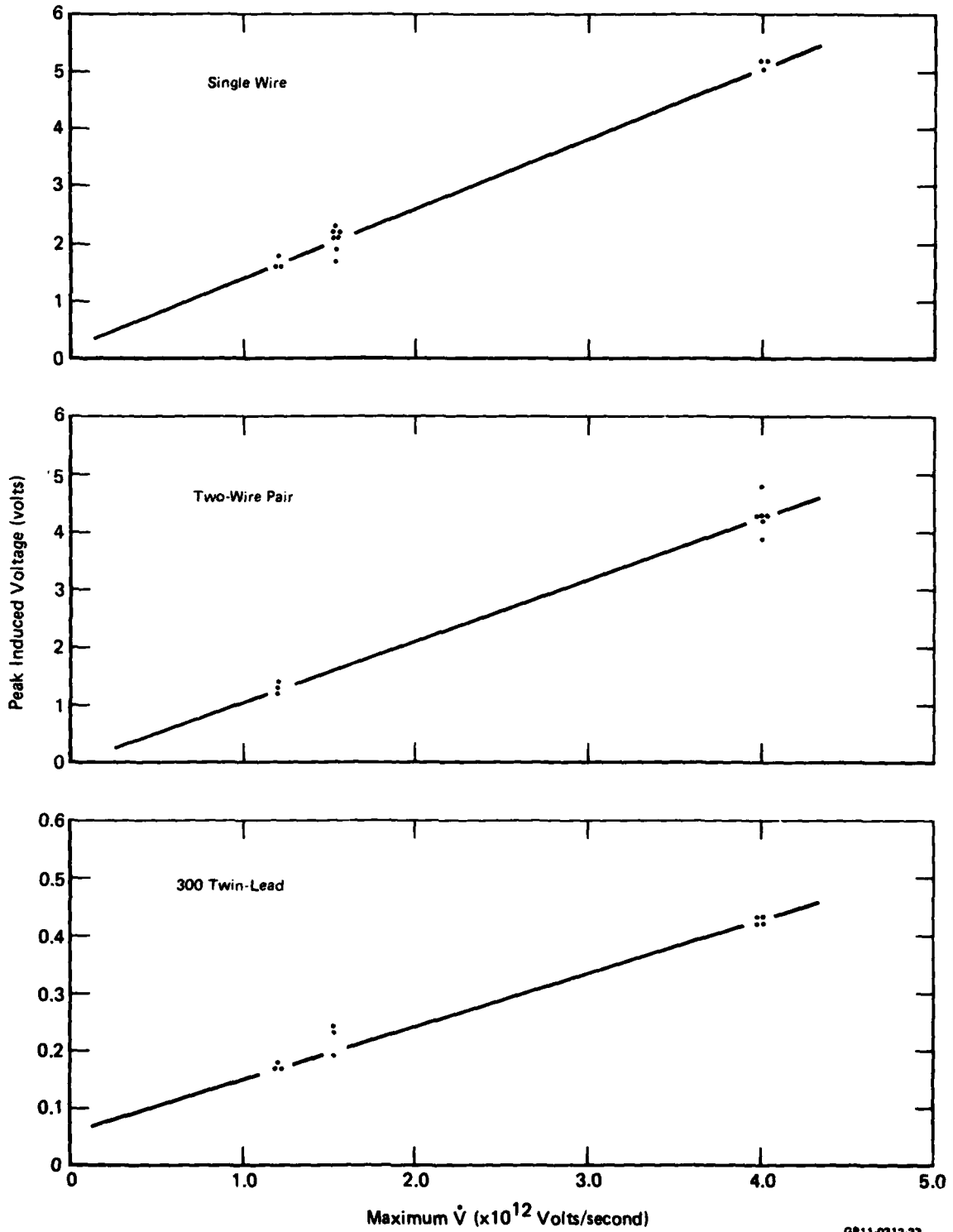   high-frequency free response of resonant modes.

FIGURE 26. INDUCED VOLTAGE VERSUS dV/dt
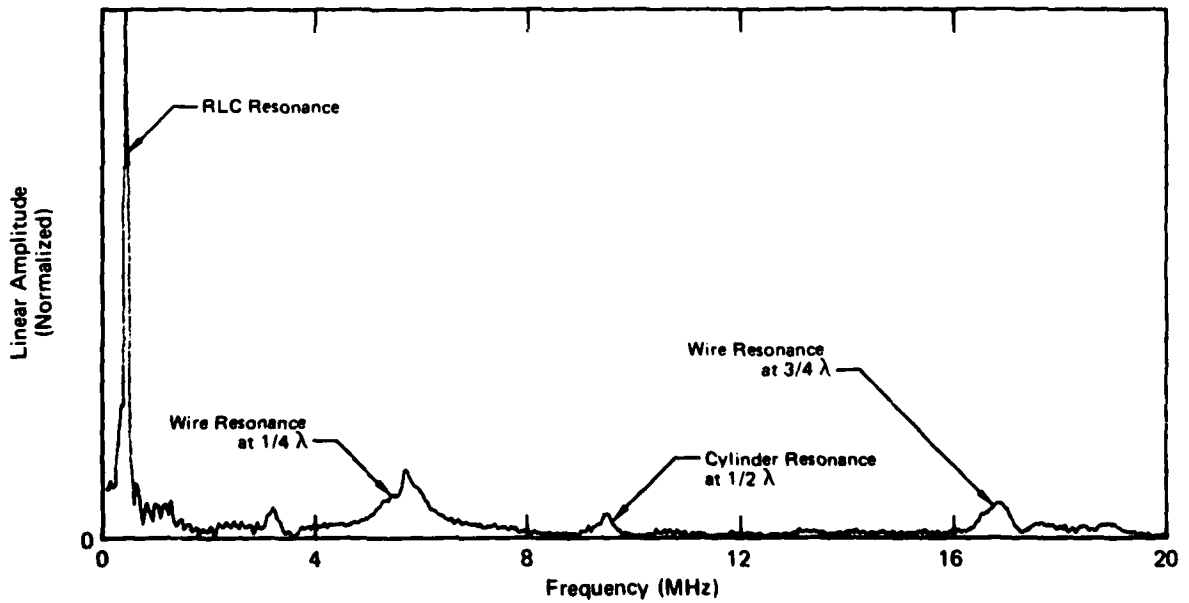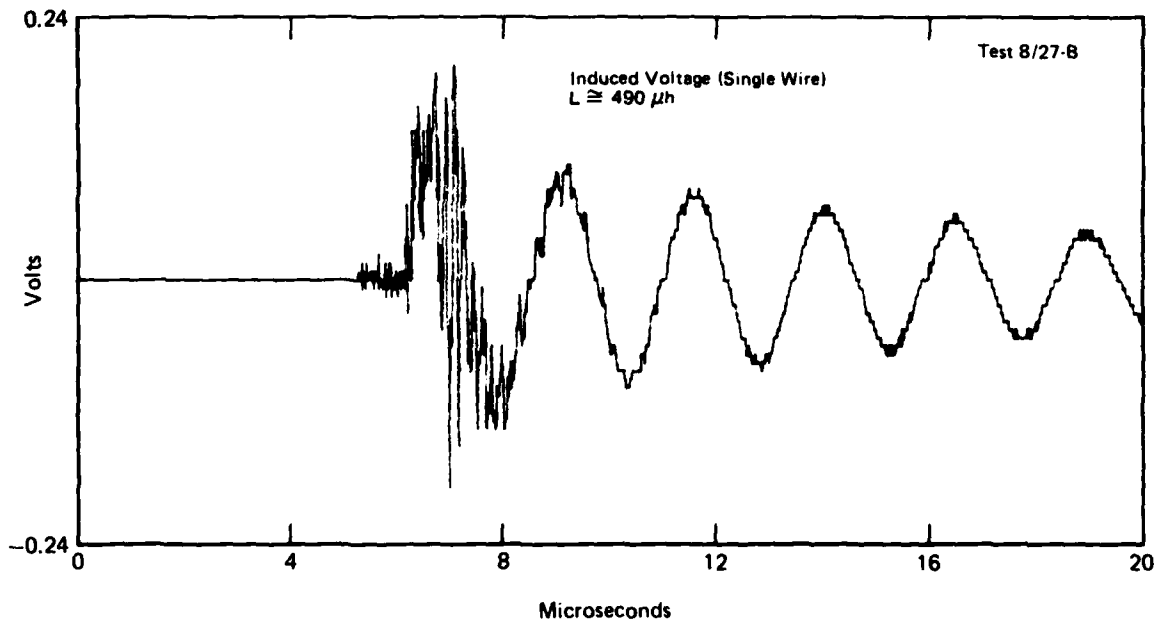Open Cylinder Configuration

GP11-0312-23

FIGURE 27. INDUCED VOLTAGE RESONANCES

In addition to the primary tests, two other system variation test sequences were run. Figure 28 shows the effect that closing the aperture has on the magnitude of the induced voltage on the interior wire. In this case, the induced voltage was attenuated by ≈33 dB. The signal waveform with the port closed is no longer the simple damped sinusoid, since coupling can occur only at joints around closed ports or at cylinder-to-cylinder connections. This brief experiment was run several times throughout the cylinder test program for different system configurations. The attenuations varied from ≈15 dB to ≈34 dB for these tests.

The second experiment was to determine the effect of wire orientation on the induced voltage response. For this test, the two-wire differential circuit was selected because its orientation is readily defined. Figure 29 shows the induced voltage for two perpendicular wire configurations. The horizontal orientation (used in all other testing) places one wire nearer to the aperture than the other. The sketched equipotential lines show that a voltage differential will be established in this case. The vertical orientation ideally places both wires symmetrical to the aperture and, therefore, there should be less voltage gradient between them. The measured induced voltages support this argument with the asymmetric case induced voltage being ≈5 times (14 dB) that of the symmetric orientation.

2. YF-16 Charging Tests

The charging tests on the YF-16 aircraft are not as easily interpreted as those on the cylinder. In the cylinder tests, the test article was completely isolated from ground so that only the charging event took place and the interior circuit response was readily determined. Such complete isolation of the YF-16 was possible only for generator voltages less than 240 kV. Rather than reducing the generator voltage so that only the charging event would occur, the tests were conducted with a generator voltage of 240 kV and a 6-inch output arc. For this configuration, the charging response on the interior circuit is seen for approximately one microsecond before the gap breaks down and the discharging transient is excited. During the short observation time of the induced charging transient neither the form nor the peak magnitude is well defined.

Induced Voltage

Aperture Open
Open Cylinder Configuration
Single Interior Wire, $L \simeq 290\ \mu h$
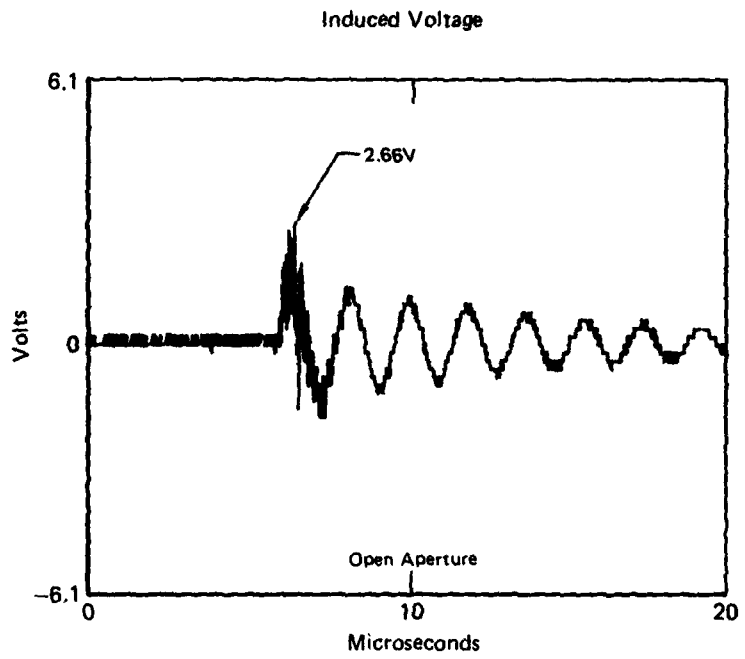
Open Aperture

Attenuation Due to Closed Aperature $\simeq 20 \log_{10} \dfrac{0.06}{2.66} = -33\ dB$

Induced Voltage

Same Conditions as Above Except
Aperture is Closed

Closed Aperture
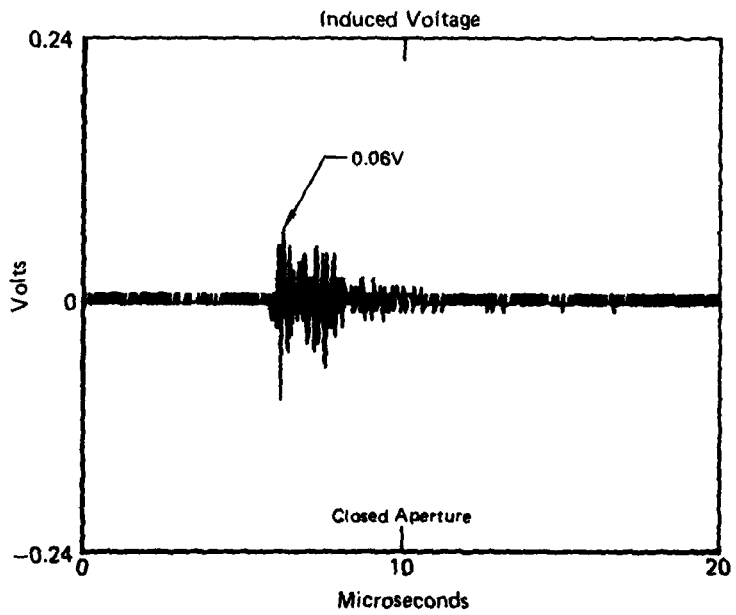
GP11-0312-28

FIGURE 28. EFFECTS OF CLOSING THE SYSTEM APERTURE

47
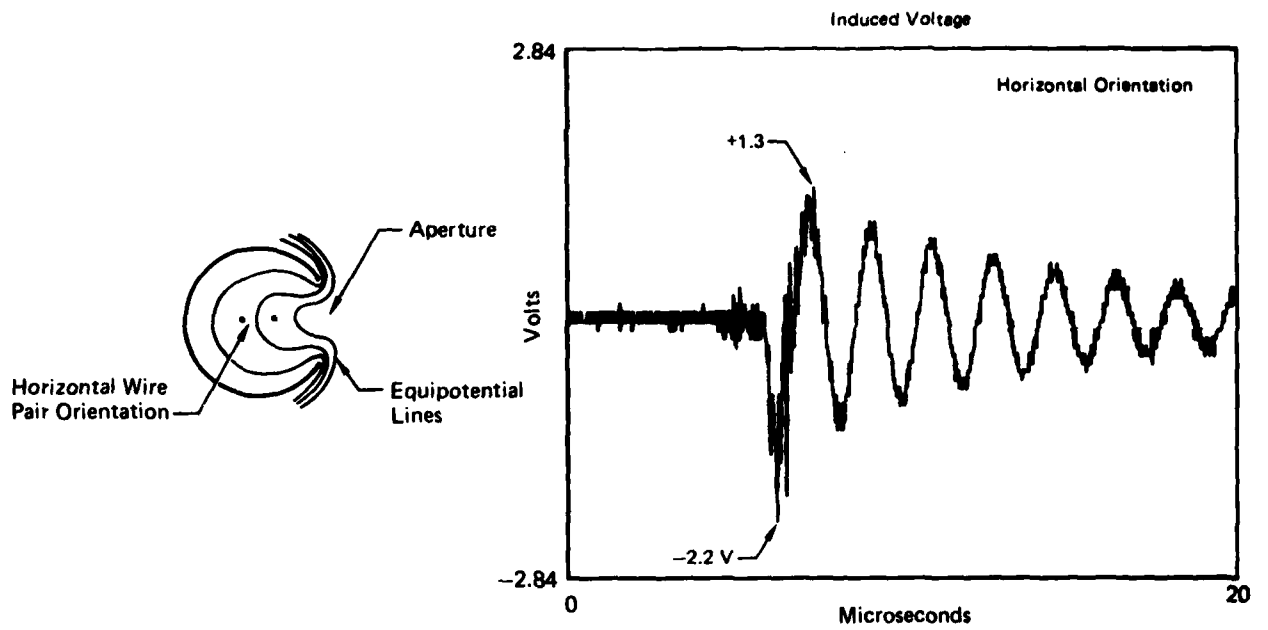
Test Conditions: Open Cylinder Configuration
Two-Wire Pair
$L \simeq 290 \; \mu h$
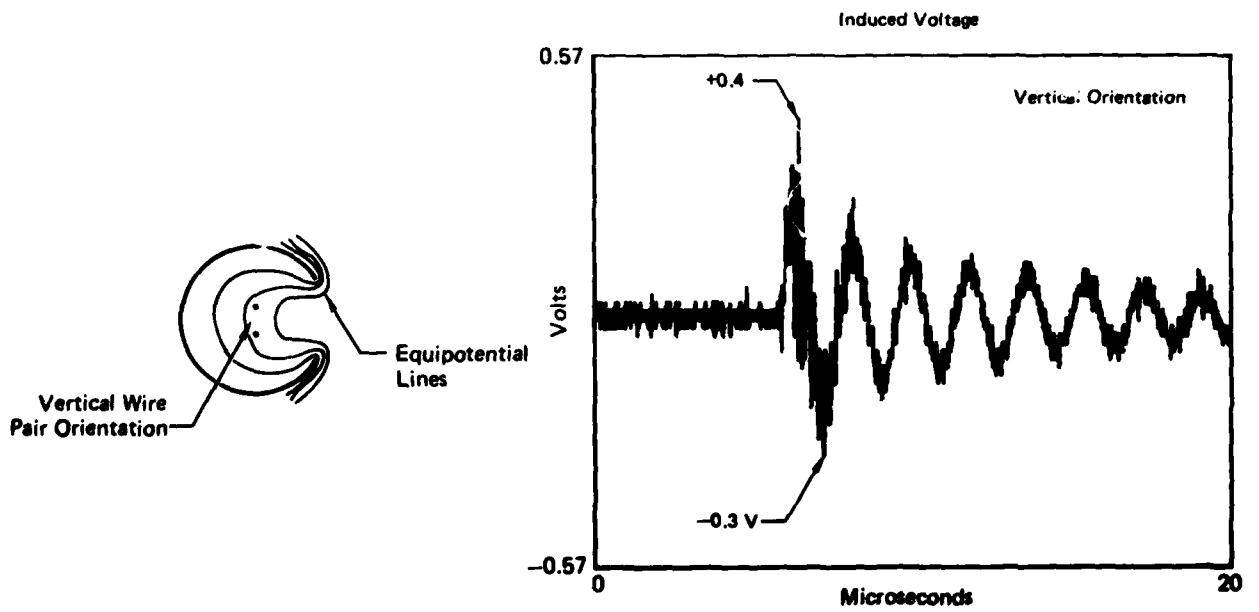
FIGURE 29. EFFECTS OF CIRCUIT ORIENTATION

48

Each of three flight control circuits was tested for three system inductance
levels (380 µh, 130 µh, and 30 µh). Figure 30 shows the relative aircraft
voltage and the induced response of the right flaperon circuit for a system
inductance of 30 µh. The form of the induced response is not clear; however,
it appears that a slower forced response is being modulated by a high-
frequency free response that is relatively large in magnitude. In general,
the measured induced transients for charging were of lower magnitude than the
discharging transients. However, when all added inductors were removed from
the system to provide the fastest charging d V_{CYL}/dt (as in Figure 30), the
magnitude of the induced charging transient was comparable to the discharge
transient.
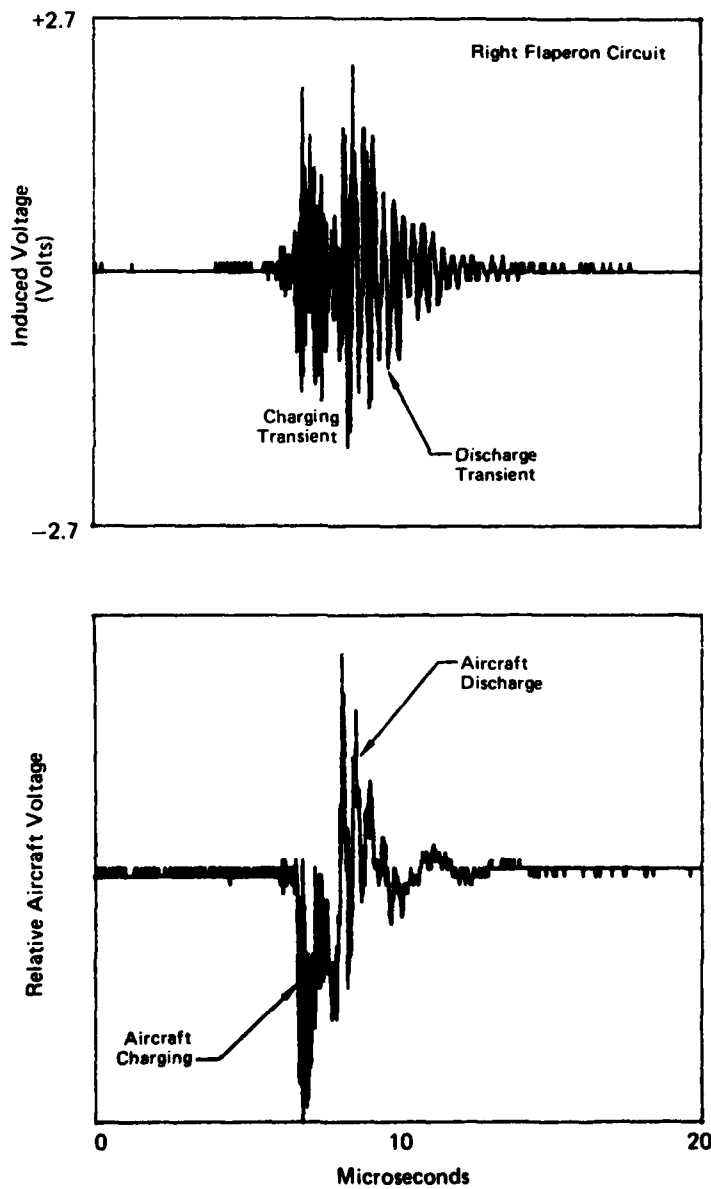
FIGURE 30. YF-16 CHARGING AND DISCHARGE TRANSIENTS
RIGHT FLAPERON CIRCUIT, 30µH SYSTEM INDUCTANCE

49

Figure 31 shows the induced voltage (peak-to-peak of the high-frequency oscil-
lations) plotted against the average d V_{F-16}/dt for the charging transients
with three different system inductances. Considerable data scatter exists,
but the data does demonstrate that the charging induced transient varies with
d V_{F-16}/dt. More data would be needed to confirm a linear scaling with
d V_{F-16}/dt as was seen for the aluminum cylinder tests.
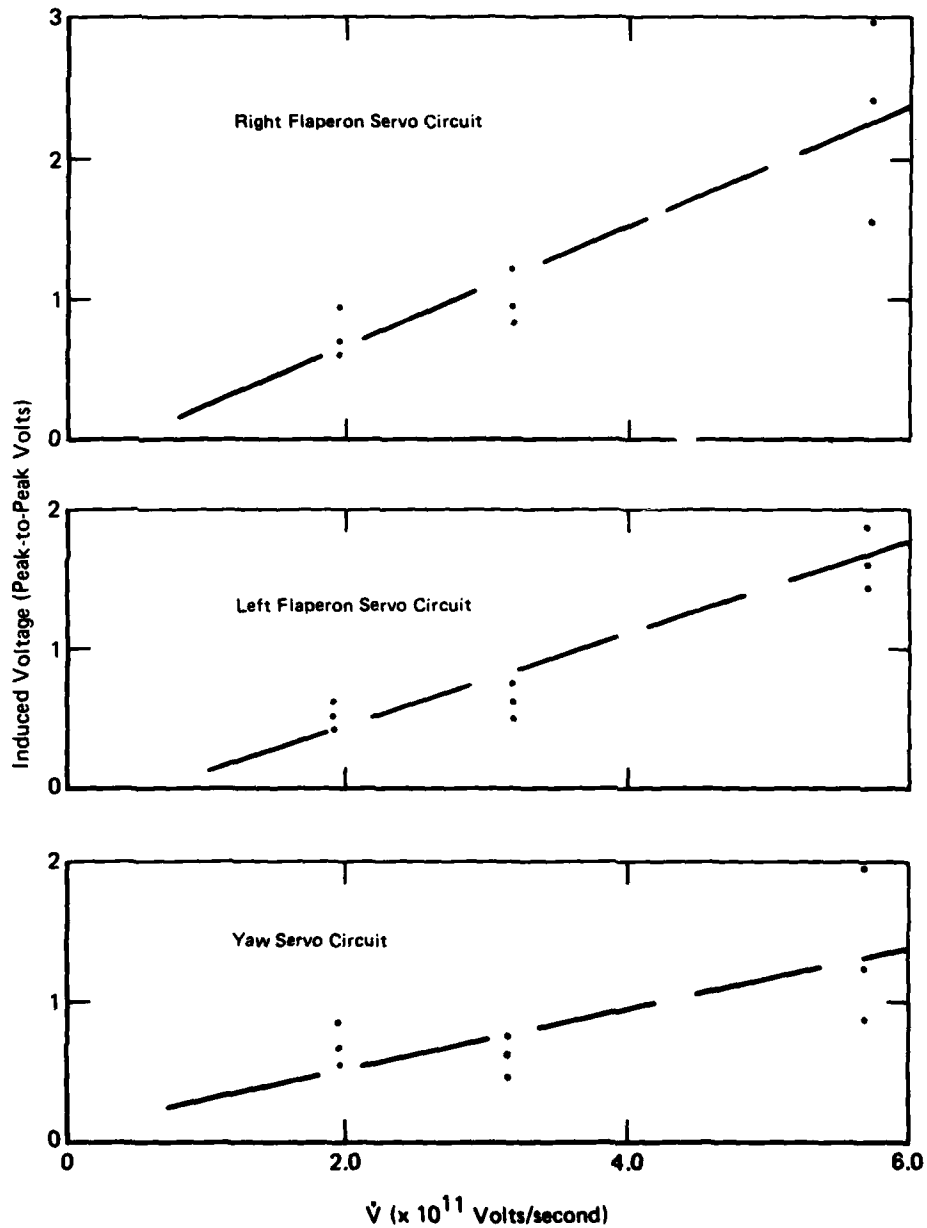
FIGURE 31. INDUCED VOLTAGE VERSUS dV/dt
YF-16 Charging Transient

SECTION VI
DISCHARGE TRANSIENTS

The induced transients produced by the current pulse and the discharge portion of the shock-excitation test technique were studied for high impedance circuits in both the long aluminum cylinder and the YF-16. These tests are intended to simulate the induced effects of the return stroke of natural lightning.

If the test article is isolated from ground potential, the only difference in the test setup for the two techniques is whether or not a spark gap is included between the test article output and the return conductor. This minor configuration change has a significant impact on the system response and the induced response of interior wires.

The presence of the output spark gap enables the test article to charge to a high voltage before the spark gap breaks down and the test article rapidly discharges toward ground potential. dV/dt's up to 10^{12} V/m-s can be generated during this fast discharge. This case is contrasted by the current pulse technique where the test article voltage is limited to the L_R dI/dt voltage drop along the ground return conductor (where L_R is the inductance between the test article and ground). For the current pulse, the dV/dt of the test article will thus go like d^2I/dt^2 and will be less than the corresponding dV/dt of the shock-excitation test. For high impedance circuits, shown to be sensitive to capacitive coupling in Section III, the induced voltages measured by the shock-excitation test should therefore be larger than those measured for the current pulse test.

The system current responses for the two test techniques show similar differences. For underdamped conditions, the current pulse technique provides the familiar damped oscillatory current waveform with a frequency primarily dependent on the generator capacitance and system inductance. The first half cycle or so of the current waveform may be modulated by a higher frequency oscillation characteristic of transmission line reflections from the short-circuited output condition (due to the hard-wire connection between the test article and the return conductors). The magnitude and frequency of these oscillations are dependent on the input circuit impedance and the transmission line

characteristics. These transmission line reflections are more exaggerated in the shock-excitation tests. In the shock-excitation technique, a fast current spike is produced as the output spark gap breaks down and the test article starts to discharge through the low resistance output arc. This current spike is partially reflected at the then "shorted" output and modulates the slower discharge of the generator through the system. The slower generator discharge is identical to that obtained in the current pulse tests; however, the test article discharge can produce a current spike with dI/dt's up to 10^{11} amps/s. The fast discharge and the resulting reflections can, therefore, strongly modulate the generator discharge.

This section first demonstrates the transmission line effects on the simple geometry of the test cylinder. Then the shock-excitation and current pulse tests on the cylinder are compared for both the single wire and coaxial return conductor configurations. Finally, the test results on the YF-16 are described.

1. Transmission Line Effects

As qualitatively described above and analytically treated in Section III, the test article/return conductor transmission line characteristics have an important impact on the system current and voltage responses which ultimately get coupled as induced voltages on interior wiring. The extent of the transmission line reflection and modulation depends on the system configuration, including the transmission line terminations, characteristic impedance, length, uniformity, and losses.

The system terminations determine the resonant mode. For all the program tests, the rise time of the modular Marx generator was slowed by a large inductor in series with the output. At frequencies different from the slow discharge response, this generator system represents a high impedance source to the test article. With the input termination set, the resonant mode is dependent only on the other end of the transmission line which is the output connection between the test article and the return conductor. When this output connection is open (as in the open cylinder tests or with a spark gap before breakdown), both ends of the line are high impedance points with

current minima. The test article/return conductor transmission line, there-
fore, exhibits a half-wave resonance which modulates the test article charging
current. When the output of the test article is shorted either by an arc or
hard-wire to the return conductor, the short circuit establishes a current
maximum at the output end while the generator is maintained as a current node.
The system transmission line will then resonate at a quarter wavelength.

Figure 32a shows the effect of the quarter-wave resonance on a 40-foot cylin-
der hard-wired to a ground plane return. A 4.5-MHz signal, which corresponds
to a propagation velocity of .77 c, strongly modulates the underdamped system
currents. The current measurement was made in the output line shorting the
cylinder to the ground plane where the reflected currents are a maximum. Fig-
ure 32b shows that the addition of a 120Ω resistor in the waveshaping network
on the input to the cylinder overdamps the system current but has little
effect on the percentage of modulation since the resistor and waveshaping
inductor in series still represent a high impedance mismatch at the generator
end. Figure 32c shows the effect of removing the 120Ω resistor from the input
circuit and putting it in the output line to approximately terminate the
cylinder/ground plane transmission line. The reflected signal is then
greatly reduced. This demonstrates that the modulating signal was indeed due
to the short circuit impedance mismatch.

A second example of transmission line resonances is given in Figure 33 which
shows the absorption nodes of the 48-foot cylinder configured with the eight-
wire coaxial return. The simple instrumentation setup simulated the quarter-
wavelength resonance conditions with the 50Ω terminator representing the short
circuit and an open circuit at the other end of the cylinder representing the
high impedance of the input waveshaping network. Strong absorption occurs at
3.9 MHz, 11.8 MHz, and ≈19 MHz which correspond, respectively, to the $\lambda/4$,
$3\lambda/4$, and $5\lambda/4$ resonances with a propagation velocity of ≈.79 c. The 3.9-MHz
resonance was the dominant modulating frequency in all coaxial return tests.

In preliminary tests on the long aluminum cylinder using a ground plane return,
the current modulation on the uniform test article due to transmission line
resonances was large, even for the hard-wired current pulse case. These modu-
lations had not been substantial in previously reported current pulse tests on
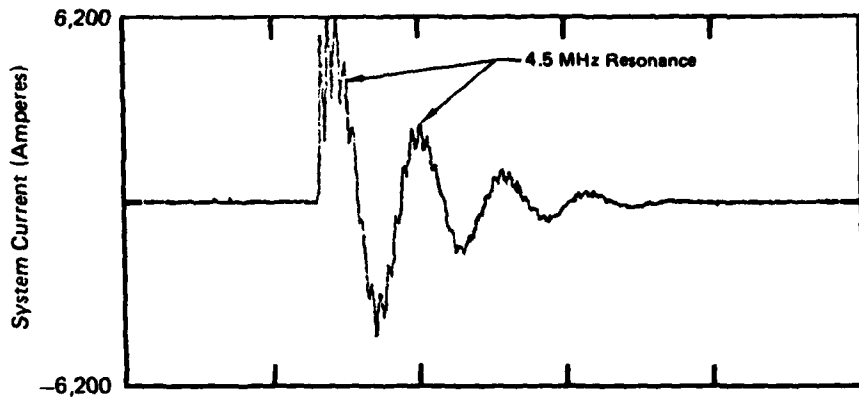
a) Cylinder hard-wired to ground plane return
(current measured in cylinder output line)
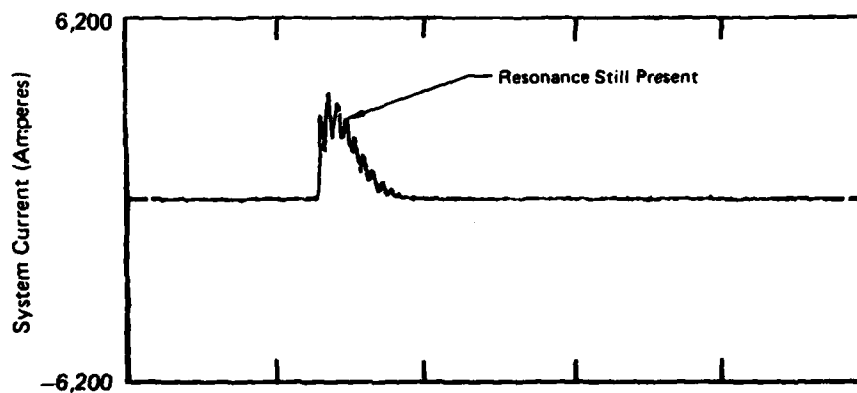
b) Same as a) with an additional 120 Ω resistor added
between the generator and the cylinder
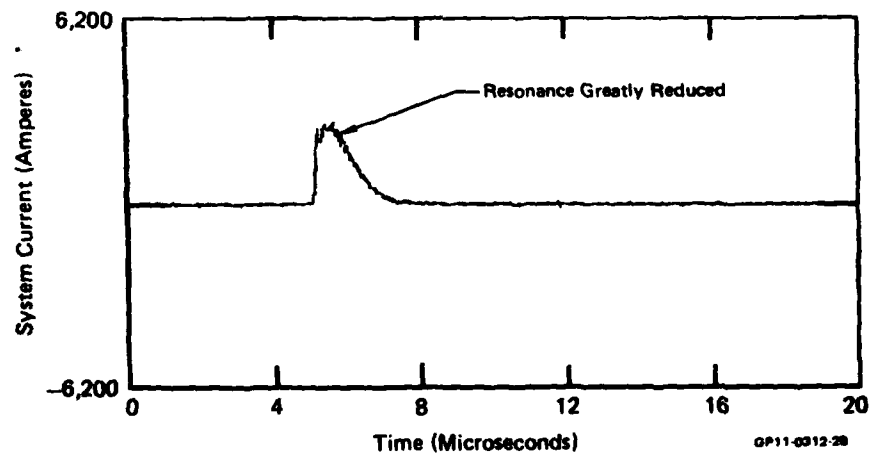
c) 120 Ω resistor moved from cylinder input to the cylinder output
to terminate the cylinder/ground plane transmission line

FIGURE 32. CYLINDER TERMINATION EFFECTS
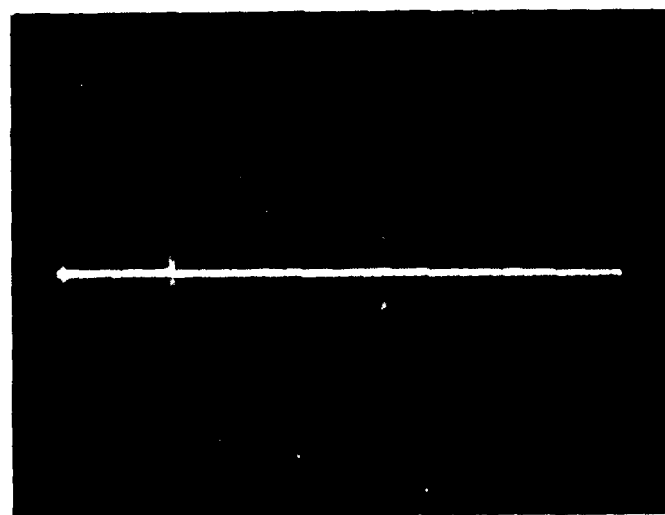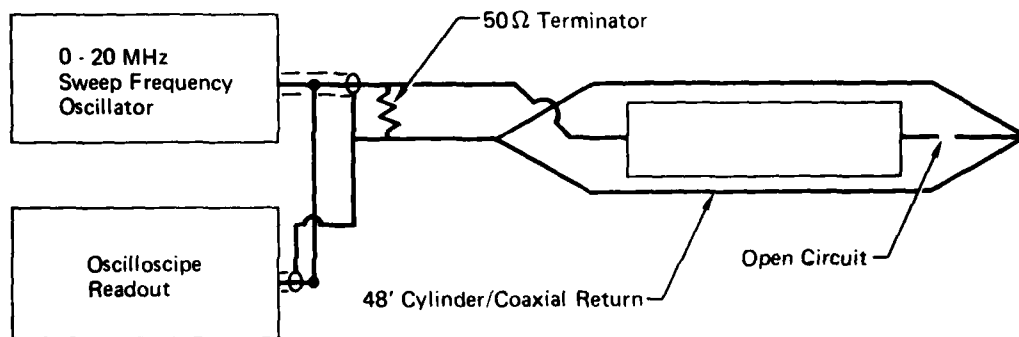
Absorption Resonances Occur at 3.9 MHz, 11.8 MHz, and 19 MHz. They
Correspond to $\lambda/4$, $3\lambda/4$, and $5\lambda/4$ at a propagation velocity of $\simeq 0.79c$.

FIGURE 33. ABSORPTION RESONANCES FOR COAXIAL RETURN CONFIGURATION

aircraft and were found to be of relatively small amplitude in our YF-16 tests. To keep these resonances to a minimum on the cylinder tests (so that the results could better be compared to the aircraft tests) two different transmission line systems were used for the cylinder tests.

In one case, the ground sheet return path was changed to a single wire return which was isolated from ground. The cylinder/single wire transmission line has a characteristic impedance approximately three times that of the cylinder/ground plane line. Thus, for a given reflected voltage, the corresponding resonant current was reduced threefold. The second case used a coaxial return wire configuration with parallel resistors added between the cylinder and return wires to approximately terminate the output end. Current pulse and shock-excitation tests were conducted for both return configurations.

2. Cylinder Tests With Single-Wire Return

The first comparisons of the current pulse (hard-wired output) and the shock-excitation (spark gap output) test techniques were done with the test cylinder supported approximately 5 feet above a single-wire return. The wire return was used to limit reflected currents at the cylinder's quarter-wave resonance. This experimental configuration is similar to that previously used in the IRAD studies and is extremely flexible. Changes in the cylinder output spark gap length or to a hard-wired condition are easily made.

A 250-microhenry inductor and 140 ohms of resistance were added as waveshaping components between the generator and the cylinder input. The inductor slows the current rise time to 1.5 microseconds which is similar to the two-microsecond rise time generally used in current pulse testing. The resistance was added to help damp the cylinder voltage oscillations before the spark gap breakdown occurs.

Tests were conducted on each of the three interior wire circuits. The system parameters varied in the tests were the generator charge voltage (200, 375, or 520 kV), the cylinder output condition (hard-wired or arc), and the length of the output spark gap where applicable. All other parameters remained the same during this portion of the test program. The measured quantities were the

system current at the cylinder output, the induced voltage on the interior circuit due to aperture coupling from one open port, and the electric field in the vicinity of the cylinder.

Figures 34 through 36 show the typical effect of the output configuration on the system and induced voltage responses. All three tests were conducted with identical system parameters; the only difference in the three was the cylinder output condition. In Figure 34 the output was hard-wired (no spark gap). The system current is the underdamped RLC response with a peak current of ≈1000 amps. Figures 35 and 36 show the shock-excitation response for the same system parameters when output spark gaps of 7.5 and 13 inches are incorporated into the setup. These figures and the results of this cylinder test series are described in the following paragraphs.

    a. Current Pulse Response (Hard-Wired Output) - When the test article was held near ground potential by a hard-wired output, the system current was the basic RLC response with very little transmission line modulation. The current pulse measurements were always made in the output connection between the test article and the return conductor where the current modulation would be a maximum. Figure 34 shows that there was virtually no modulation for the hard-wired output with the single wire return.

The induced voltage response is a high frequency oscillation that is excited to its maximum amplitude soon after the generator is triggered and system current starts to flow (denoted as time t = 0). The slowly damped free response bears no resemblance to the input system current waveform. The frequency response, shown in Figure 37, has the characteristic free response peaks at 5.7 and 16.8 MHz. These peaks were also found in the cylinder charging tests (Figure 27) and correspond to the 1/4 and 3/4λ resonances of the interior wire.

Previous analysis and cylinder tests have shown that the high impedance interior wire circuit is sensitive to capacitive ($\approx$ dV/dt) coupling. For the hard-wired case, dV/dt at the aperture is proportional to L_R d^2I/dt^2. The second derivative of the current has a large value at t = 0+ and is relatively low in value thereafter since the current pulse is a smooth sinusoid for times
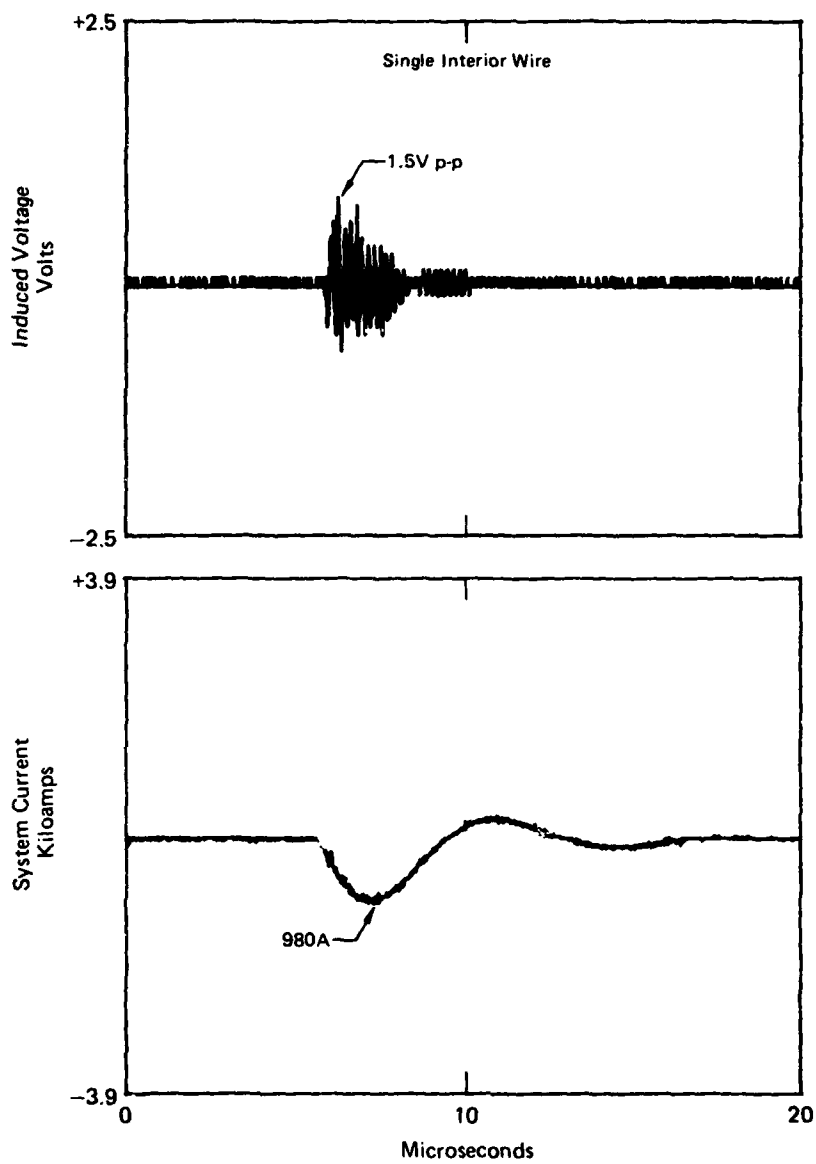
FIGURE 34. SYSTEM RESPONSE WITH HARDWIRED OUTPUT
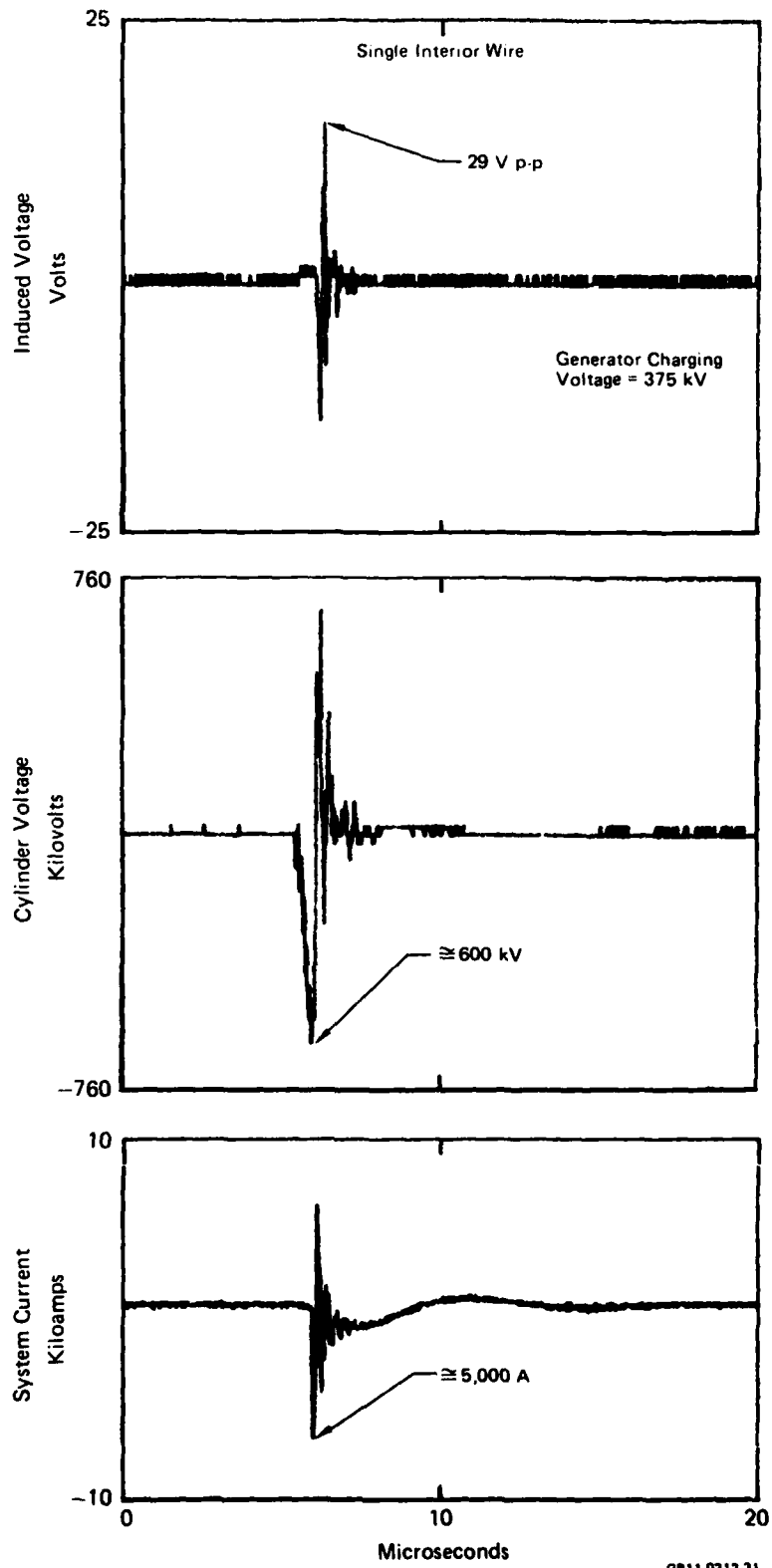
FIGURE 35. SYSTEM RESPONSE WITH 7.5" OUTPUT ARC
Cylinder Near Peak Voltage
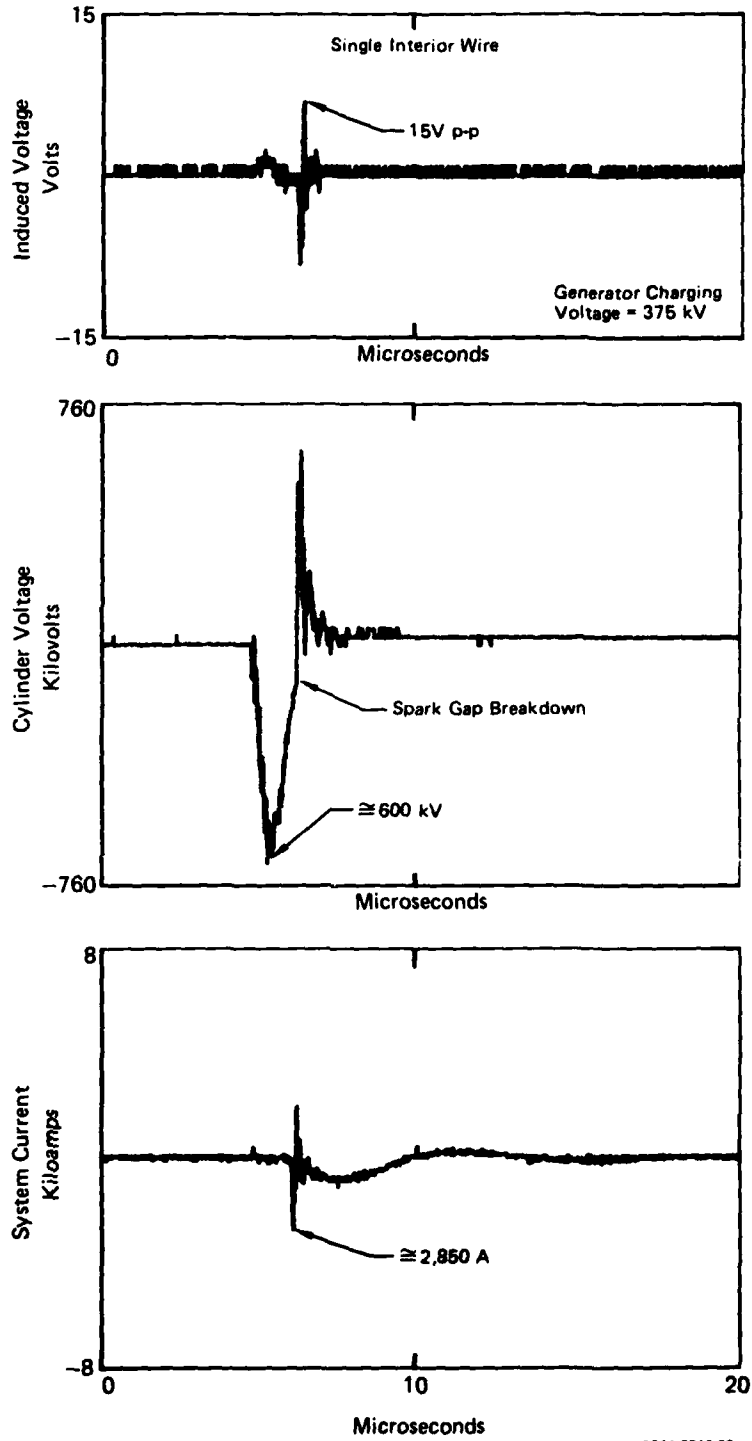
FIGURE 36. SYSTEM RESPONSE WITH 13" OUTPUT ARC
Cylinder Near Minimum Voltage

60
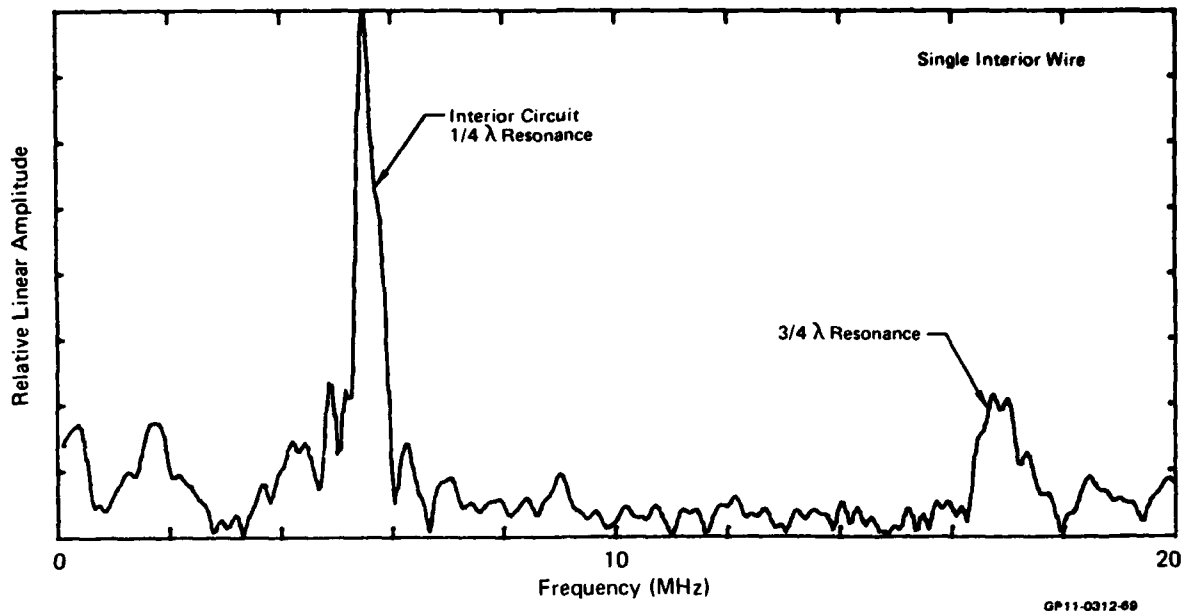
FIGURE 37. INDUCED VOLTAGE FREQUENCY RESPONSE
(Hard-Wired Output)

greater than 0. The large value of d^2I/dt^2 at $t = 0$ is dependent on the triggering conditions of the generator since $dI/dt = 0$ for time $t = 0-$, and dI/dt is a damped cosine function (which has its maximum amplitude at $t = 0+$) for times greater than $t = 0$. The transition between these two dI/dt conditions produces the high instantaneous d^2I/dt^2 at $t = 0+$ which can excite the free response of the interior wire. The amount of coupling to the interior circuit and the damping of the induced free response is dependent on the particular interior wire circuit and configuration.

The response of the three different wire types was measured for generator output voltages of 200, 375, and 520 kV. These generator voltages corresponded to peak system current levels of approximately 500, 980, and 1350 amperes, respectively. The induced voltage response of the three wires is plotted in Figure 38. The data generally scales linearly; however, some data scatter exist due to the impulse nature of the coupling which is dependent on the repeatability of the generator triggering. The induced voltage levels were only a few volts, and the two-wire and single-wire configuration voltages were approximately ten times that of the 300Ω twin-lead.

61
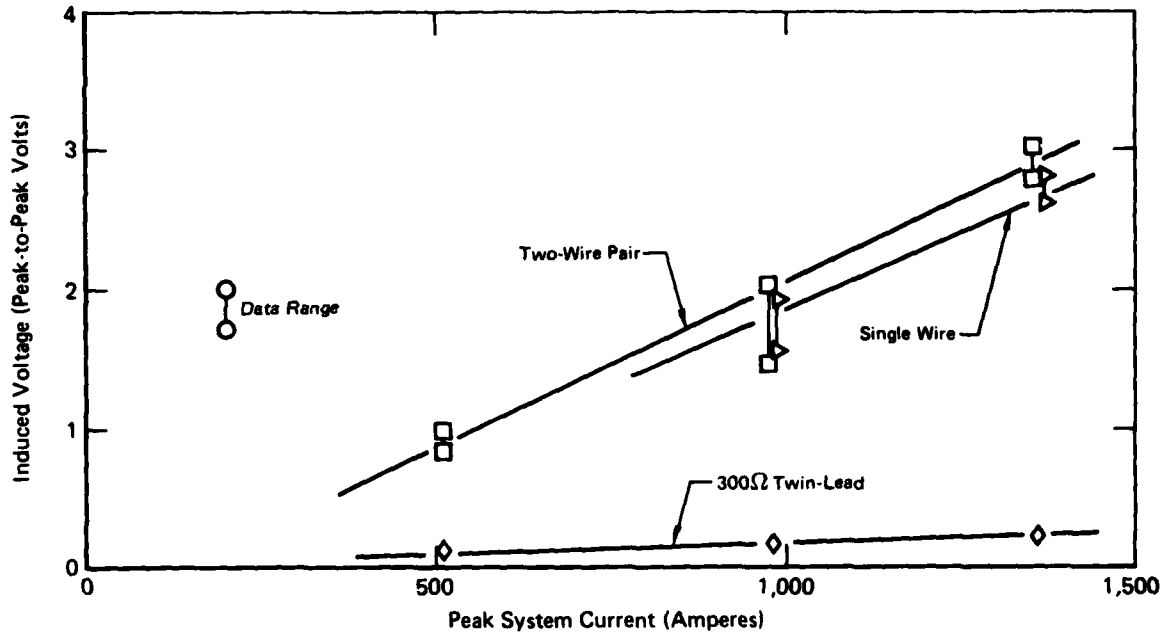
FIGURE 38. CURRENT PULSE TEST RESPONSE
(HARD-WIRED OUTPUT, WIRE RETURN)

b. <u>Shock-Excitation Response (Spark Gap Output)</u> - When a spark gap is
inserted in the cylinder output line, the cylinder first charges to a high
potential, as described in Section V. For a large output gap and the system
parameters used in this test sequence, the cylinder voltage will rise to a
peak 1.6 times the initial generator voltage and will then oscillate about
the initial generator voltage level. When gap breakdown occurs, the cylinder
voltage quickly discharges and oscillates about ground potential. Accom-
panying the rapid voltage change is a sharp current spike which produces high-
frequency ringing on the cylinder (oscillating at the quarter-wavelength
resonant frequency). The current spike and its reflections modulate the early
portion of the slower RLC system discharge which is identical in magnitude to
that of the hard-wired output case.

Figures 35 and 36 show that both the system current and voltage waveforms have
fast oscillations (and therefore high first derivatives) at the 3.8-MHz
quarter-wavelength resonance. The aperture coupling of the cylinder transients
excites a forced response on the interior wire circuit. The forced response

has the same 3.8-MHz frequency and has a maximum amplitude when the spark gap breakdown occurs. Since the voltage and current transmission line oscillations are at the same frequency and related by the characteristic impedance of the cylinder/return conductor line, the particular coupling mechanism cannot readily be determined from the test data but must be inferred from the circuit configuration and previous tests. For the high impedance interior circuit and aperture coupling near a high impedance location, capacitive coupling is the dominant mechanism, as has been shown in the previous tests.

The shock-excitation tests studied the variation of the induced voltage response with changes to dV_{CYL}/dt during the cylinder discharge. The data comparison was simplified by using the variation of the cylinder voltage at breakdown as an approximation of the relative dV_{CYL}/dt's for various tests. For the cylinder test setup, the quarter-wave resonance determines the transmission line frequency and, therefore, the period of fast oscillations. For parameter changes that do not affect this resonance, the time between positive and negative peaks of the high frequency voltage (or current) oscillations is a constant, and the cylinder potential at breakdown is approximately proportional to dV_{CYL}/dt at breakdown. The proportionality generally holds well for most of the cylinder tests. A few exceptions were found for low cylinder voltages at discharge. In these cases (see Figure 36), the voltage discharge is not symmetric about ground potential so the cylinder voltage at breakdown under-approximates the actual dV_{CYL}/dt.

During this test series, the cylinder voltage at breakdown was varied in two ways. For a fixed generator voltage, the output spark gap distance was varied to change the time (and thus the cylinder voltage) between triggering the generator and cylinder discharge. This effect is demonstrated in Figures 35 and 36 where the only difference in the test setup is the length of the output spark gap. In Figure 35, the discharge occurs near the peak cylinder voltage, and in Figure 36, the discharge occurs near the voltage minimum after the first peak. The second method of varying the cylinder voltage is to increase the generator voltage which in turn proportionately increases the entire charging waveform.

Table 3 is a summary of all the data recorded in this test sequence. Each element represents the average of at least two (and generally three) shots with the same conditions. The table includes the spark gap distance, the peak-to-peak induced voltage level, and the cylinder voltage (at the time of gap breakdown) as a percentage of the peak cylinder voltage (1.6 times the initial generator voltage). The data in Table 3 show that the induced voltage for the fast discharge of the isolated cylinder is an order of magnitude larger than the corresponding hard-wired case for the same generator voltage. The fast transmission line oscillations caused by the discharge greatly increase the coupled voltage on the interior circuit.

For a given interior circuit and generator voltage, the induced voltage generally follows the cylinder voltage at breakdown (percent of peak cylinder voltage column) which approximates dV_{CYL}/dt. The induced voltage waveform was always a fast oscillatory transient driven by the transmission line resonances of the cylinder/return conductor line. For these reflections, the cylinder current is directly related to the oscillating voltage by the characteristic impedance of the line. Thus, the peak current of the fast discharge

TABLE 3. DATA SUMMARY - CYLINDER WITH WIRE RETURN

Generator Voltage	200 kV			376 kV			520 kV		
Wire Type	Arc Length (in.)	Induced Voltage (Volts)	% of Peak Cylinder Voltage	Arc Length (in.)	Induced Voltage (Volts)	% of Peak Cylinder Voltage	Arc Length (in.)	Induced Voltage (Volts)	% of Peak Cylinder Voltage
Single Wire		No Data Taken		HW* 6 7 1/2 9 13	1.7 21 29 28 17	72 100 90 28	HW 6 9 13 20	2.8 28 37 40 28	77 83 90 45
Two-Wire Pair	HW 5 1/2 7 1/2 9	0.85 12+ 6.7 2-5	90 45	HW 6 9 13	1.6 ≫5+ 31 11-17	76 100 14-40	HW 6 9 13 18 20	2.9 27 35.5 34 32 11-18	65 90 90 70
300Ω Twin-Lead	HW 6 7 1/2	0.24 2.2+ 1.2	100 43	HW 6 9 13	0.28 3.0 3.9 2-3	74 100	HW 6 9 13 20	0.36 5.7 6.5 6.1 2.4-3.5	73 100 92

*HW = Hard-Wired (No Arc)

GP11-0312-33

64

should also vary like the cylinder discharge voltage and the induced voltage. For a more limited data base, the peak of the current pulse was found to be proportional to the induced voltage. The frequency response of the current transformers and difficulties in keeping the fast current spike in the linear region of the fiber optic system limited the amount of current data obtained.

The linear trend of the induced voltage with the magnitude of the fast oscillations was also found to hold when the generator output voltage was changed. Figure 39 is a plot of induced voltage versus the cylinder voltage at breakdown. The plotted values are for cases when the cylinder discharge occurred near the peak cylinder charging voltage for each of the three generator charging levels. The graph shows that some data scatter exists, but that the linear trend is generally established. The coupling to the single wire and the two-wire pair is again seen to be approximately the same and an order of magnitude larger than the coupling to the 300Ω twin-lead.
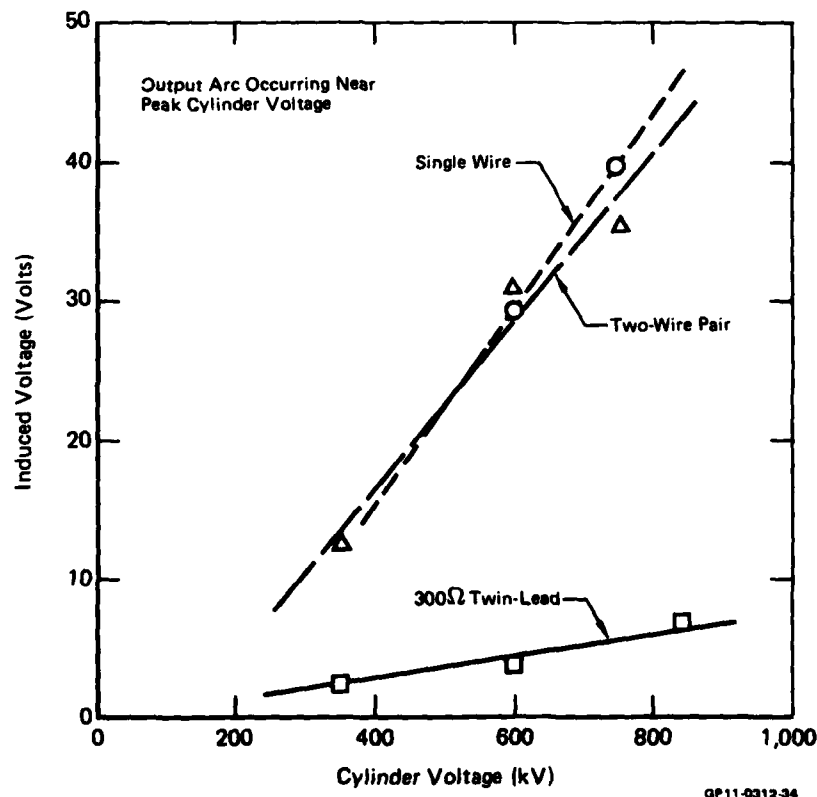

FIGURE 39. INDUCED VOLTAGE VERSUS CYLINDER
VOLTAGE FOR OUTPUT ARC CONFIGURATION

3. Cylinder Tests With a Coaxial-Wire Return

A second comparison of the current pulse and shock-excitation tests was made using an eight-wire coaxial return to provide a symmetric electromagnetic field distribution around the cylinder's circumference. The modular Marx generator was hard-wired to the input end of the cylinder through a 250-micro-henry inductor and a 20-ohm resistor. When the cylinder output was shorted to the coaxial return, either by a wire or an output arc, very large oscillating currents were produced on the low-impedance transmission line. These slowly damped oscillations were produced at the system's resonant frequencies (shown in Figure 33). To eliminate the large oscillating currents, parallel resistors were added between the end of the cylinder and the return wires. The resistance of the parallel combination was 125 ohms, and effectively terminated the cylinder/return transmission line whose characteristic impedance was approximately 120 ohms.

The comparison of the two techniques was made on the single- and two-wire high impedance circuits for three generator voltages. The shock-excitation tests were run with a fixed 6-inch output spark gap due to limited space in the cylinder output when the resistors were incorporated in the setup. The electric field sensor was located outside the coaxial return wires. In this location, the sensor is somewhat shielded from the cylinder voltage by the return wires but does sample the leakage fields. The tests were conducted similar to those using the single wire ground return. Multiple shots were run for each variation to ensure reproducibility, and the only configuration difference between the two techniques was whether or not the output spark gap was included in the cylinder circuit.

Figures 40 and 41 demonstrate the response of an open-circuited single interior wire for the hard-wired and spark gap cases at a generator voltage of 240 kV. In the hard-wired case (Figure 40), the smooth underdamped system current response shows that the terminating resistors were effective in limiting transmission line resonances. However, the addition of the resistors did alter the voltage characteristics of the cylinder. The voltage at the cylinder aperture is given by $V_{CYL} = IR + L_R \, dI/dt$. The cylinder potential is a combination of the inductive potential drop (as in the previous tests) and the
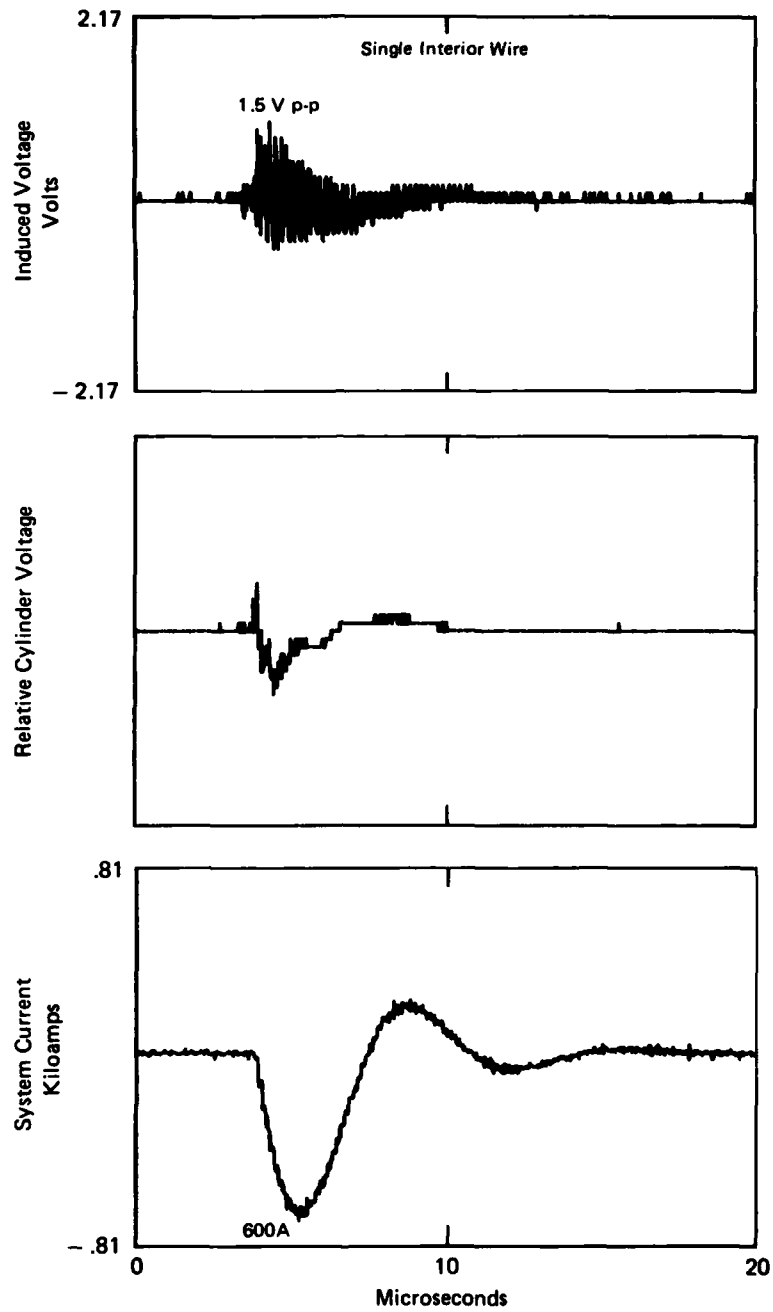
FIGURE 40. CYLINDER WITH COAXIAL RETURN
Hard-Wired Output, Interior Wire Isolated
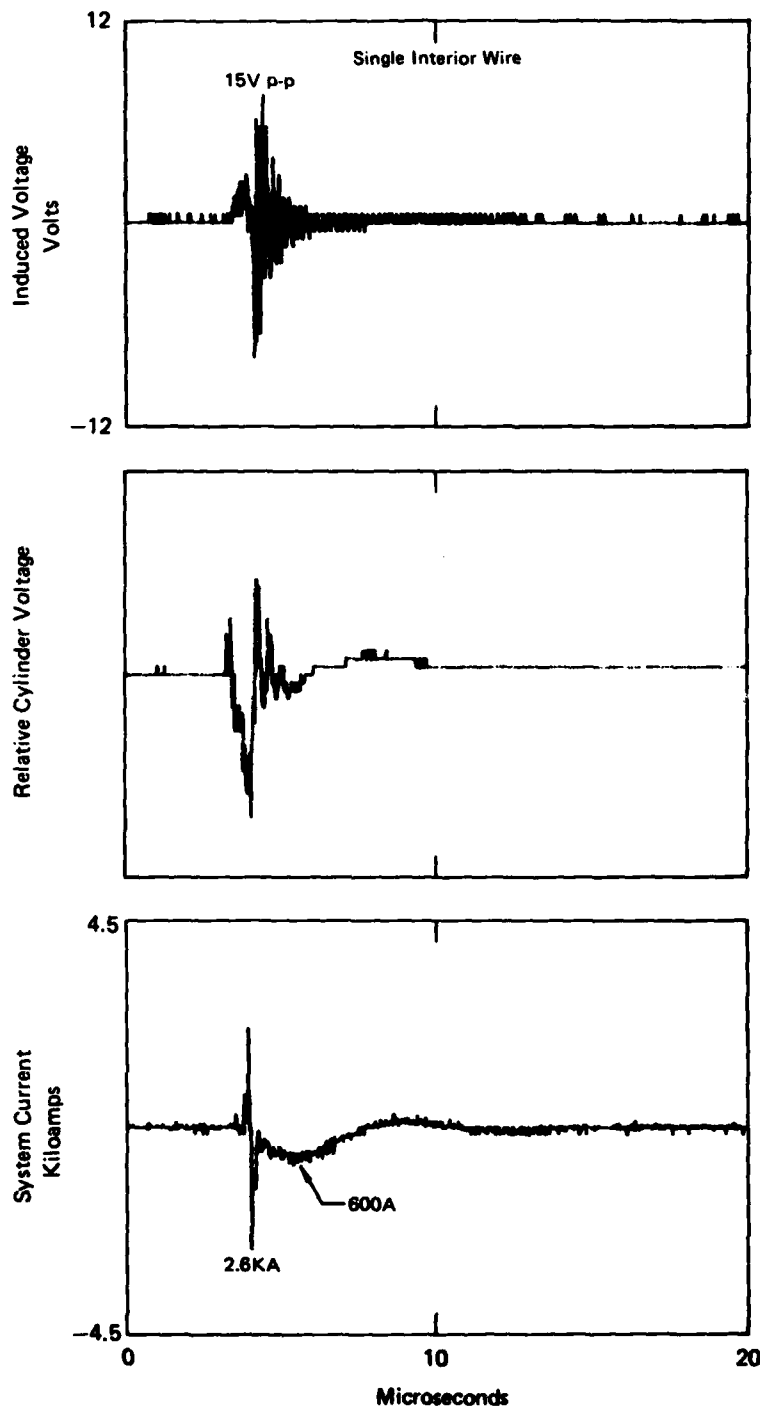
FIGURE 41. CYLINDER WITH COAXIAL RETURN AND 6-INCH SPARK GAP
Interior Wire Isolated

resistive drop across the large output resistors. The effect of the two out-of-phase terms is shown in the more complicated E-field sensor response. The induced voltage response has the characteristic free (5.8 MHz) oscillation which is initiated at generator triggering by the $L_R \, d^2I/dt^2$ term of d V_{CYL}/dt. The presence a second smaller component is also seen in the induced voltage response. The waveshape of this smaller term is difficult to discern because of the larger fast oscillations, but the component should vary like R dI/dt for capacitive coupling.

The system current with the spark gap output (Figure 41) shows a single cycle of the fast cylinder discharge. The reflections, which were present in previous tests, are damped by the terminating resistors leaving only the large amplitude current spike followed by the system current. The cylinder voltage first increases during the charging and then rapidly discharges at spark gap breakdown. The induced voltage of the open-circuited single wire has a smaller charging response before breakdown and the large damped oscillatory response after breakdown. As in the previous tests, the induced voltage transient for the shock-excitation technique was approximately an order of magnitude larger than that for the current pulse technique.

Even though the induced voltage responses for the coaxial return conductor configuration are similar to those of the single-wire return, the results of the scaling tests at three generator charging voltages are somewhat different and are presented in Table 4. The table gives the average peak-to-peak induced voltage for three shots in each condition. The induced voltage does not vary significantly with a change in the generator charging voltage.

TABLE 4. INDUCED VOLTAGE DATA FOR CYLINDER WITH COAXIAL WIRE RETURN

Test Configuration	Average Induced Voltage (V)		
Generator Voltage	240 kV	360 kV	480 kV
Hard-Wired Output			
Single Wire	2.2	2.3	2.6
Two-Wire Pair	1.4	2.3	2.3
6" Spark Gap Output			
Single Wire	15.5	13.5	18.3
Two-Wire Pair	13.0	—	13.4

GP11-0312-36

The reason for the lack of variation is not understood for the hard-wired output case. The current waveforms were smooth damped sinusoids and scaled with increased generator voltage. The fast, free oscillations were excited to their peak induced voltage when the generator was triggered. The likely impulsive driving function, which excites the free response, is the $L_R d^2I/dt^2$ term of $d V_{CYL}/dt$. Why the impulse apparently does not vary linearly for this system configuration requires further study.

The shock-excitation tests also showed a lack of variation with generator voltage; however, it is more readily explained. Since the output spark gap was limited to a length of 6 inches, breakdown occurred on the leading edge of the first cylinder charging oscillation. The breakdown voltage of a spark gap is primarily dependent on its geometry and on the time variation of the applied voltage. For these tests, the charging rate of the cylinder increased with the generator voltage; however, the voltage standoff capability of the spark gap was quickly exceeded in each case so that breakdown occurred at nearly the same voltage level regardless of the generator voltage. Since the breakdown voltage remained relatively fixed (≈ 20 percent variation), the $d V_{CYL}/dt$ at breakdown should also remain fixed and the capacitive coupling to the interior wire should not vary with increased generator voltage.

To provide a better understanding of the coupling mechanisms for the coaxial configuration, the interior single wire was shorted (instead of open-circuited) to the cylinder for a few shots. This change converts the high impedance interior circuit where capacitive coupling dominates into a low impedance circuit where inductive coupling should dominate. Figures 42 and 43 show the effect of the change. The system current and cylinder voltage waveforms are identical to the open-circuited case; however, the induced voltage responses are very different. Both the hard-wired and arc output cases demonstrate the dI/dt coupling to the slower oscillating system current. The fast current spike, generated during the cylinder discharge, produces a large, high-frequency transient superimposed on the slower system response. The high-frequency oscillations on both induced voltage transients are at approximately 12 MHz. This frequency is characteristic of the $1/2\lambda$ resonance of the interior transmission line which has a low impedance at both ends. Figure 44 is the fast Fourier transform of the induced voltage response for the shock-excitation case.
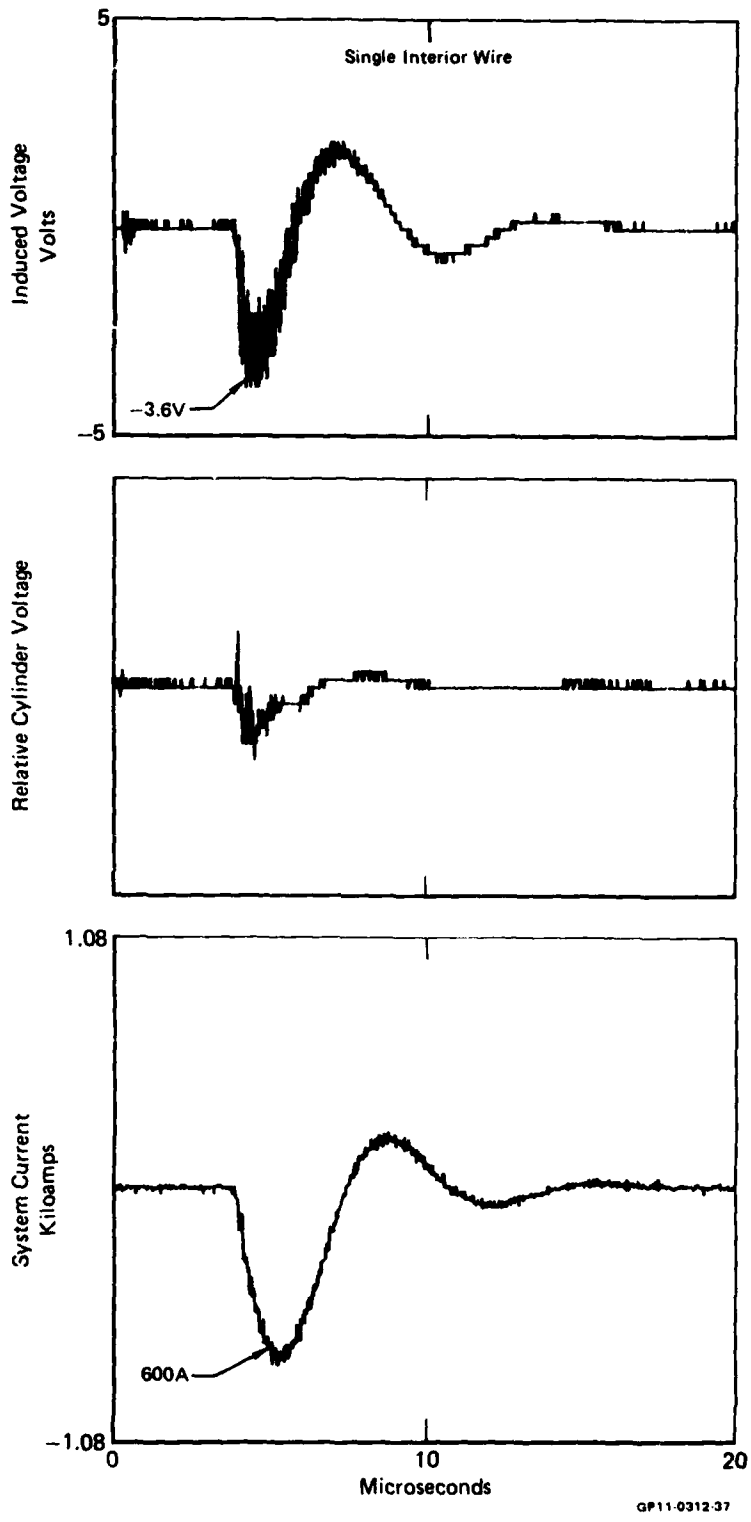
70

FIGURE 42. CYLINDER WITH COAXIAL RETURN
Hard-Wired Output, Interior Wire Shorted to Cylinder

71
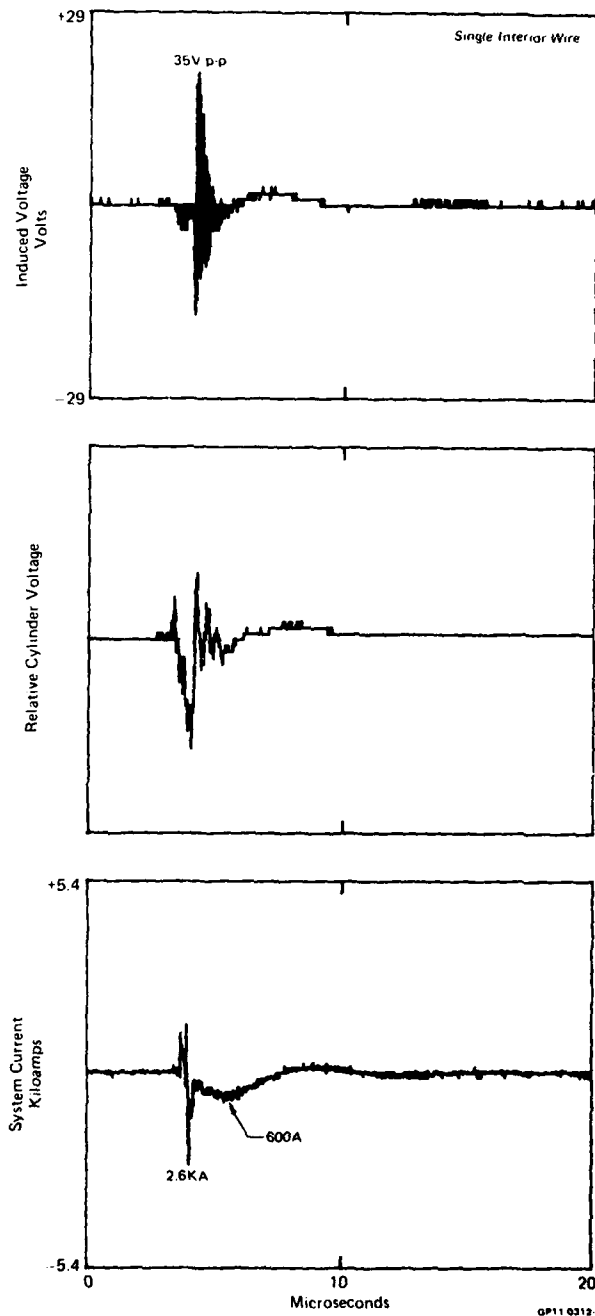
FIGURE 43. CYLINDER WITH COAXIAL RETURN 6-INCH SPARK GAP,
INTERIOR WIRE SHORTED TO CYLINDER
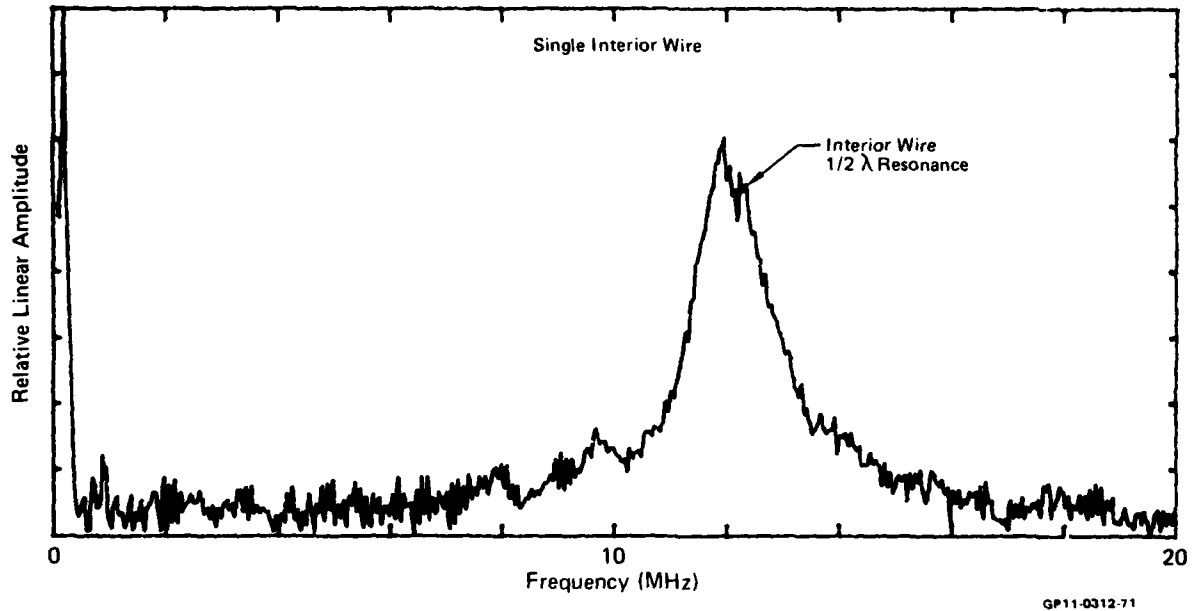
FIGURE 44. INDUCED VOLTAGE FREQUENCY RESPONSE
Interior Wire Shorted to the Cylinder

4. Induced Transients of YF-16 Flight Control Circuits

The induced transients of three YF-16 flight control circuits were measured using both the current pulse and shock-excitation test techniques. A diagram and photographs of the test setup are presented in Section III.2. The initial system inductance of the generator/aircraft/sheet return circuit was 30 µh. Two wire-wound coils (350 µh total) were added between the generator and the air-craft's pitot tube to slow the current rise time to 1.85 µs, which is compar-able to the 2-µs rise time used in past current pulse test programs. Three generator voltage levels (240, 360, 520 kV) were used to produce peak under-damped system currents of approximately 720, 1080, and 1550 amps, respectively.

The only configuration difference between the shock-excitation and current pulse test techniques was the presence or absence of a spark gap in the output connection between the engine exhaust duct and the coaxial sheet return con-ductors. A 6-inch spark gap was used in most tests. The voltage breakdown threshold of the 6-inch gap was approximately the same value regardless of the generator charge voltage, and limited the voltage applied to the aircraft to

73

about 300 kV. Varying the generator voltage from 240 to 520 kV produced no more than a 20 percent change in the breakdown voltage. The exact percent change could not be accurately determined due to the increased level of high-frequency noise that was present on the E-field sensor output for the 520 kV generator voltage.

The yaw and the left and right flaperon circuits of Branch C were tested. All three flight control servos were supposed to contain identical position linear voltage differential transformers. The transformers have three separate primaries and one secondary winding. The primaries are driven by op-amps in the flight control computer. The secondary is a position sensor which supplies position feedback information to the computer control circuit. The circuits tested were one of the three redundant branches from the computer to the servos primaries. The design characteristics of each servo is 0.2 henries inductance and 35 ohms DC resistance. At megahertz frequencies, the large inductive load has a very high impedance.

The tested YF-16 had previously undergone many lightning test programs. Some circuits may have been damaged or modified during this previous testing. For example, one open yaw circuit was found during preliminary checkout of possible test circuits. A second example was the significant difference in the circuit characteristics of the right flaperon circuit (see Table 1 in Section IV). The yaw and left flaperon circuits had nearly identical values for their pin-to-pin (81 ohms) and pin-to-airframe (100 and 181 ohms) resistances. The right flaperon circuit had one of its differential wires shorted to the airframe and 476 ohms pin-to-pin resistance. The wire shorted to the airframe causes the differential right flaperon circuit to have some common mode transient characteristics that differed from the responses of the other two circuits.

a. Waveform Comparison - Figures 45 and 46 show the typical system and induced voltage response of the right flaperon circuit for the two test techniques. These tests were conducted with a generator output voltage of 240 kV, and their only difference is that a 6-inch output spark gap was used for the shock-excitation case.

The aircraft response to the two test techniques is very similar to that discussed in the cylinder tests (Figures 35 and 36). Again the simple output
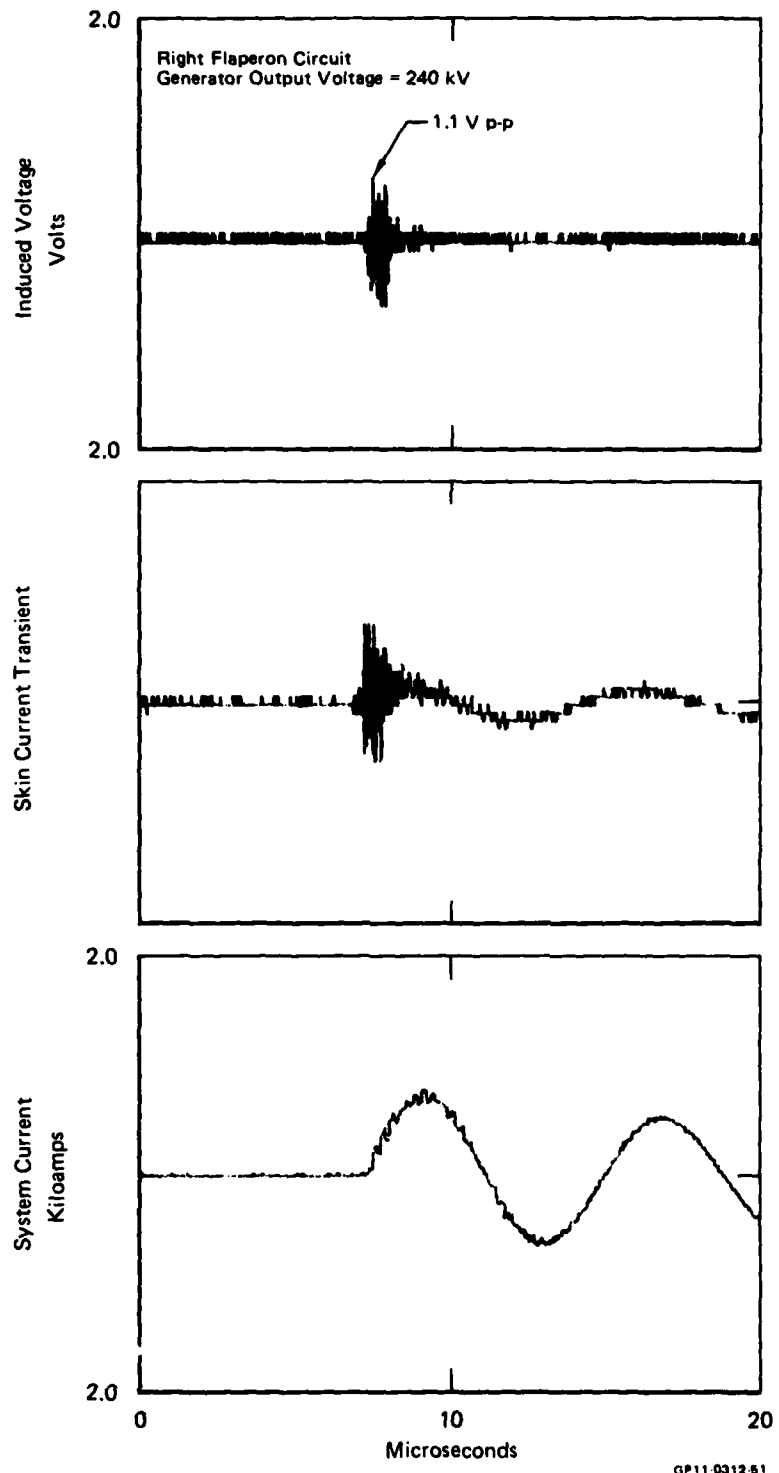
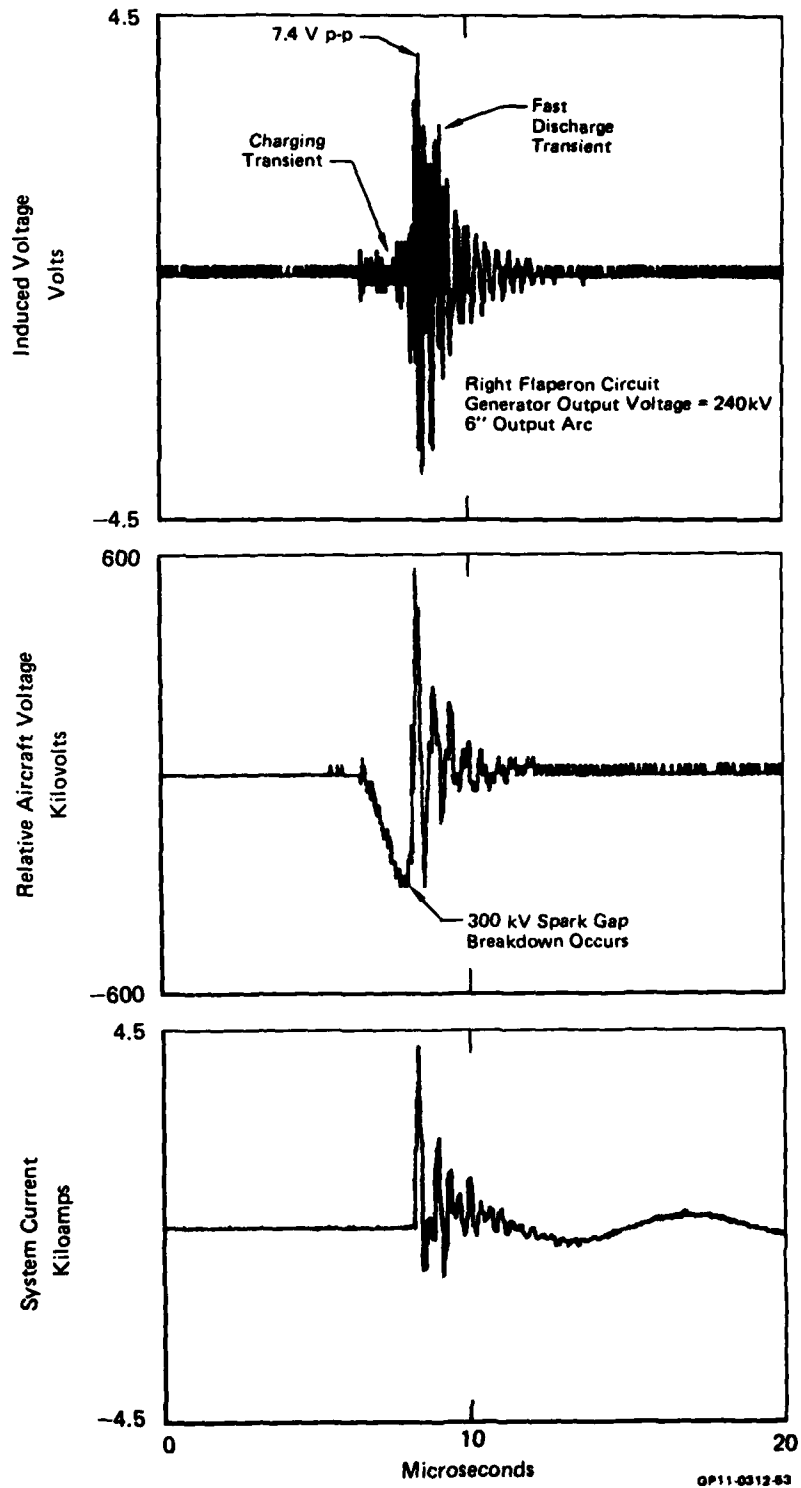FIGURE 45. TYPICAL YF-16 TEST WITH HARD-WIRED OUTPUT

FIGURE 46. TYPICAL YF-16 TEST WITH SPARK GAP OUTPUT

configuration change produces very different system and induced voltage responses. The shock-excitation case shows the aircraft charging to high voltage followed by fast discharge that modulates the slower generator discharge. The induced voltage responses have only a high-frequency oscillatory response like the high impedance capacitively-coupled cylinder circuits. They do not contain any slower dv/dt component typical of inductive coupling. The induced voltage response for the hard-wired output is the circuit's free response to a stimulus that occurs as soon as the generator is triggered. The high-frequency free response (FFT peaks at 14, 17, and 22.5 MHz) is totally damped before the first quarter cycle is completed. The induced voltage response for the spark gap output is excited to its peak amplitude by the fast discharge and is exponentially damped. The principal frequency of the shock-excited response is a 3.2-MHz transmission line resonance also seen on the aircraft voltage and current waveforms. This "forced" response at the exterior circuit's resonance occurred only for the right flaperon circuit which had one wire shorted to the airframe. The differential yaw and left flaperon circuits had a similar induced voltage waveshape but included only the high-frequency response (17 to 25 MHz) characteristic of the interior circuit and not the 3.2-MHz response of the exterior circuit. Increasing the generator output voltage had no effect on the system or induced voltage waveshapes.

b. YF-16 Current Pulse Tests - Current pulse tests were run on each of the three flight control circuits at three generator voltage levels. Three shots were generally run for each test case to determine the extent of the data scatter. The system current (in the output wires between the engine duct and the return conductors), the skin current (on the forward fuselage above the air inlet), and the induced voltage (near the computer end of the circuit) were measured for each case. The system current (Figure 45) contained a low-level 3.2- and 4.0-MHz modulation due to transmission line reflections caused by the shorted output. The skin current response displays both a high-frequency transient at the generator firing and the slower system current response.

The hard-wired shots at 240 kV were the first test sequence run on the aircraft besides the preliminary system checkout shots. These initial tests gave widely scattered values for the induced voltages and skin current levels. The

total system current was nearly identical for all shots, but the current distribution in the aircraft was varying from shot to shot, as indicated by the inconsistent skin current and induced voltage responses. As testing proceeded, the data scatter reduced. This finding indicated that the current distribution around the fuselage was becoming more repeatable. The initial hard-wired tests at 240 kV were repeated near the end of the aircraft tests, and the data were far more consistent.

The current pulse test data are summarized in Figure 47. The figure shows a general upward trend of the measured induced voltage plotted versus the applied system current, but the "best-fit" lines do not pass through zero as would be expected in a direct linear relationship. The impulse-excited form of the induced voltage response indicates that turn-on characteristics are the important parameters. More testing would be required to determine the coupling mechanism for this complex system; however, analogy to the simple cylinder tests would indicate that capacitive coupling should dominate for the high-impedance flight control circuits. If capacitive coupling is dominant, then the induced voltage response would be dependent on the free circuit response of the interior wire when it is excited by the d^2I/dt^2 impulse at generator triggering.

c. <u>YF-16 Shock-Excitation Tests</u> - The aircraft shock-excitation tests produced system responses similar to those of the cylinder tests. The aircraft discharge transients are dominated by transmission line reflections that strongly modulate the RLC response. The magnitudes of dI/dt and dV/dt for the fast discharge approach the accepted "full threat" levels of 10^{11} A/s and 10^{12}, respectively. Figure 46 is a typical shock-excitation test. (Appendix A provides more waveform detail, since these data were used to demonstrate the data manipulation capabilities of the data acquisition computer.)

As previously mentioned, most of the shock-excitation tests were conducted with a fixed 6-inch output spark gap that limited the aircraft's voltage at breakdown. The E-field sensor (positioned aft of the wing and ≈20 feet from the fuselage) indicated that the relative breakdown voltage was approximately constant, while the current transformer (immediately aft of the spark gap) showed that the magnitude of the fast current oscillations increased with
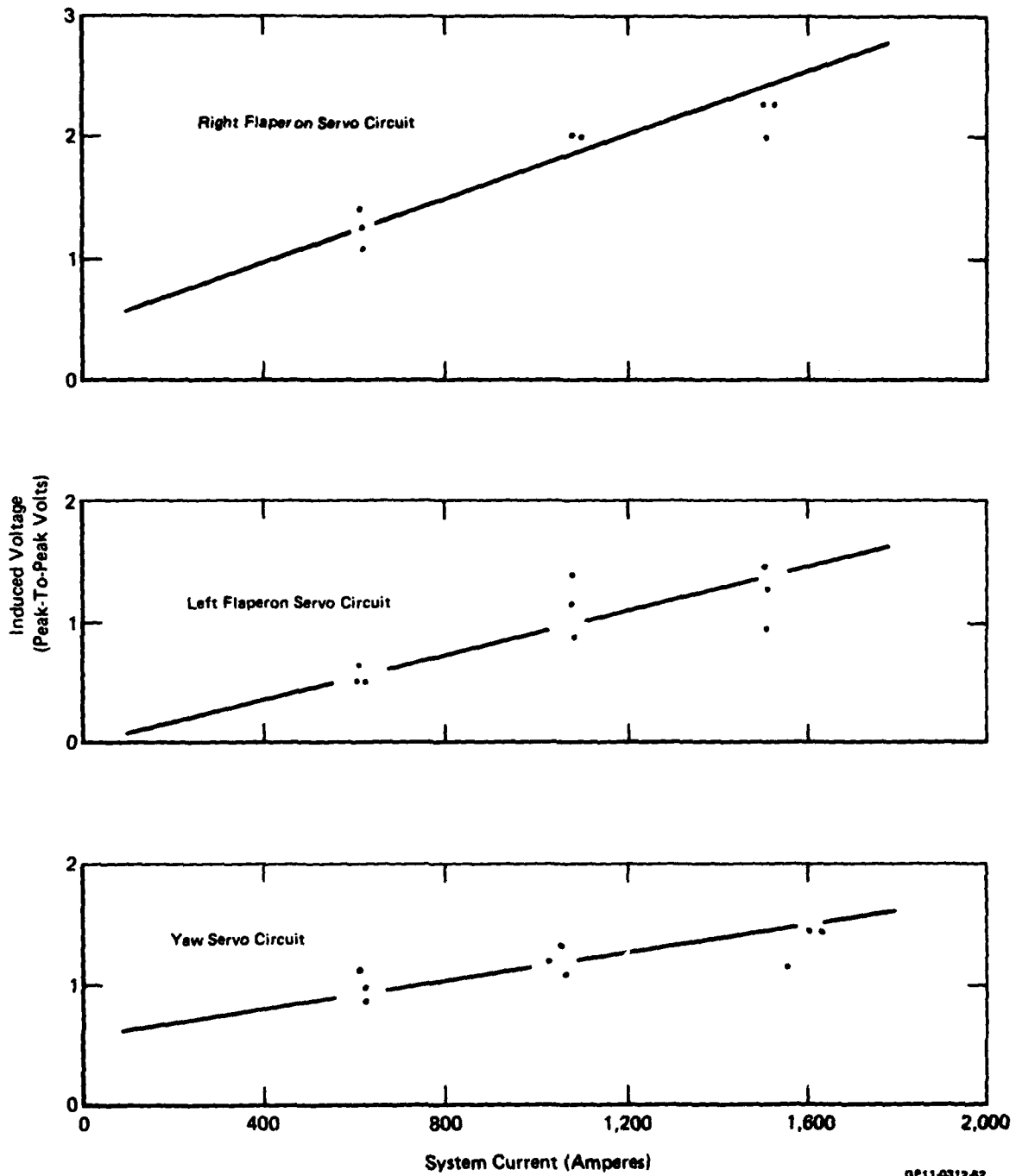
FIGURE 47. YF-16 INDUCED-VOLTAGES VERSUS CURRENT
Current Pulse Test Configuration

higher generator potential. If the output arc impedance is independent of the generator (as one would expect), then the magnitude of the current pulse should not vary as long as the breakdown potential remains constant. Why the current pulse consistently increased with higher generator voltages in these tests is not understood from the available data and would require more detailed testing.

Table 5 presents a summary of the induced voltages and current pulse levels for the three generator output voltages. The induced voltage levels were quite low. The peak-to-peak magnitudes were generally less than five times the hard-wired values even though the transmission-line effects produced very high dV/dt and dI/dt levels. The tests show that the yaw circuit induced voltage increased like the current pulse, while the right and left flaperon circuits remained relatively constant for the three generator charging levels.

TABLE 5. INDUCED VOLTAGE LEVELS FOR YF-16 SHOCK-EXCITATION
DISCHARGE (6-INCH SPARK GAP)

Generator Output Voltage	240 kV		360 kV		520 kV	
Circuit Monitored	Induced Voltage (V)	Current Pulse (Peak) (A)	Induced Voltage (V)	Current Pulse (Peak) (A)	Induced Voltage (V)	Current Pulse (Peak) (A)
Yaw Servo	$3.84\,^{+0.12}_{-0.09}$	4,100	$4.21\,^{+0.18}_{-0.19}$	4,840	$5.05\,^{+0.25}_{-0.48}$	5,600
Right Flaperon	$7.89\,^{+0.47}_{-0.38}$	4,100	$7.55\,^{+0.12}_{-0.05}$	4,900	$7.44\,^{+0.22}_{-0.12}$	5,600
Left Flaperon	$3.78\,^{+0.04}_{-0.09}$	4,100	$3.71\,^{+0.13}_{-0.24}$	5,120	$3.96\,^{+0.24}_{-0.30}$	6,000

GP11-0312-87

The somewhat different responses of the three flight control circuits were not further investigated in this test configuration. The preliminary resistance checks had shown the yaw and left flaperon circuits to be electrically similar and the right flaperon to have one lead shorted to the airframe. No attempt was made to fully characterize each circuit in this limited YF-16 test program.

To determine the effect of changing the aircraft voltage at breakdown, a test sequence was run on the right flaperon circuit. In this sequence, the generator output voltage was held constant (240 kV), and the spark gap distance was varied. Figure 46 is the 6-inch spark gap case, and Figure 48 shows the

E-field sensor data for the 3- and 9-inch spark gaps. Similar sequences were tried at higher generator voltages, but arcing occurred between the wings and the nearby return conductor and prevented data from being obtained for spark gaps longer than 6 inches.
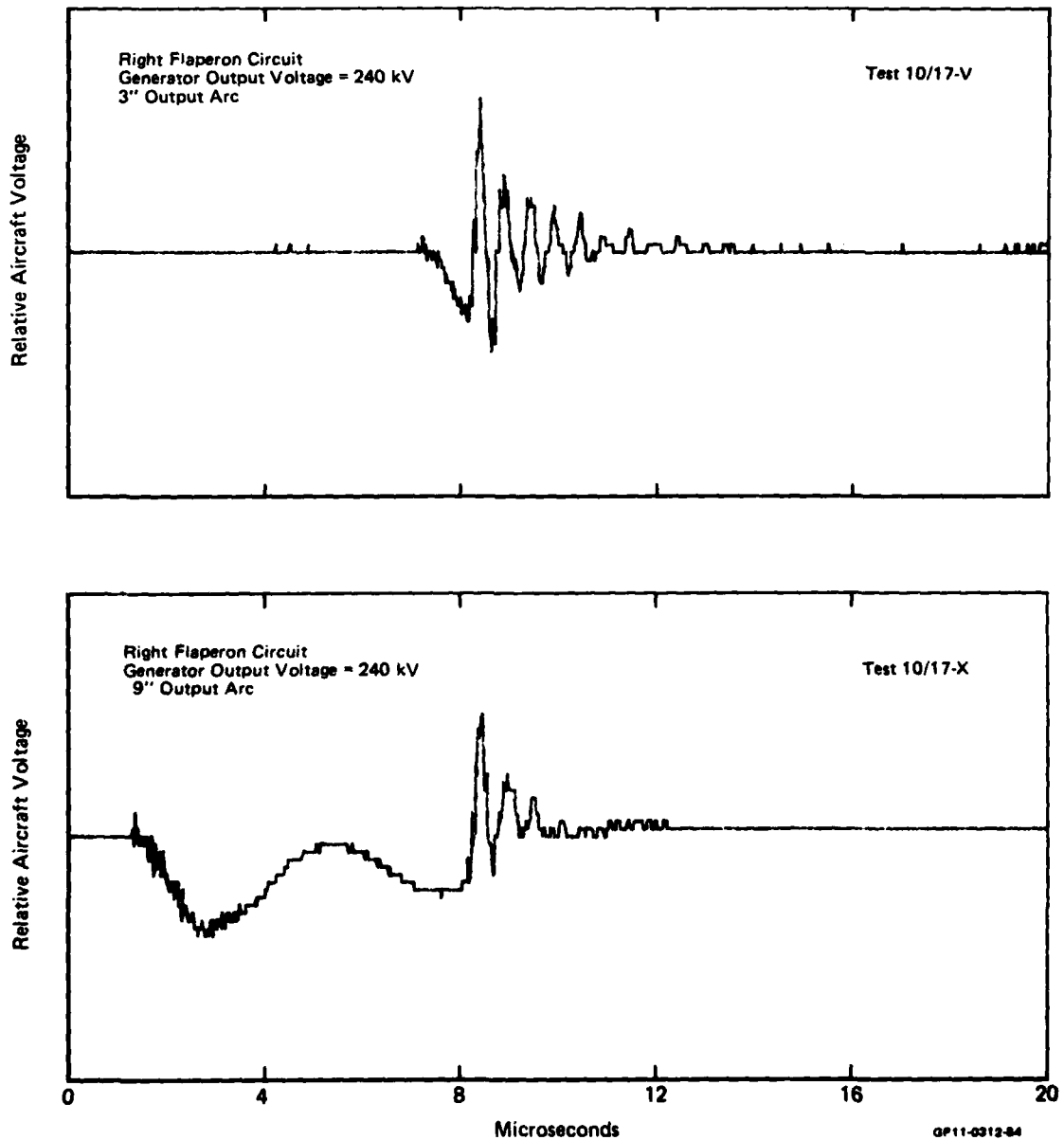

FIGURE 48. YF-16 VOLTAGE WAVEFORM VARIATION WITH OUTPUT ARC LENGTH

The results of this test sequence are shown in Table 6. For this case, the normalized rates of change for system current and voltage are nearly identical, and both rates of change closely track the right flaperon induced voltage response. Either capacitive or inductive coupling would excite such a response.

Without a more detailed test program, it is difficult to generalize the shock-excitation test results from the limited data base. From an analogy to the cylinder tests and analysis, one would expect that capacitive coupling should be the dominant coupling mechanism in the high impedance differential circuits; however, in the shock-excitation case, the transmission-line dominated discharge current and voltage are closely related, and, therefore, it is difficult to separate the coupling contributions.

TABLE 6. RIGHT FLAPERON INDUCED VOLTAGE VARIATION
WITH SPARK GAP LENGTH

Test	Induced Voltage (V)	Normalized[1] Induced Voltage	Normalized[1] dV/dt	Normalized[1] dI/dt
10/17 U	7.51	1.00	1.00	1.00
10/17 V	5.67	0.75	0.77	0.77
10/17 W	4.68	0.62	0.57	0.57
10/17 X	5.04[2]	0.67	0.59	0.54

Notes: 1. Normalized to 10/17 U values

2. Excluding a nonrepresentative voltage spike.

GP11-0312-58

The presence of capacitive coupling is supported by the fact that induced voltage waveshapes for the aircraft tests are similar to those of the cylinder tests and contain no slower $d\phi/dt$ component. The right and left flaperon circuits showed no induced voltage variation when the breakdown potential (and therefore dV/dt) was held fixed by the 6-inch output spark gap. In addition, the right flaperon induced voltage varied linearly when the voltage and current rates of change were varied by changing the output spark gap distance.

The only data that does not support the presence of capacitive coupling is the variation of the yaw circuits induced voltage when the output spark gap was held fixed. Figure 49 is a log-log plot of the induced voltage of the yaw circuit versus dI/dt. The maximum dI/dt for the hard-wired tests occurs near $t = 0$ and varied from $\approx 5 \times 10^8$ to $\approx 2 \times 10^9$ A/s, while the maximum dI/dt for the shock-excitation case are transmission-line excited and varied from $\approx 5 \times 10^{10}$ to $\approx 2 \times 10^{11}$ A/s. Thus, two orders of magnitude change in dI/dt resulted in only a three-time increase in the induced voltage. This apparent weak scaling with dI/dt [proportional to $(dI/dt)^{1/4}$] can, however, be quite misleading. Even though the trend appears well-established by the five data sets, the impact of several factors must be recognized. First, the discharge stimulus for the current pulse and shock-excitation cases are very different and dI/dt is not the only varied parameter. Secondly, the current's time rate of change was measured in the output line and not at the location of the circuit coupling (wherever that may be), and the relative magnitudes of transmission-line dependent voltage and current stimuli are position dependent. Thirdly, the induced voltage response for the current pulse technique has no resemblance to the driving current waveform, yet the voltage magnitudes are plotted against dI/dt. These factors (like others) point out the complexities of understanding induced voltage measurements and attempting to derive appropriate scaling laws.
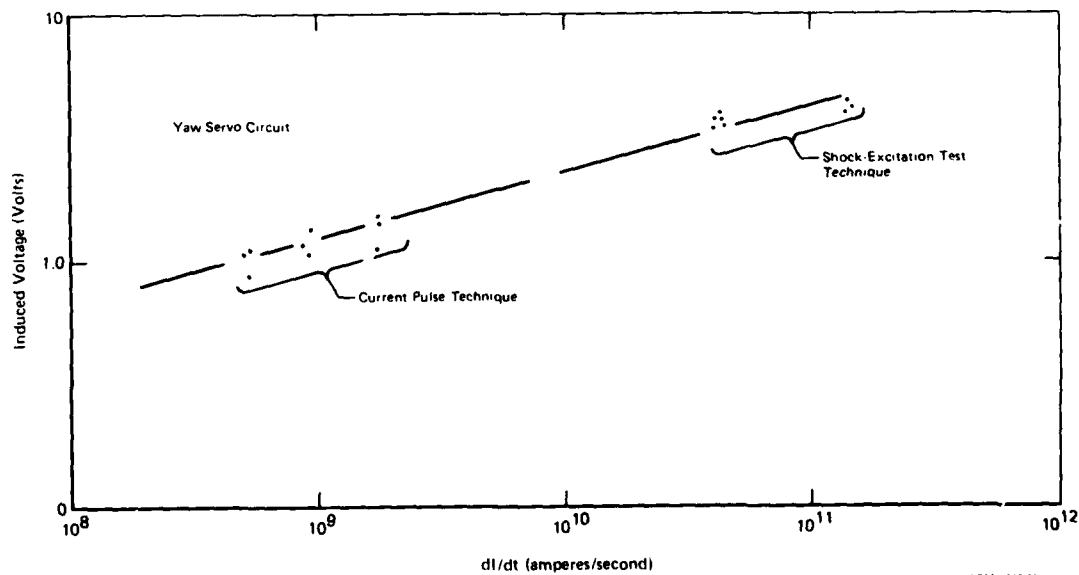

FIGURE 49. INDUCED VOLTAGE OF THE YAW SERVO CIRCUIT VERSUS dI/dt

In summary, the YF-16 system current and voltage responses to the shock-excitation technique are similar to those of the simple cylinder. The induced voltage responses of the more complicated flight-control circuits have the same general waveshape as their cylinder counterparts; however, a clear understanding of the coupling mechanisms involved must be deferred to more detailed testing.

d. **YF-16 Frequency Domain Summary** - The frequency domain characteristics of the aircraft transient responses were obtained by fast Fourier transformation of the digitally recorded data traces. In addition, the characteristic line lengths of the aircraft/return transmission line and the three interior circuits were measured by time domain reflectometry (TDR). The data, presented in Table 7, show that line length resonances are important for the aircraft/return transmission line, but do not appear important to the response of the interior circuits.

TABLE 7. YF-16 FREQUENCY DOMAIN SUMMARY

	TDR Down and Back Time (ns)	Projected Frequency Peaks		Measured Frequency Peaks (FFT), (MHz)
		$\lambda/2$ Freq (MHz)	$\lambda/4$ Freq (MHz)	
Aircraft/Return	$\simeq 200^*$	5.0	2.5	2 or 4**, 3.2
Yaw Servo	150	6.6	3.3	17, 18, 7, Others
Left Flaperon Servo	120	8.2	4.1	17, 10, 12.5, Others
Right Flaperon Servo	120	8.2	4.1	17, 3.2, Others

* Transit time is not well defined since the line impedance varies substantially along the fuselage.   QP11-0312-69

** 4 MHz resonance for hard-wired output, 2 MHz resonance for spark gap out; RLC system resonance dominates the FFT

The flight-control circuits have complicated induced voltage spectra with high-frequency oscillations dominating any lower frequency components. The spectra for hard-wire and spark gap output are generally comparable; however, the spark gap spectra are more complex. The spectra do not correlate with higher order quarter-wavelength resonances (like the cylinder tests) or with series resonances caused by the large servo inductance. The commonality of the 17 MHz peak does indicate that the size or location of a coupling aperture

could be the cause. No attempt was made to locate the source.

During disassembly of the YF-16 test setup, a few tests were run with the electrostatic shield removed from the generator. The shield was directly in front of the aircraft and within two feet of the coaxial sheet returns. The presence of the shield had a significant effect on the effective impedance of the generator end of the aircraft/return transmission line, as shown in Figures 50 and 51. Figure 50 shows the typical system current transient for the output spark gap configuration with the electrostatic shield in position. Figure 51 is the response for the same output condition with the shield removed. Both the waveshape and the frequency response of the transmission line system are changed significantly. Since the current and cylinder voltage resonances establish the characteristic system period, this frequency and waveform shift could have a significant effect on the values of dV/dt and dI/dt experienced by the aircraft. The effect of the electrostatic shield on the aircraft/return transmission line must be considered in the design of future aircraft tests where transmission line resonances are important.
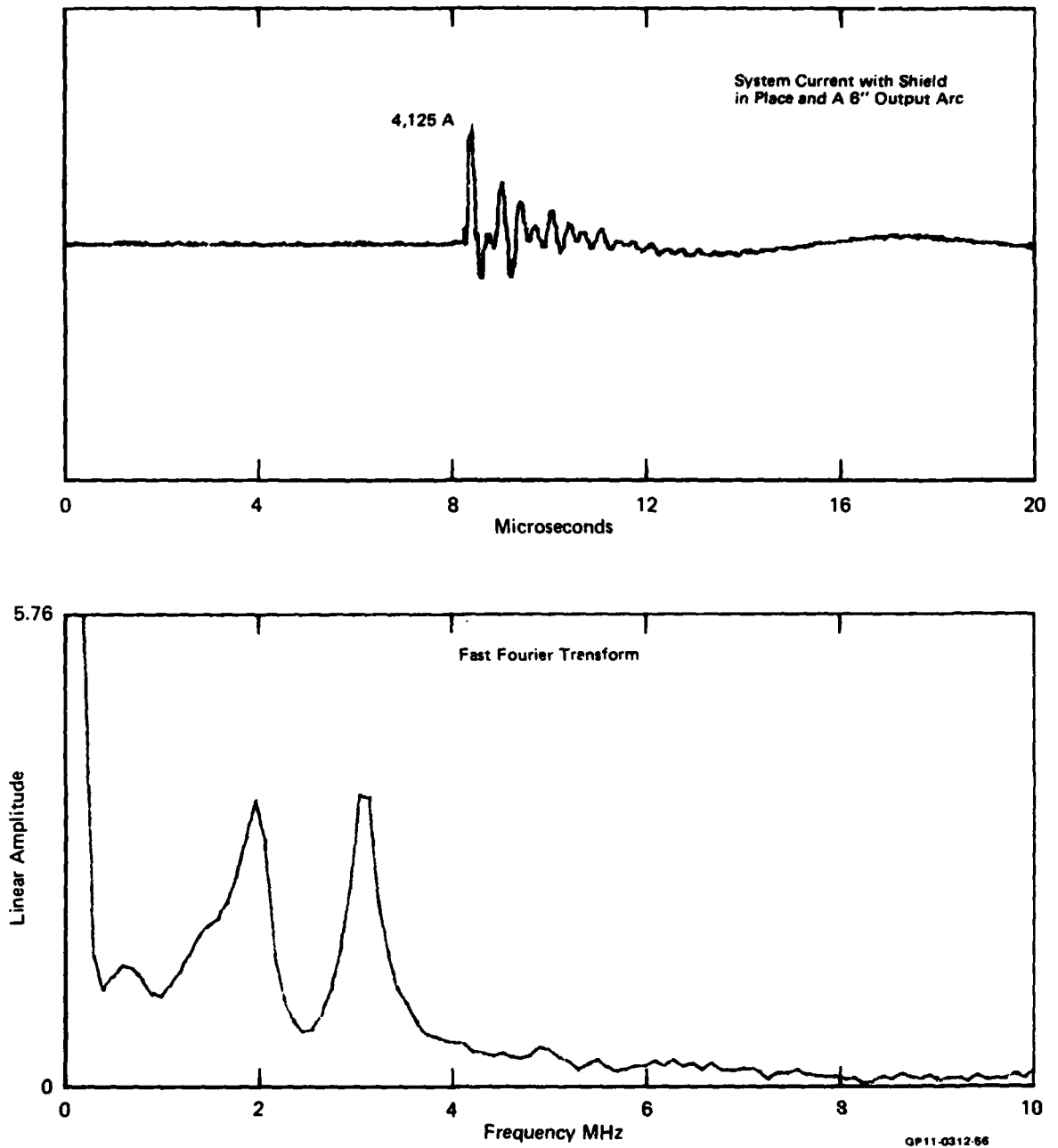
FIGURE 50. SHOCK-EXCITATION SYSTEM CURRENT WITH SHIELD IN PLACE

1.0

1.1

1.25 1.4 1.6
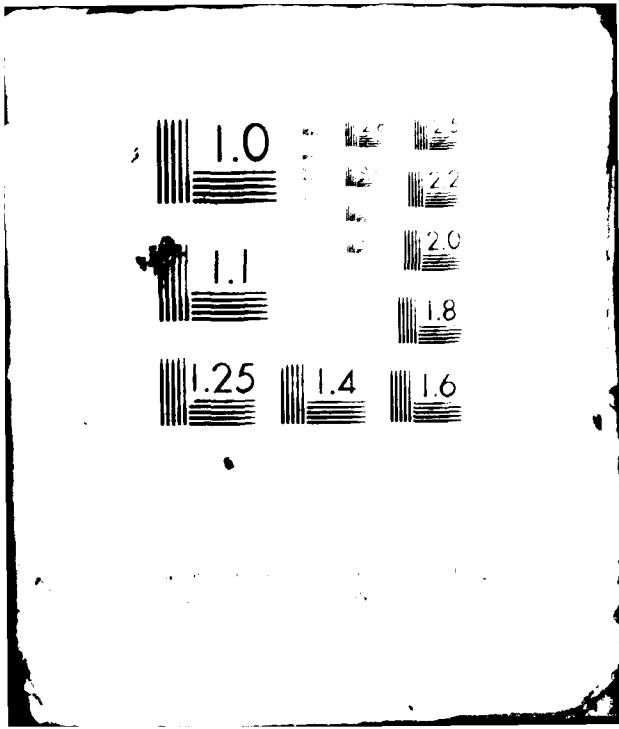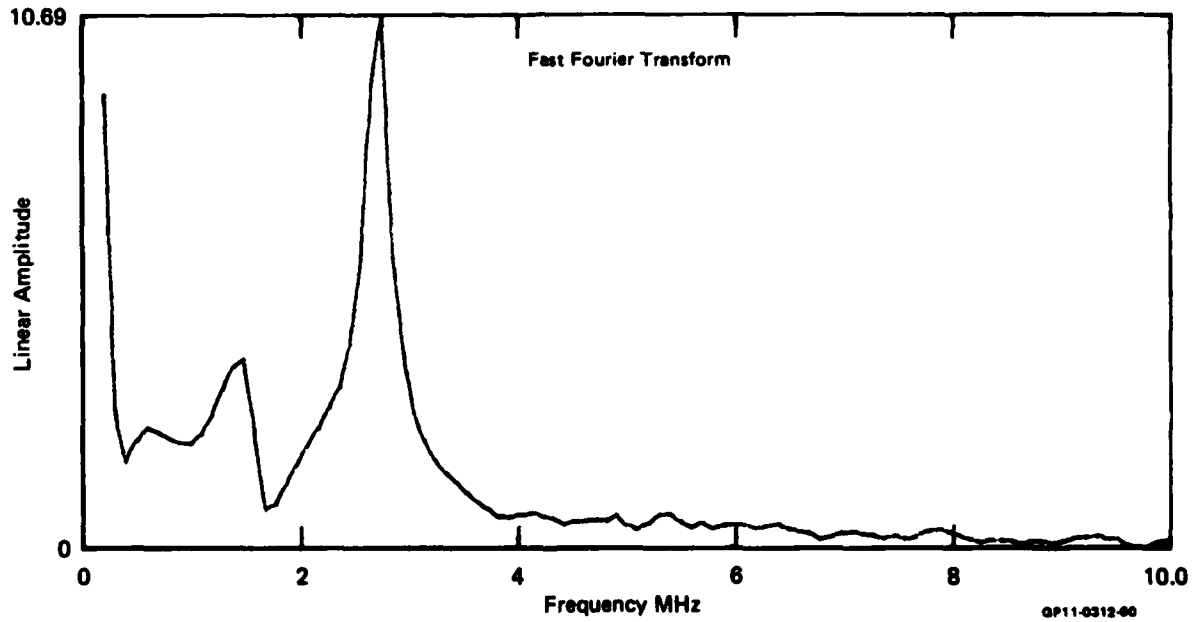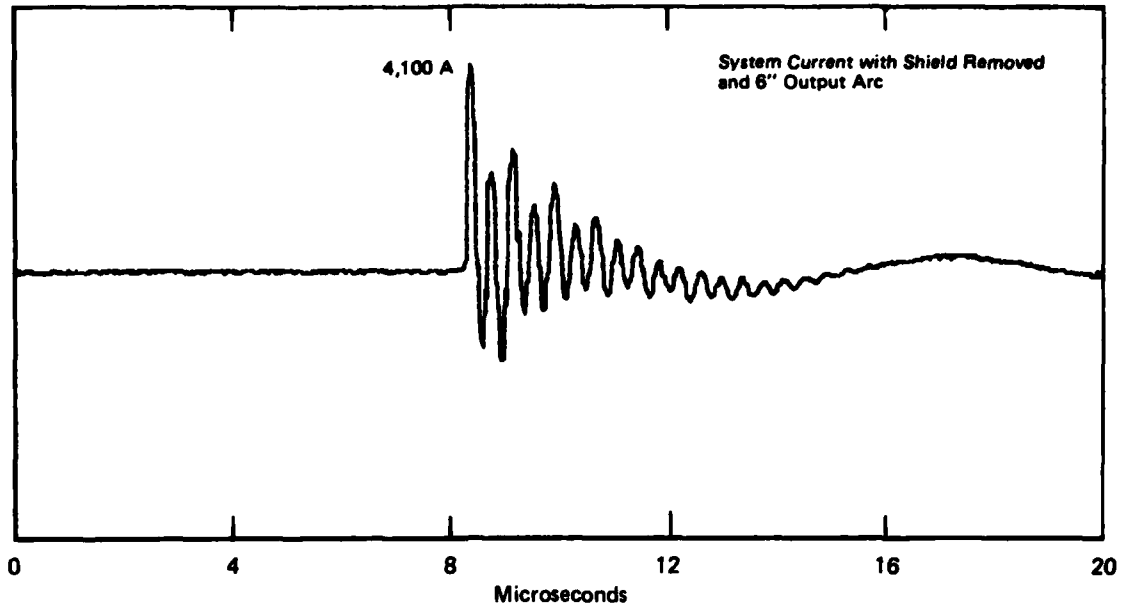
2.2

2.0

1.8

FIGURE 51. SHOCK-EXCITATION SYSTEM CURRENT WITH SHIELD REMOVED

SECTION VII
CONCLUSION

The program objective was to assess the current pulse and shock-excitation test techniques on both a simple cylindrical structure and the YF-16 fighter aircraft. The comparison was made on high-impedance differential wire pairs typical of many flight critical circuits in use in advanced aircraft. The current pulse technique applies primarily a current stimulus to the test article, while the shock-excitation technique first charges the test article with displacement currents and then applies a rapid voltage/current pulse when the spark gap breaks down. The fast discharge and its transmission line reflections have very high dV/dt and dI/dt oscillations that are capable of exciting larger induced voltages.

The analysis of the cylinder test configuration demonstrated that both test techniques could be modeled as two coupled transmission line circuits. The transmission lines may incorporate either distributed or lumped components. Simple RLC circuit modeling was sufficient to predict the induced voltage behavior during cylinder charging tests. The more complicated models were necessary to describe the transmission line effects that are important for the discharge transients. A time-dependent arc impedance was required to provide the damping observed when the output spark gap was incorporated into the system.

The analysis showed that for the cylinder test configuration capacitive coupling should dominate for high impedance circuits while inductive coupling would dominate for low impedance circuits that were not tested. Sensitivity studies showed that the aperture location, cylinder dissipation, cylinder characteristic impedance, and cylinder length were important parameters.

The flexible cylinder test configuration permitted complete separation of the shock-excitation charging transient. The charging transient agreed well with the waveshape and scaling predicted for capacitive coupling. Discharge transients were compared for the current pulse and shock-excitation test techniques. The current pulse tests produced low-level "free" circuit responses at generator triggering and no slower dφ/dt coupling. The shock-excitation tests produced an induced voltage charging transient followed by a larger

discharge transient initiated by the spark gap breakdown. For the same test conditions, the induced voltage for the current pulse test was approximately an order of magnitude less than that for the discharge transient of the shock-excitation test. The shock-excitation discharge transient scaled well with dV_{CYL}/dt for both generator voltage and arc length variations.

The YF-16 tests on the flight control circuits produced time domain waveforms that were similar to those of the cylinder tests. The complexity of the aircraft system was most evident in the frequency domain where system resonances could not readily be explained and in the test technique complications caused by the physical size and weight of the aircraft. The aircraft isolation from ground and the return conductors of approximately 300 kV did not permit the complete separation of the charging and discharge transients and limited the output spark gap to 6 inches for most tests.

The current pulse tests on the YF-16 produced only a fast oscillatory induced transient at generator triggering. The shock-excitation tests produced induced voltages only two to five times as large as the respective current pulse tests; however, the dI/dt of the fast discharge current was approximately two orders of magnitude larger than the initial current rate of change in the current pulse tests. Differences in the three circuits' responses and an apparent inconsistency in the fast discharge current and voltage data for the 6-inch arc tests complicate the understanding of the coupling mechanism and induced voltage scaling; however, capacitive coupling does appear to be important for the high impedance circuits tested.

More detailed shock-excitation tests are necessary to adequately access the induced voltage variation with different test parameters and circuit types. Near threat level rates of voltage and current change are produced during the fast discharge and its subsequent transmission line reflections. The relationship of the induced effects of the shock-excitation stimulus compare   those predicted for natural lightning is the primary objective in the future de. lopment of the shock-excitation test technique.

APPENDIX A
DATA ANALYSIS CAPABILITIES

Appendix A shows the various data representations that are used to analyze the test data. Figure A-1 is the standard output format. The rest of the figures are data manipulations of the standard output.

Since the data are sensed by digital transient recorders that are controlled by an HP 9825 microcomputer, both real time data analysis and storage of the digital signals on magnetic tape for future data reduction are readily accomplished. The computer software is structured so that one controlling program is used to call any of 28 subroutines to perform the basic data recording, display, storage, and processing tasks. Data manipulations such as signal averaging, grid expansions, fast Fourier analysis, and cross-power correlations are each accomplished with a single command.

For program flexibility all outputs are displayed in terms of the measured voltages. The voltage levels are converted to the appropriate current or field measurement values by multiplying by the sensitivity of the parameter's sensor. For this test, a conversion factor of 80 amperes per volt is required for the system current transformer, and approximately 4.3 kV (aircraft potential) per volt of E-field sensor output is required for the aircraft voltage measurements.
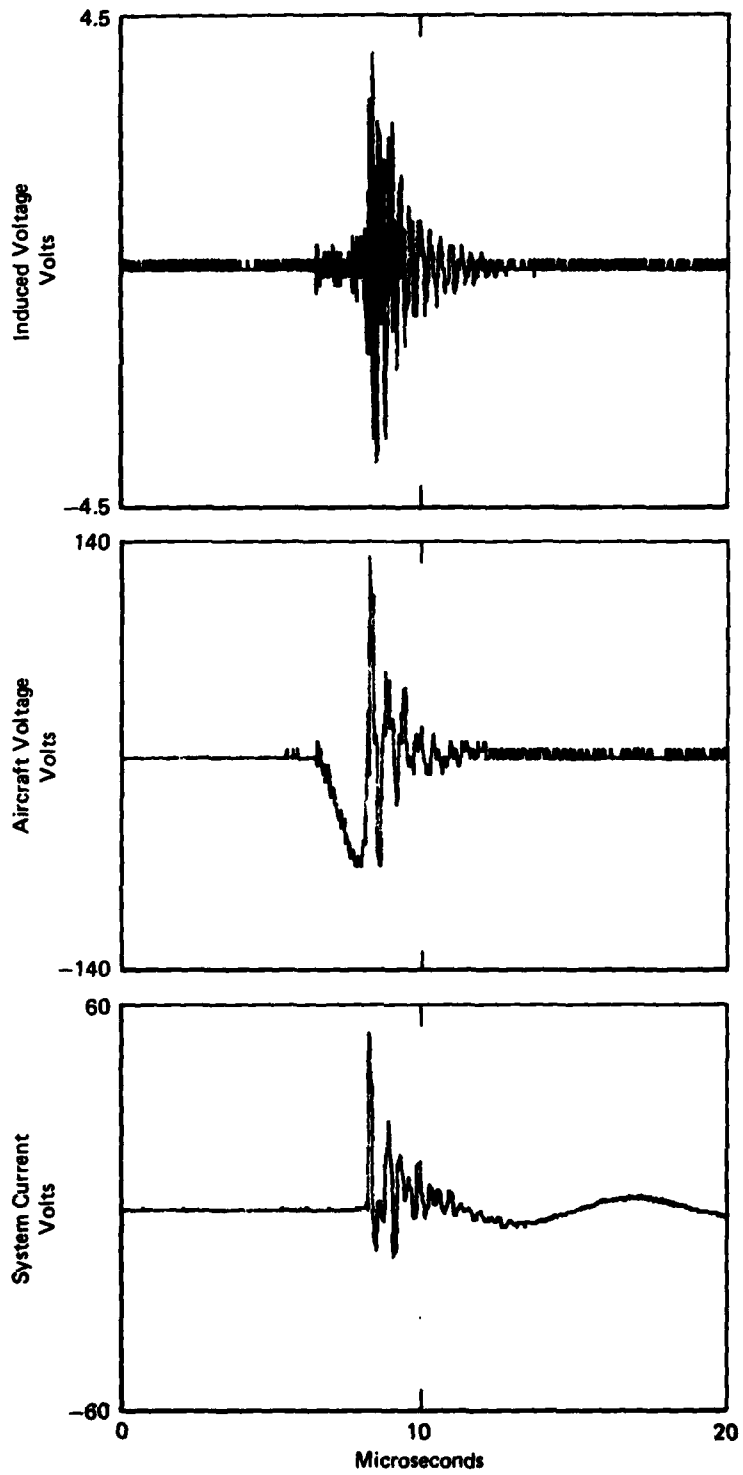
FIGURE A-1. STANDARD OUTPUT

OP11-0312-81
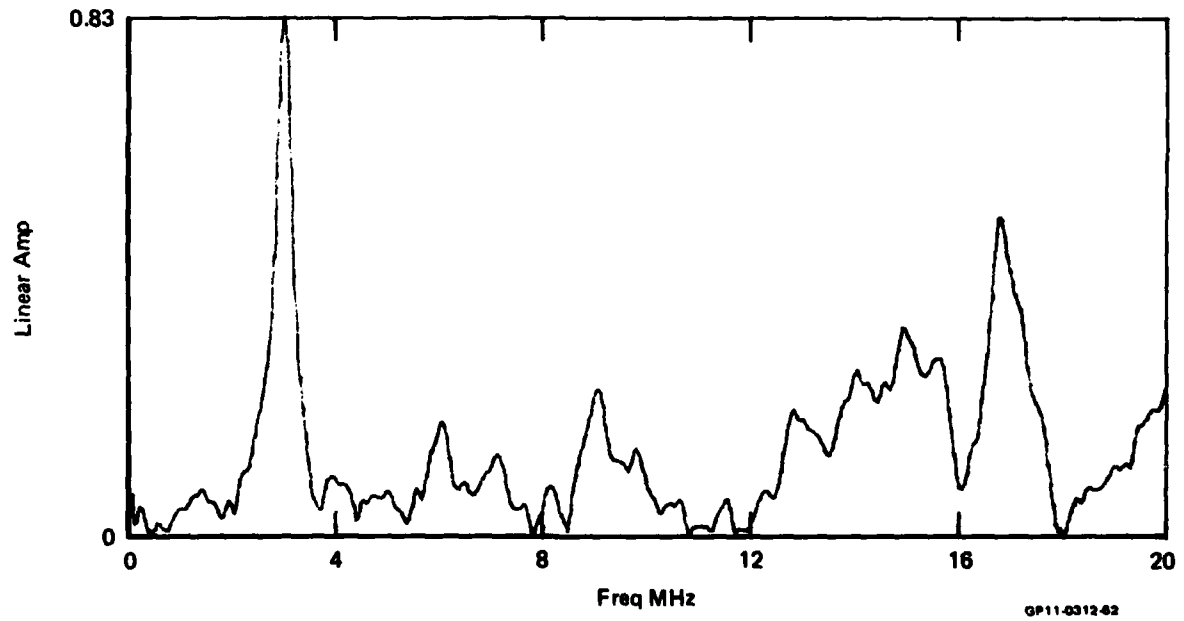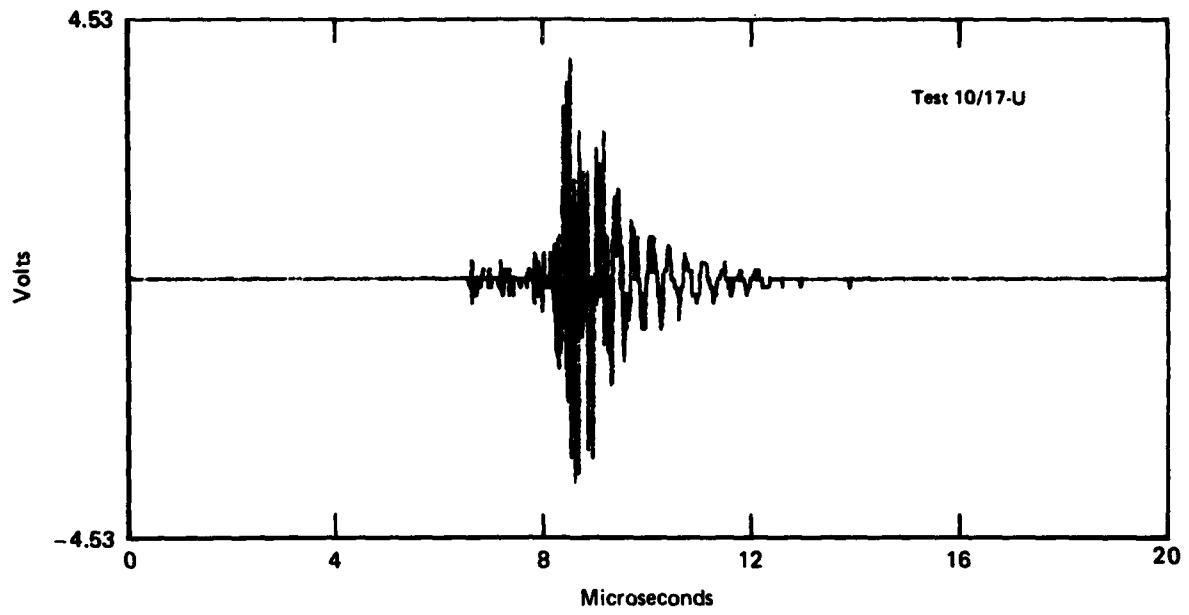
FIGURE A-2. INDUCED VOLTAGE AND ITS FAST FOURIER TRANSFORM
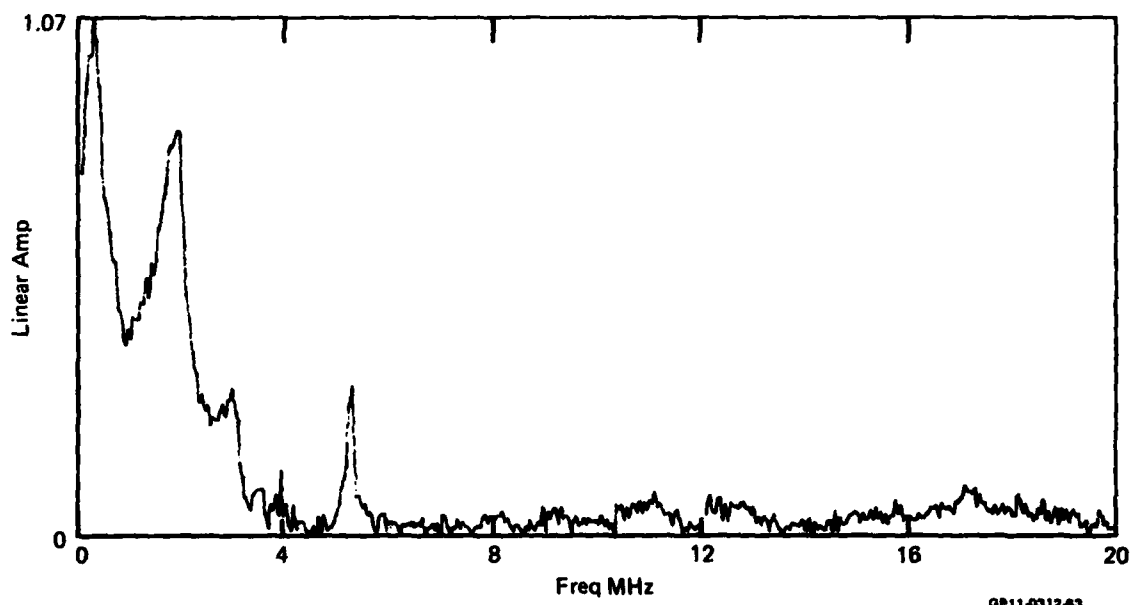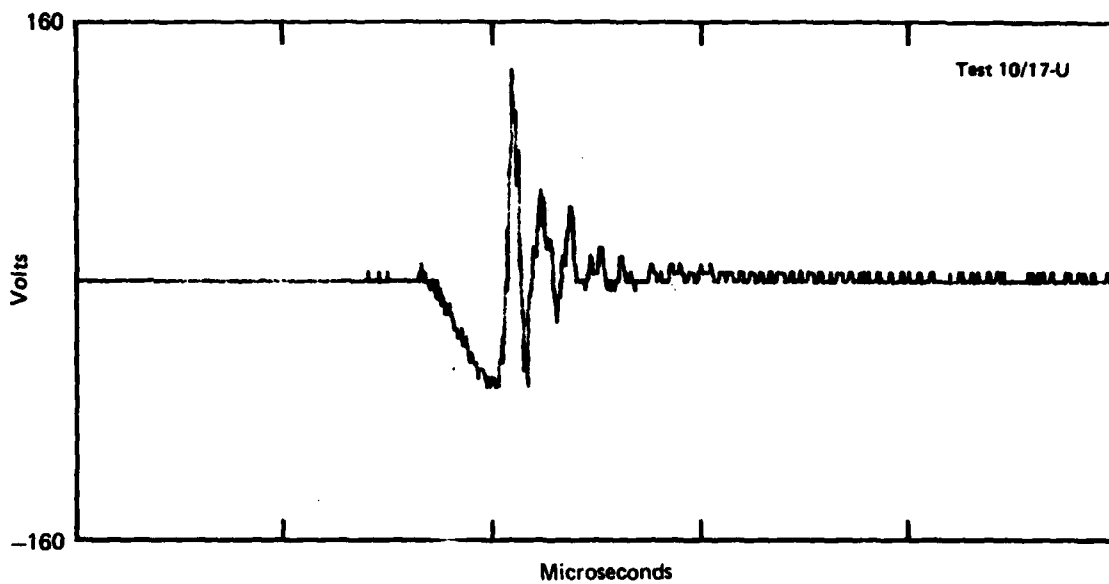
FIGURE A-3. AIRCRAFT VOLTAGE (AS MEASURED WITH THE E-FIELD
SENSOR) AND ITS FAST FOURIER TRANSFORM

94

Test 10/17-U
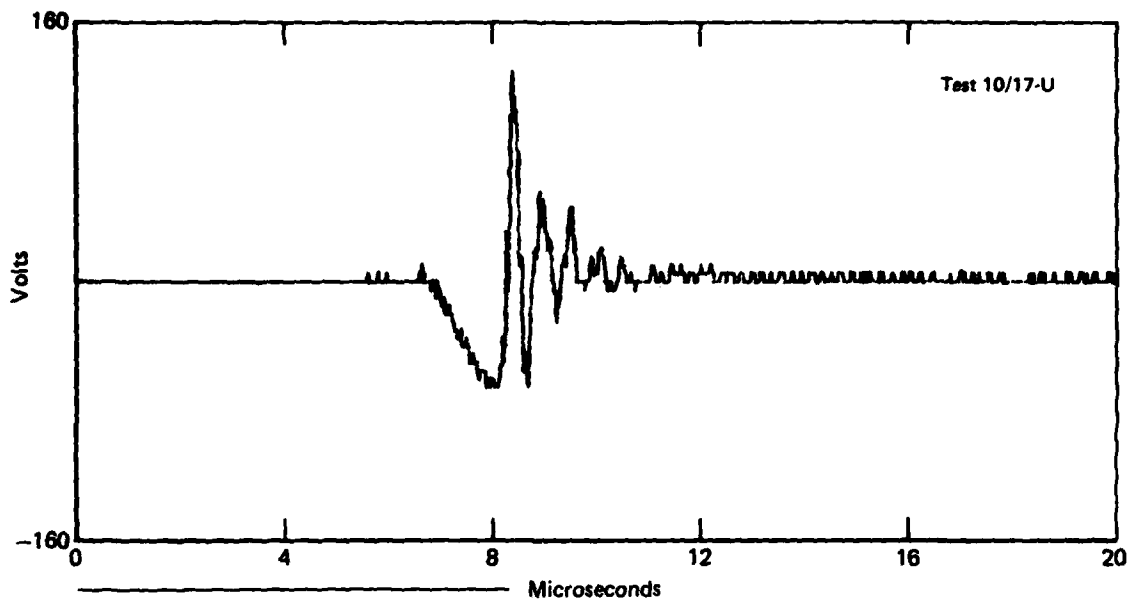
The portion of the transient which has a line
beneath it is zeroed before the transform is made.

FIGURE A-4. AIRCRAFT VOLTAGE AND A PARTIAL FAST FOURIER TRANSFORM

GP11-0312-64

FIGURE A-5. EXPANDED AIRCRAFT VOLTAGE WAVEFORM

FIGURE A-6. CROSS-POWER CORRELATION OF THE
INDUCED VOLTAGE AND AIRCRAFT VOLTAGE

96
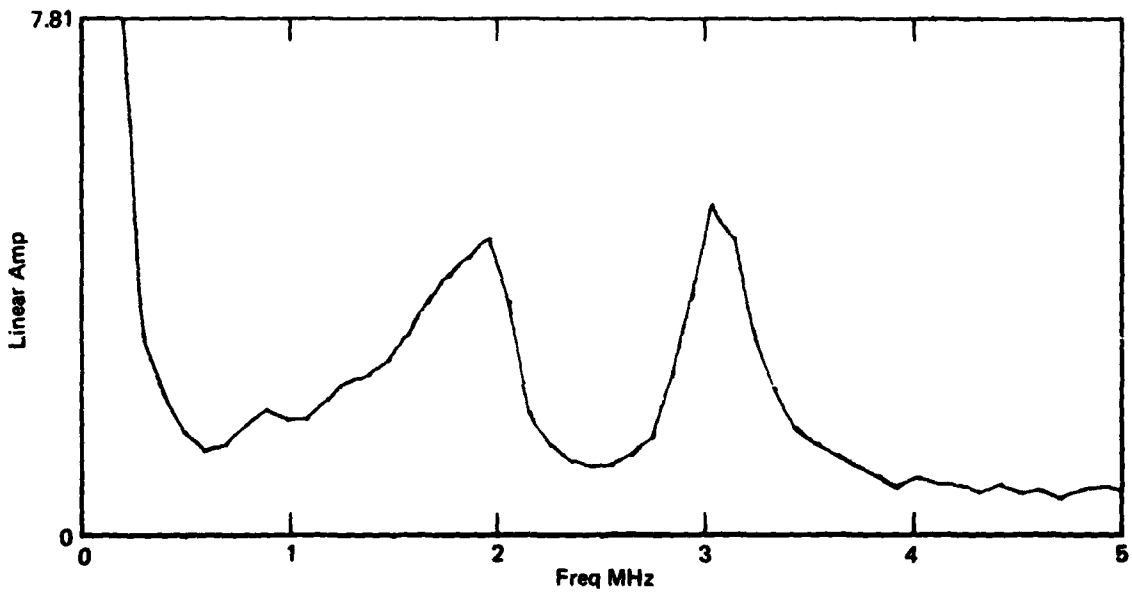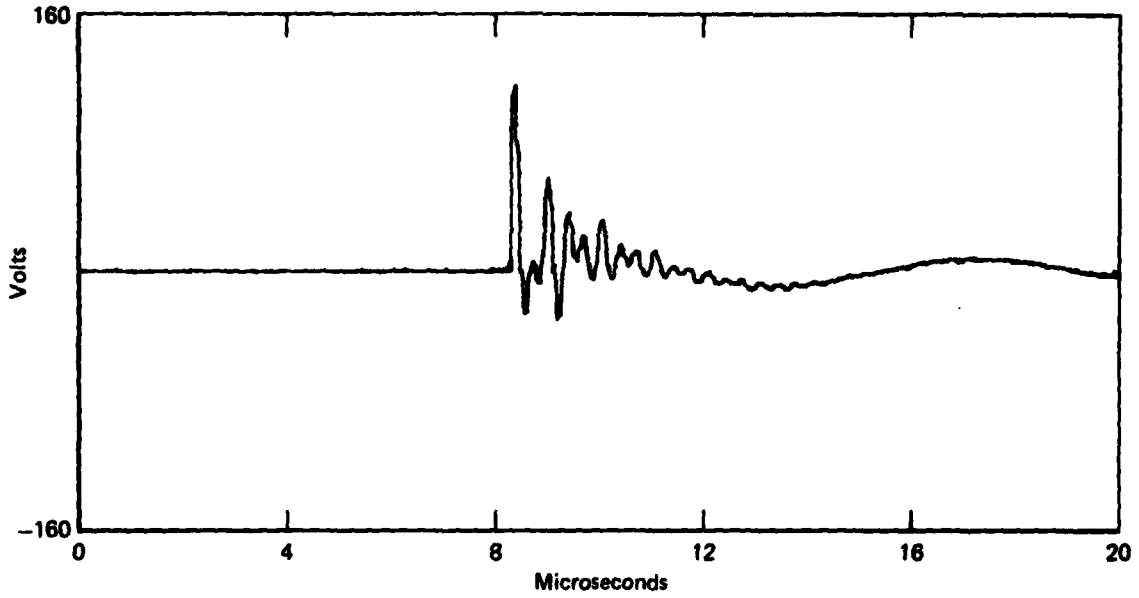
FIGURE A-7. SYSTEM CURRENT AND ITS FAST FOURIER TRANSFORM

APPENDIX B
ANALYTICAL DETAILS

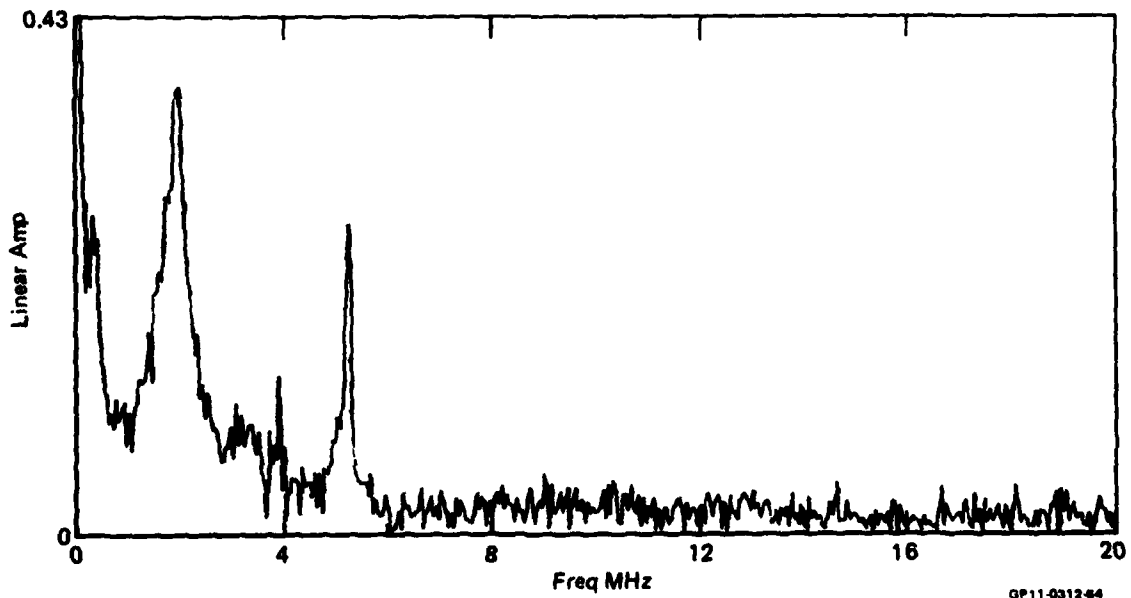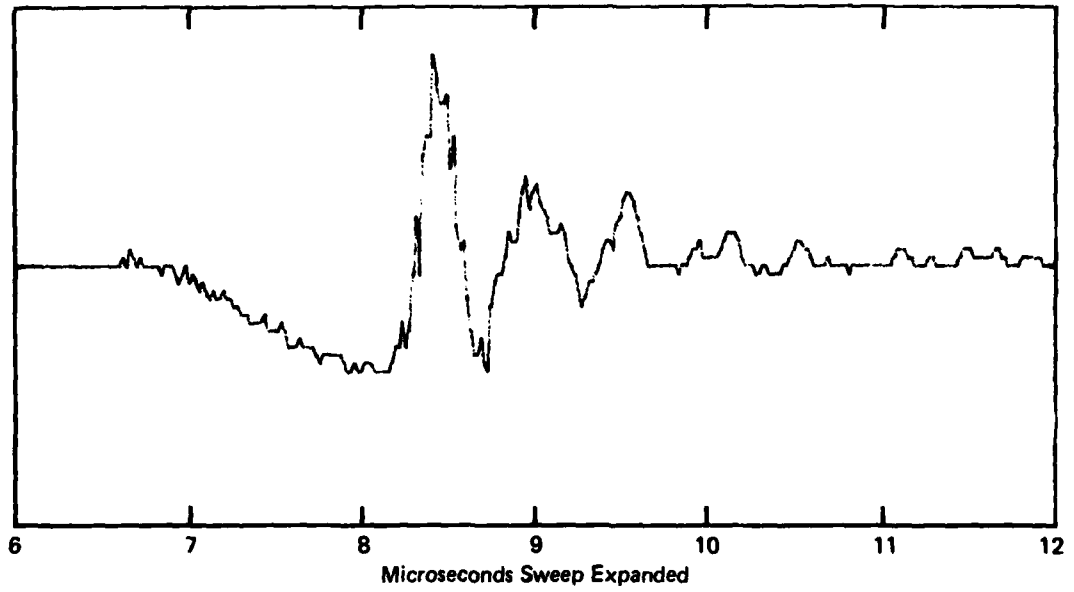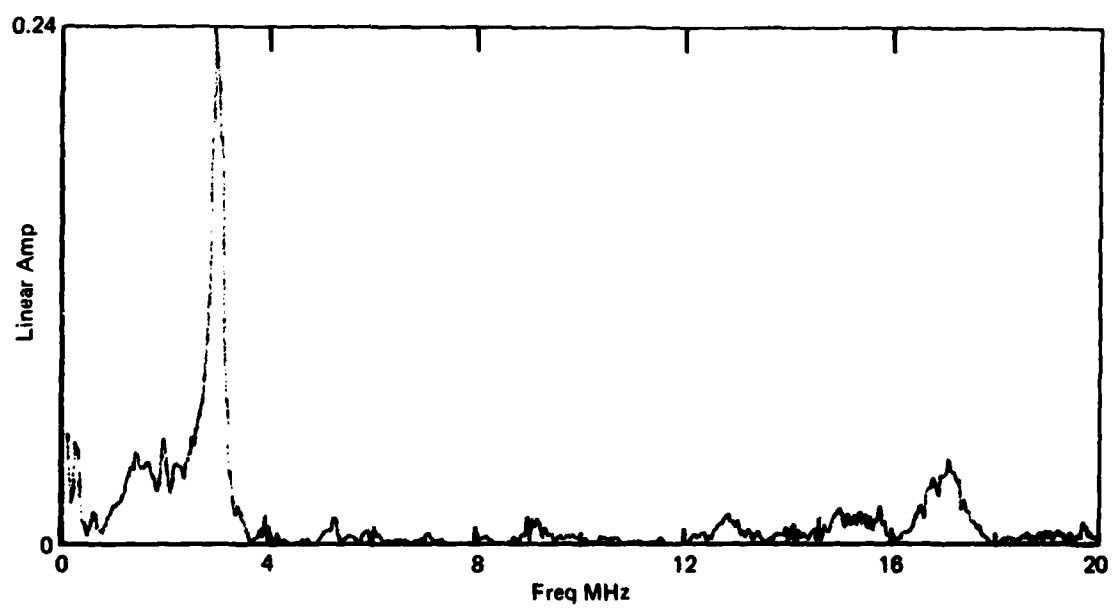### 1. Estimate of Effective Aperture Mutual Inductance

For a rough approximation, assume a current I flowing down a cylinder of
radius r that distributes itself uniformly around the cylinder everywhere
except the sector $2\theta_0$ subtended by the aperture of size ℓ.
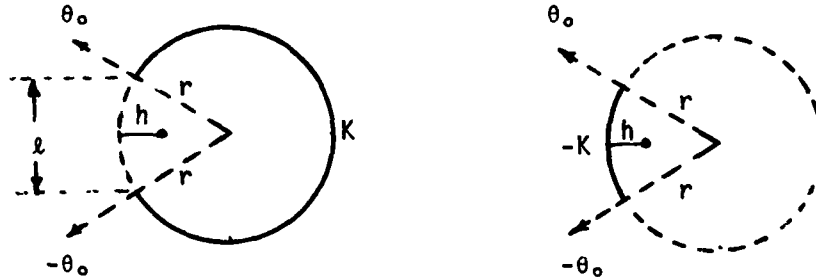
By superposition, the magnetic field <u>inside the cylinder</u> generated by the cur-
rent sheet $K = \dfrac{I}{(2\pi - 2\theta_0)r}$ on the left is equivalent to the sum of the field
generated by a current sheet K that exists around the entire cylinder plus a
current sheet -K along the aperture portion only. Symmetry and Ampere's Law,
however, require that the former component is identically zero, so that only
the component due to the aperture current remains. Integrating over this cur-
.ent distribution, the normal component of magnetic field at a distance h
along a radial line from the center of the aperture is derived as:

$$B_n(h) = \frac{\mu_0 I}{4\pi(r - h)(\pi - \theta_0)}\left[2\tan^{-1}\left(\frac{2 - \frac{h}{r}}{\frac{h}{r}}\tan\frac{\theta_0}{2}\right) - \theta_0\right]$$

The magnetic field at the aperture itself (h = 0) reduces to

$$B_{APERTURE} = \frac{\mu_0 I}{4\pi r}$$

while at the center of the cylinder ($h = r$) it reduces to

$$B_{CENTER} = \frac{\mu_o I}{2\pi r} \frac{\sin \theta_o}{\pi = \theta_o}$$

For an 11.2-inch aperture in a 14.7-inch-diameter cylinder ($\ell = 11.2"$, $r = 7.35"$, $\theta_o = 0.76$ rad), the field strength at the center conductor relative to the field strength at the aperture is

$$\frac{B_{CENTER}}{B_{APERTURE}} = 0.58$$

Approximating the normal magnetic field between the center conductor and the aperture as the average,

$$B_{AVG} = \frac{1}{2} [B_{CENTER} + B_{APERTURE}] = 0.79 \frac{\mu_o I}{4\pi r}$$

the mutual flux is approximated as

$$\Phi = B_{AVG} \ \ell r = 0.79 \frac{\mu_o I \ell}{4\pi}$$

so the aperture mutual inductance $L_{12} = 0.79 \frac{\mu_o \ell}{4\pi} = 22$ nanohenries.

2. Estimate of the Aperture Mutual Capacitance

The mutual capacitance C_{12} is derived indirectly from the mutual inductance L_{12}. Considering the cylinder with its ground plane or external wire return as one loss-less transmission line, and the inner conductor with its inner cylinder wall return as the other loss-less transmission line, the product of the inductance and capacitance matrices for the two coupled transmission lines is a diagonal matrix

$$\tilde{L}\tilde{C} = \mu \, \epsilon \, \tilde{I}$$

from which it follows that $C_{12} = -\dfrac{C_{22}'}{L_{11}'} L_{12}'$

where $\quad C_{12}'$ = mutual capacitance per unit length

L_{12}' = mutual inductance per unit length

C_{22}' = self capacitance per unit length (coaxial line) = $2\pi\epsilon_o / \ell n \dfrac{r}{a}$.

L_{11}' = self inductance per unit length (cylinder/ground return)

$$= \frac{\mu_o}{2\pi} \, \ell n \, \frac{2h}{r}$$

r = cylinder radius

h = cylinder height

The lumped mutual capacitance for the aperture is then easily determined:

$$C_{12} = (-C_{12}')\ell = (\frac{C_{22}'}{L_{11}'} L_{12}')\ell = \frac{C_{22}'}{L_{11}'} L_{12}$$

$$C_{12} = (\frac{(2\pi)^2 \mu_o/\epsilon_o}{\ell n \frac{r}{a} \, \ell n \frac{2h}{r}})L_{12} = 1.5 \times 10^{-5} \, L_{12}$$

Thus, for the aperture mutual inductance previously calculated:

L_{12} = 22 nanohenries

$C_{12} = 1.5 \times 10^{-5} \, (22 \times 10^{-9}) = 0.33$ picofarad

These values for mutual inductance, when used in the SPICE simulation, resulted in induced waveforms closely resembling the measured induced waveforms but whose amplitudes were overpredicted by one order of magnitude. When the mutual capacitance was adjusted down from .33 to .03 pf, the capacitive component of induced voltage closely matched the actual data. The inductive

component of induced voltage matched available data when the mutual inductance was adjusted down from 22 to 1.7 nh.

The relationship of the adjusted capacitance and inductance is:

$$\frac{C_{12} \text{ ADJUSTED}}{L_{12} \text{ ADJUSTED}} = \frac{.03 \times 10^{-12}}{1.7 \times 10^{-9}} = 1.8 \times 10^{-5}$$

The fact that the ratio of these adjusted parameters remains reasonably constant, considering the crudeness of the approximations and experimental error, helps support the transmission line approach in modeling the cylinder. The difference between calculated and adjusted values of the coupling parameters is probably due to the fact that the assumption of a uniform current distribution is not valid. Even for the quasi-static case, the fact that the aperture has a finite length along the cylinder axis skews the current distribution. At frequencies on the order of 1 MHz, the current will distribute itself in such a way as to exclude magnetic field lines from the cylinder wall, so that all magnetic field lines must enter and leave through the aperture, significantly decreasing the field levels.

3. Modeling the Arc Impedance

The gap impedance was assumed an open circuit prior to breakdown, simulated by a one-megaohm resistance. Well after establishment of an arc, a one-ohm resistance was used to model the low arc impedance, in series with an arc inductance of several microhenries.

The particular way in which the transition between high and low impedance was modeled was heavily constrained by the modeling options available in the SPICE program and other practical considerations having to do with pecularities of the code in execution.

The arc resistance was modeled as the sum of two components: $R(t)$, a component that makes a smooth transition from 10^6 ohms at t_1 (initiation of breakdown) to one ohm at t_2 (several hundred microseconds later); and $r(t)$, an intermediate component of 200 ohms that persists for about a microsecond after initiation.

(a) $t < t_1$ $\quad R(t) = 10^6$

$\qquad\qquad\qquad r(t) = 200$

(b) $t_1 \leq t \leq t_2$ $R(t) = \dfrac{1}{a + b(t - t_1)^9}$ where $a = 10^{-6/9}$

$\qquad\qquad\qquad\qquad\qquad\qquad\qquad\qquad\qquad\qquad\qquad\qquad b = \dfrac{1 - 10^{-6/9}}{t_2 - t_1}$

$\qquad\qquad\qquad r(t) = 200\, e^{-(t - t_1)}$

(c) $t > t_2$ $\quad R(t) = 1$

$\qquad\qquad\qquad r(t) = 200\, e^{-(t - t_1)}$

103/104
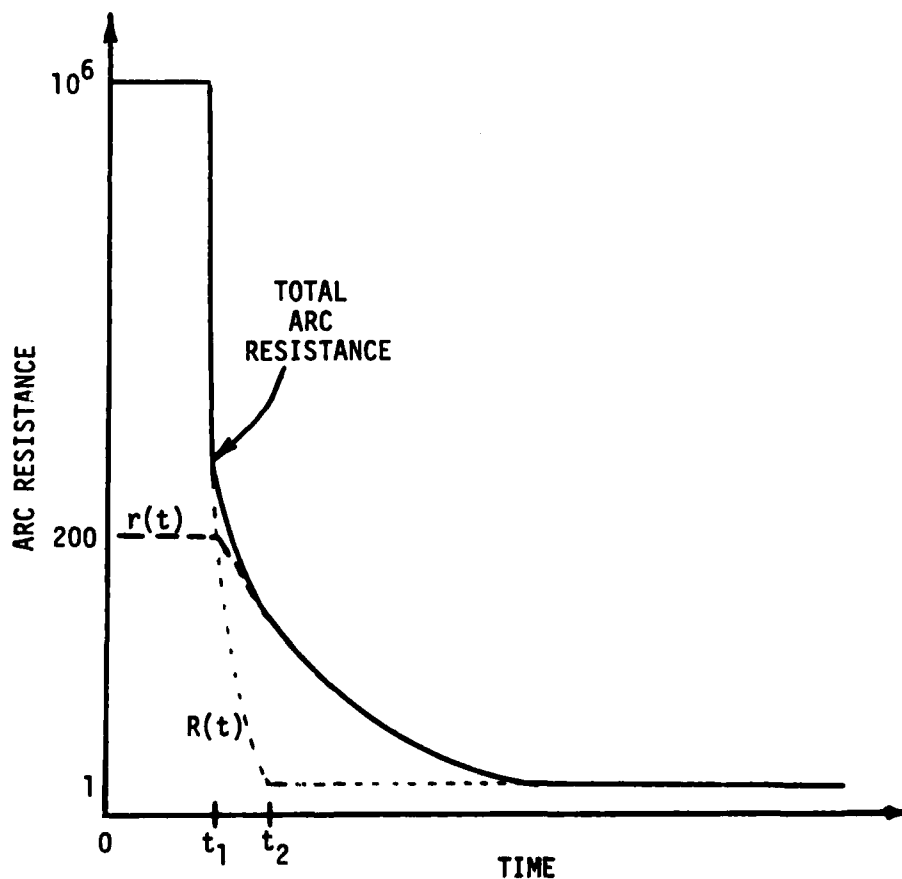
APPENDIX C
PRINCIPAL TEST EQUIPMENT

To enhance the correlation of the cylinder and YF-16 tests, the same test
equipment and instrumentation was used in both test phases. The principal
test components are briefly described in the following paragraphs.

1. High-Voltage Generator System

The high-voltage generator system was specifically designed for remote site
testing. The high-voltage Marx generator is modular in construction. Its
output voltage is readily varied from 50 kV to 1.5 MV by changing the number
of stages. The generator charging system is pneumatically controlled for
isolation and is fail-safe in its operation.

Figure C-1 is a schematic of the system which includes the high-voltage Marx
generator, a power supply, and an oil-filled charge/dump switch. The genera-
tor, shown in Figure C-2, is built in modules with each shelf being an inter-
changeable generator stage. Up to 15 stages can quickly be assembled using
only the shelves and nylon support posts for mechanical support. Each shelf
contains the capacitor, three resistors, spark gap switch, trigger electrode,
and a grading ring. Each capacitor stage is rated at 0.032 µf and 100 kV.
Interchangeable 40 KΩ copper sulfate resistors interconnect the capacitor
terminals and trigger electrodes from one stage to the next. Each stage is
triggered with an electrode biased at approximately half the potential between
the copper-sphere spark gap electrodes. A grading ring is used on each shelf
to suppress corona and produce a smoother electric field distribution.

Control of the generator system is provided by a pneumatically-operated charge/
dump switch which totally isolates the generator from ground during firing.
This system minimizes ground loops and coupling to the power supply and pro-
vides excellent operator safety. To charge the generator, the operator must
depress a spring-loaded valve to apply air pressure to a pneumatic actuator
which connects the power supply to the generator. When the valve is released,
the following sequence quickly occurs: 1) the power supply and its ground are
disconnected from the generator, 2) a trigger signal is applied to the trigger

circuit, 3) the generator erects to high voltage, and 4) both sides of the capacitor string are connected to ground. If for some reason the generator does not fire at step 3, the sequence continues and in step 4 the generator is discharged to ground through the charge/dump relay system.
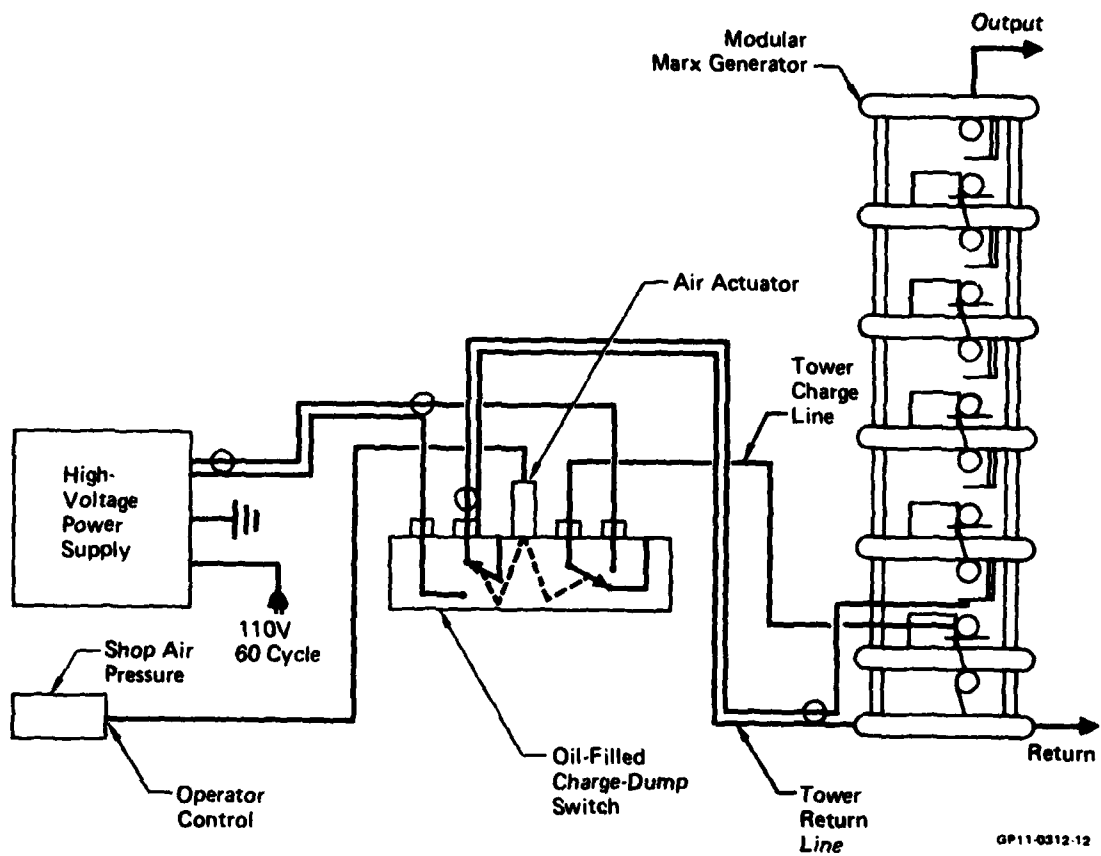
FIGURE C-1. HIGH-VOLTAGE GENERATOR SYSTEM DIAGRAM

One Marx-Stage
per Shelf

Trigger
Electrode

Aluminum
Grading-Ring

Copper Sphere
Spark Gap

Nylon Rod
Mechanical
Supports

Interchangeable
Resistors

Oil Filled
Charge/Dump
Switch

100 kV, 0.032 μf
Capacitor

GP11-0312-13
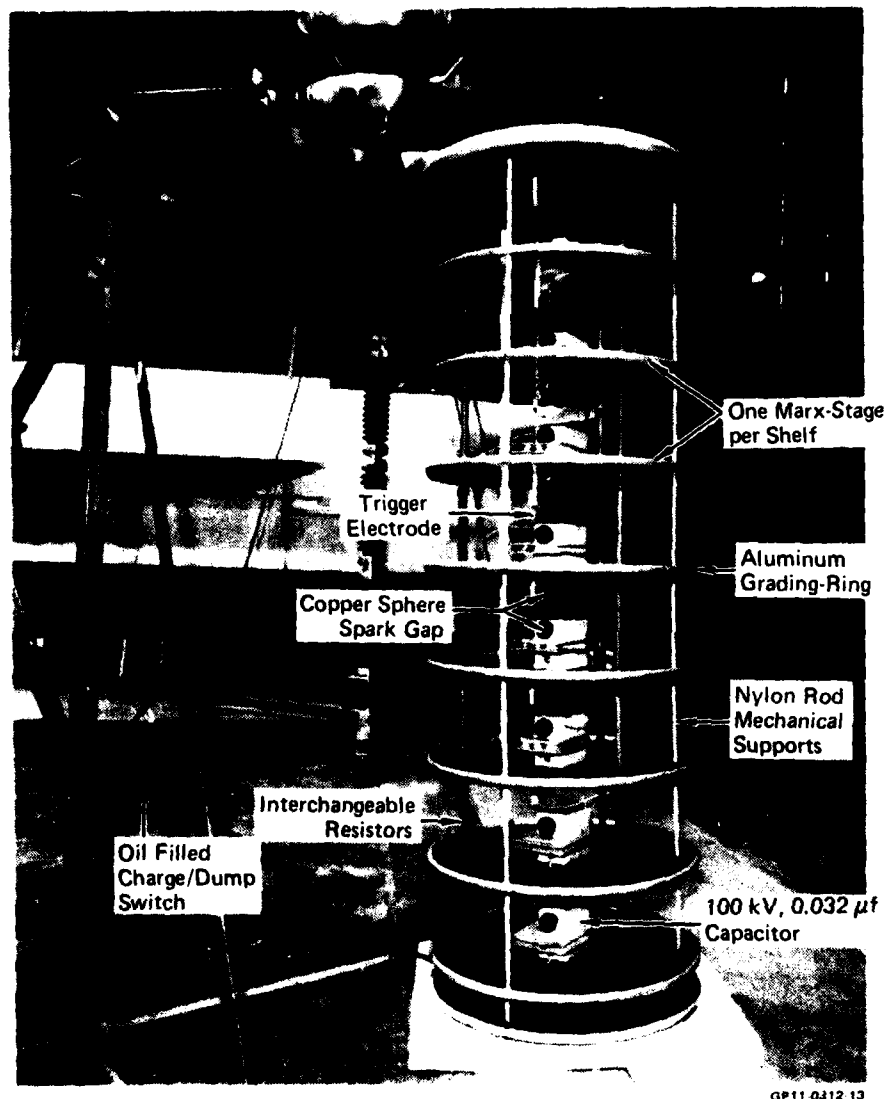
FIGURE C-2. MODULAR HIGH-VOLTAGE GENERATOR

2. Fiber Optic System

The fiber optic data links, pictured in Figure C-3, were designed and con-
structed at MCAIR. These units were used in all tests to transmit the elec-
trical response measured at the sensor to the recording equipment located in
an RFI tight screen room. The use of fiber optics eliminates common mode
interference and ground loop problems caused by the severe electromagnetic
test environment.

The MDC fiber optic transmitter uses a high impedance differential amplifier
to drive a current amplifier which in turn drives the light-emitting diode

within its linear range. The output is a signal modulated light pulse which can be transmitted through up to 20 meters of multistranded fiber optic cable to the receiver located in the screen room. The transmitter has common mode rejection of $\approx$40 dB at 15 MHz and can produce variable voltage gains from one to $\approx$150. The transmitter is battery-powered with a usable charge life of $\approx$4 hours. It can, therefore, be utilized anywhere in the test environment without external power and common mode signal problems. The dielectric fiber optic cable provides excellent high-voltage isolation.

The fiber optic receiver reconverts the optical signal into its electrical equivalent. The main receiver components are the receiver diode, a video amplifier, and a current amplifier to drive the 50Ω input impedance of the transient recorders. The entire fiber optic system has undergone several modifications during its development to improve reliability and bandwidth. The current system has a bandwidth of 25 MHz.

GP11-0312-14

FIGURE C-3. FIBER OPTICS COMPONENTS

3. Data Recording and Reduction

The data recording system, shown schematically in Figure C-4 and photographically in Figure C-5, is housed in a shielded enclosure for testing. The main components include two Biomation 6500 transient recorders, one Biomation 8100, and a Hewlett-Packard 9825 microcomputer with additional plotter and floppy-disk capability.
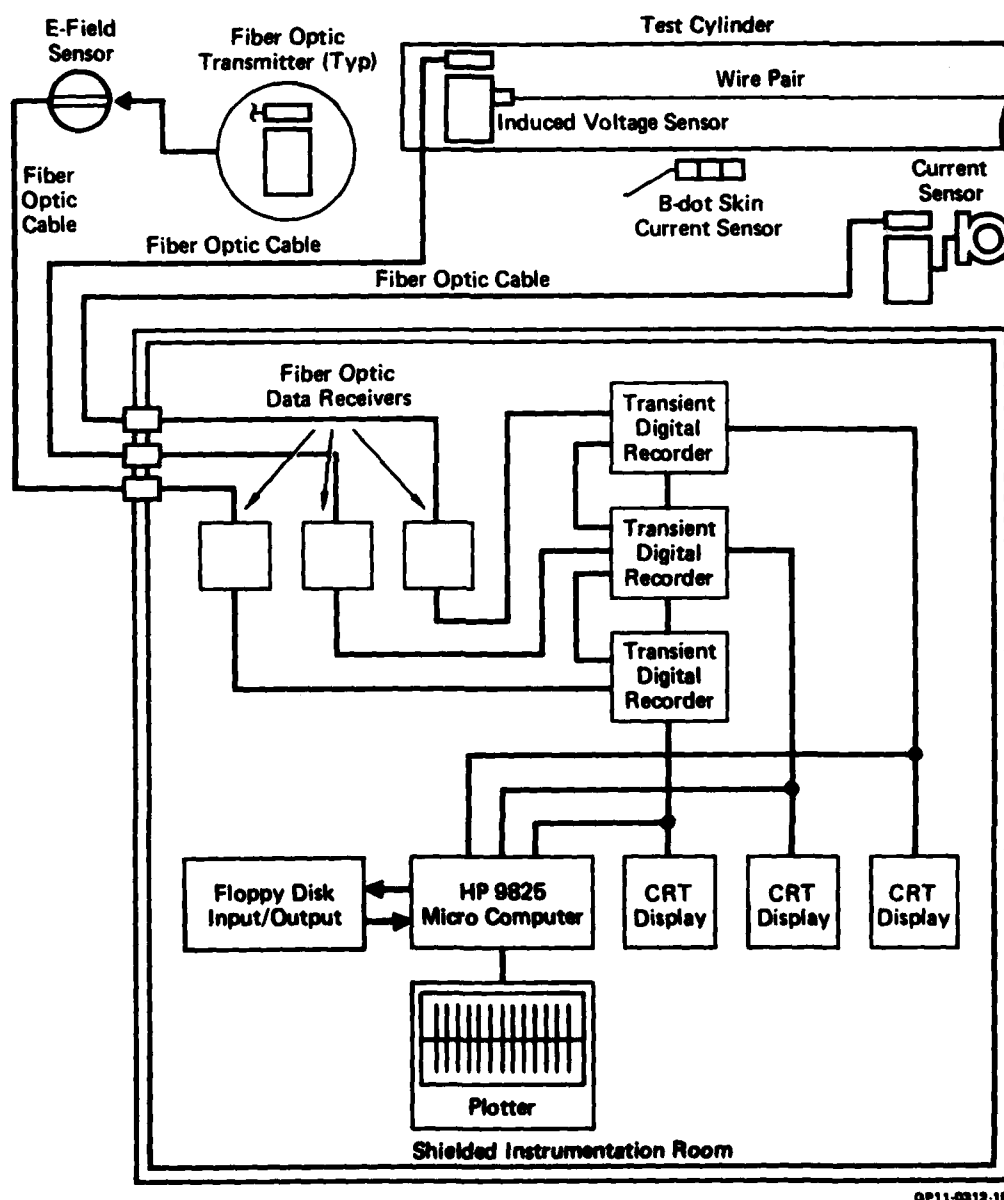

FIGURE C-4. INSTRUMENTATION SYSTEM FOR INDUCED COUPLING

The Biomations are operated in their "pretrigger" mode so that the baseline and leading edge of the transient response can be recorded. The 8100 samples 2,048 data points with nominal 8-bit resolution at a sampling rate of one datum point every ten nanoseconds. The 6500's have 6-bit resolution and sample every 20 nanoseconds for a total of 1,024 data points. All three recorders are triggered from the Biomation 8100 and can be synchronized to better than 50 nanoseconds.

The entire data acquisition system is controlled by the HP 9825 with software developed for transient analysis testing. The software is structured so that one controlling program is used to call any of 28 subroutines to perform the basic data recording, display, storage, and processing tasks. Memory space is held to a minimum by having only the controlling program and a binary FFT program in memory at any time. Data are stored on magnetic tape to provide a permanent record. Appendix A shows an example of the format and data processing routines available to aid in analyzing the test response.
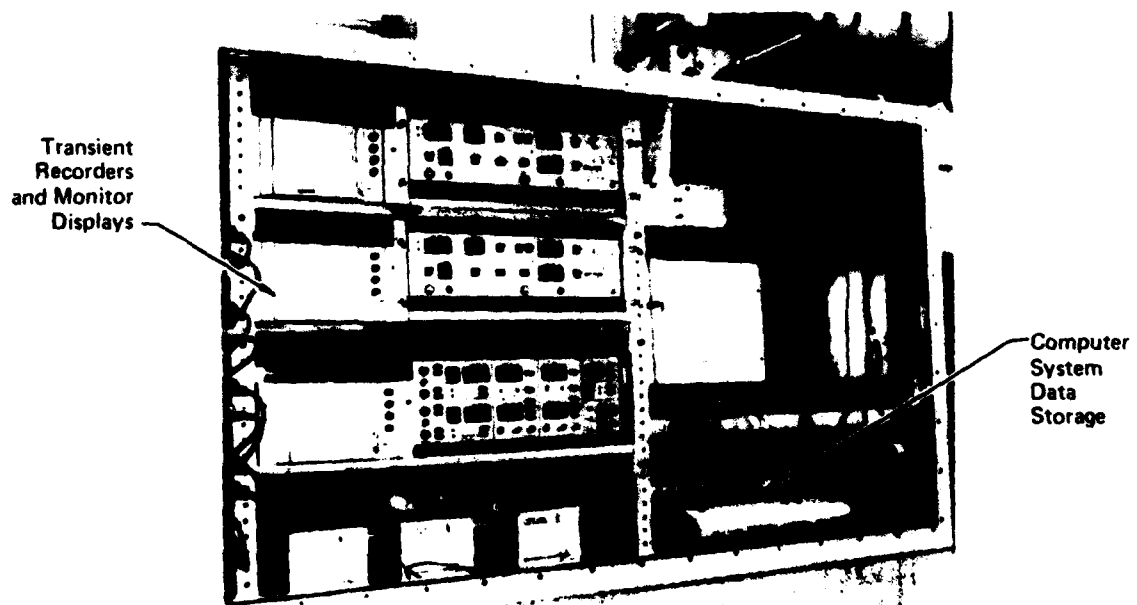

Transient Recorders and Monitor Displays

Computer System Data Storage

GP11-0312-16

FIGURE C-5. ADVANCED PORTABLE DATA SYSTEM

4. Data System Calibration

Prior to each test series, the total data system including the fiber optics, the transient recorder, and the computer is calibrated for bandwidth and linearity. To do this, a high-frequency triangular wave is applied at the fiber optic transmitter of each data channel. The wave is adjusted in amplitude up to the point that nonlinearity can be seen on the recorder's monitors. This known amplitude then establishes the maximum point at which data can be recorded and still maintain accuracy. The bandwidth is checked by using a high-frequency on the triangular wave.

The triangular calibration signal that is in the transient recorder memory is loaded into the computer. This signal with its calibrated peak-to-peak voltage is used to establish all of the recorded signal levels.

5. Sensors

Three types of electrical sensors were used during the tests. These were total current (I), surface current density (B-dot), and electric field (E). The total current sensor was a Pearson model 3025 with a sensitivity of .025 volts/amp. The surface current density measurements were made using the EG&G model MGL-S7A sensor. The electric fields (indirect cylinder voltages) were made using the McDonnell Douglas E-field probe with a sensitivity of .010 volt per volt/meter. The E-field sensor is a noncontacting spherical dipole antenna whose output is proportional to the E-field at the sensor. The voltage on the test article has the same waveshape as the field measured at the sensor, and the relative magnitude is inferred by comparison to calculated values.

6. Dielectric Isolation System for Aircraft Wheels

The lightning test article must be isolated from ground potential to utilize the shock-excitation test technique. Isolation for the long aluminum cylinder is readily provided by fiber glass tripod support stands. The isolation of an 11-ton fighter aircraft whose nose-wheel hub is only 3 inches above ground is more difficult. Surface tracking along a dielectric or arcing to ground

111

potential from the wheels or other extremities near ground provide alternate current paths which greatly reduce shot-to-shot repeatability and complicate test understanding.

Figure C-6 and C-7 are a schematic and photograph of the dielectric pads used to isolate the YF-16 nose and landing gear wheels. The base of the pad consists of eight 1/4-inch-thick, 4'x4' Lexan sheets. The inner and outer sidewalls are each a continuous sheet of Lexan 1/8-inch thick by 12 inches wide wrapped to give six complete turns. The sidewalls were installed in 1/2-inch recesses cut from the top three layers of the base. The extreme inner and outer edges of the two sidewalls were sealed with RTV-11 silicone rubber, and the segmented area between the sidewalls was filled with oil to prevent surface tracking under the sidewalls. *The pads withstood over 250 kV in the YF-16 tests without any surface tracking or arcing.*
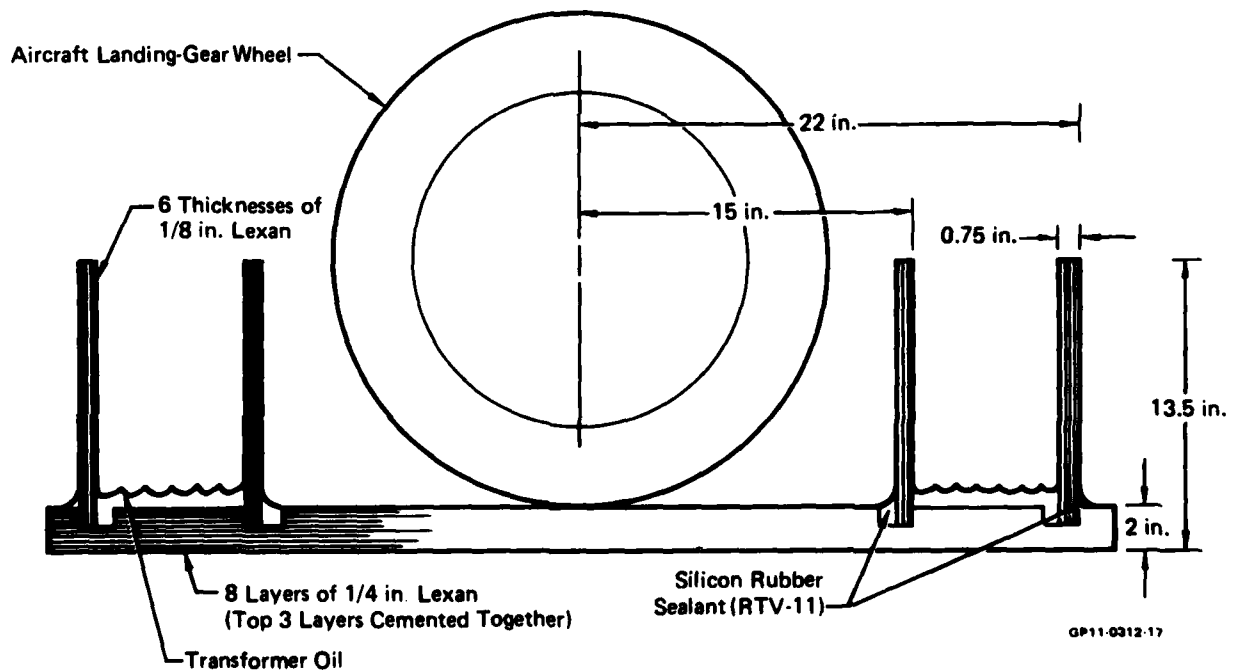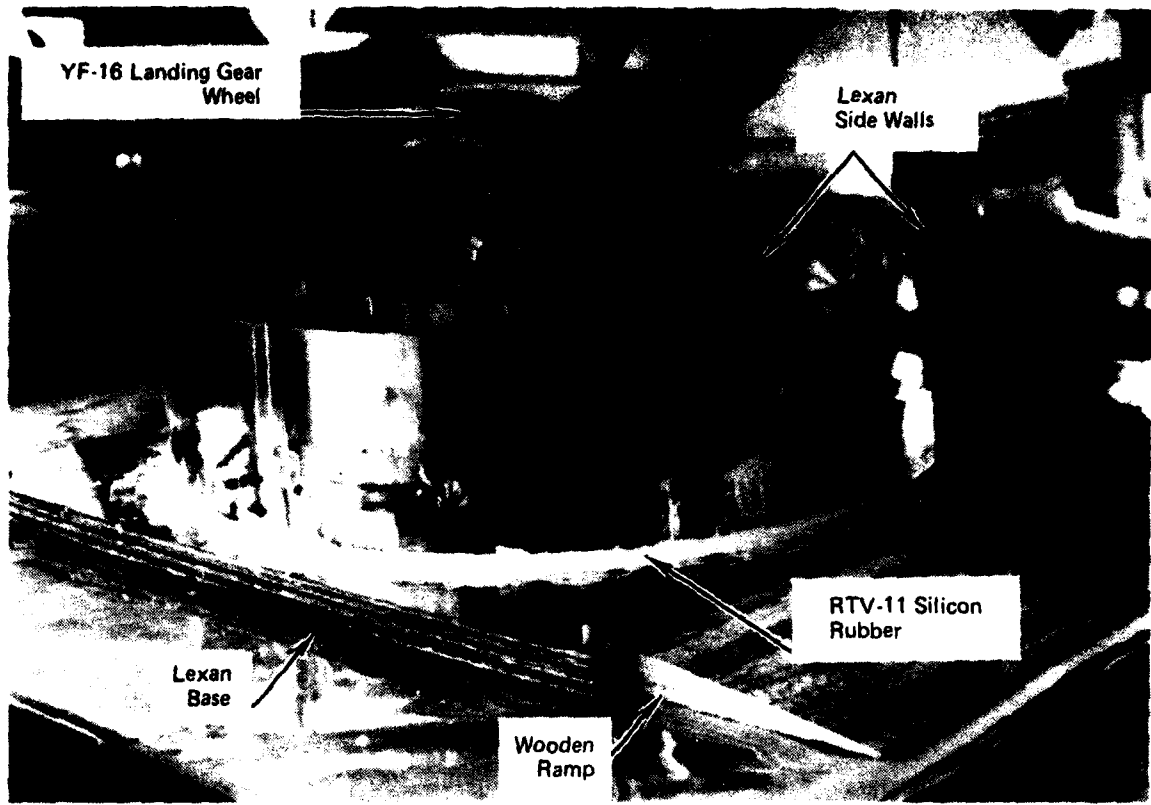

FIGURE C-6. DIELECTRIC ISOLATION PAD SCHEMATIC

FIGURE C-7. DIELECTRIC PAD PHOTOGRAPH

APPENDIX D

LIST OF EQUIPMENT AND INSTRUMENTS

ITEM	MANUFACTURER AND MODEL NUMBER	SERIAL NUMBER
TRANSIENT RECORDER	BIOMATION	
	6500	A082418
	6500	A082417
	8100	65433-1
MONITOR	TEKTRONICS	
	620	82425
		82426
		82427
COMPUTER PLOTTER	HEWLETT-PACKARD	
	9825A	73609
	9862A	73609-1
FIBER OPTIC RECEIVER	MCDONNELL AIRCRAFT	
	AFO-3R	73878-1
		73881-1
		73882-1
		73883-1
FIBER OPTIC TRANSMITTER	MCDONNELL AIRCRAFT	
	AFO-3T	71462
		73879
		73880
		73881
		73882
		73883
B-DOT SENSOR	MCDONNELL AIRCRAFT	
	LL1	-
	LL2	-
E-FIELD SENSOR	MCDONNELL AIRCRAFT	
	BLL1	-
CURRENT TRANSFORMER	PEARSON ELECTRONICS	
	3025	651731
HIGH-VOLTAGE POWER SUPPLY	UNIVERSAL VOLTRONICS	
	BAM 70-15	67267

(cont'd)

OSCILLOSCOPE	TEKTRONICS 7704	B151765
DIFFERENTIAL COMPARATOR	TEKTRONICS 7A13	A63704
TIME BASE	TEKTRONICS 7B70	A63711
TDR/SAMPLER	TEKTRONICS 7S12	B141636
SAMPLING HEAD	TEKTRONICS S-6	B87633
PULSE GENERATOR HEAD	TEKTRONICS S-52	B87634
FUNCTION GENERATOR	WAVETEK 145	B307619
SCOPE/DMM	TEKTRONICS 213	B044347

(cont'd)

OSCILLOSCOPE	TEKTRONICS 7704	B151765
DIFFERENTIAL COMPARATOR	TEKTRONICS 7A13	A63704
TIME BASE	TEKTRONICS 7B70	A63711
TDR/SAMPLER	TEKTRONICS 7S12	B141636
SAMPLING HEAD	TEKTRONICS S-6	B87633
PULSE GENERATOR HEAD	TEKTRONICS S-52	B87634
FUNCTION GENERATOR	WAVETEK 145	B307619
SCOPE/DMM	TEKTRONICS 213	B044347

REFERENCES

1. K. J. Lloyd, J. A. Plumer, and L. C. Walko, "Measurements and Analysis of Lightning-Induced Voltages in Aircraft Electrical Circuits," NASA CR-1744, February 1971.

2. L. C. Walko, "A Test Technique for Measuring Lightning-Induced Voltages on Aircraft Electrical Circuits," NASA CR-2348, February 1974.

3. J. A. Plumer, "YF-16 #1 Lightning Transient Analysis Test Report," General Dynamics Report 16PR051, June 1975.

4. K. E. Crouch and J. A. Plumer, "Improved Test Methods for Determining Lightning-Induced Voltages in Aircraft," NASA CR-3329, September 1980.

5. W. G. Butters, R. J. Lauber, and K. S. Zeisel, "Evaluation of Lightning-Induced Transients in Aircraft Using the E-Dot, V-Dot and I-Dot Shock-Excitation Techniques," McDonnell Douglas Corporation Report MDC A5683, December 1978.

6. D. W. Clifford and K. S. Zeisel, "Evaluation of Lightning-Induced Transients in Aircraft Using High-Voltage Shock-Excitation Techniques," 1979 IEEE International Symposium on Electromagnetic Compatibility, San Diego, California, October 1979.

7. W. G. Butters, D. W. Clifford, and J. E. Lenz, "Experimental Resolution of System Resonances Produced by Simulated Lightning Excitation," FAA/NASA/FIT Symposium on Lightning Technology, Hampton, Virginia, April 1980.